THE UNIVERSITY OF CHICAGO

EVOLUTION OF BIOMECHANICAL NOVELTIES AND THE MECHANICAL PROPERTIES OF CRANIAL LIGAMENTS IN WRASSES AND PARROTFISHES (FAMILY: LABRIDAE)

A DISSERTATION SUBMITTED TO
THE FACULTY OF THE DIVISION OF THE BIOLOGICAL SCIENCES
AND THE PRITZKER SCHOOL OF MEDICINE
IN CANDIDACY FOR THE DEGREE OF
DOCTOR OF PHILOSOPHY

GRADUATE PROGRAM IN INTEGRATIVE BIOLOGY

BY

SAMANTHA MARIE GARTNER

CHICAGO, ILLINOIS

JUNE 2023

For my grandma, Love you forever.

Table of Contents

LIST OF TABLES

LIST OF FIGURES

ACKNOWLEDGEMENTS

I have so many people to thank for the support and help given across the five years of my dissertation. First, I want to thank Mark Westneat for providing insightful and helpful comments on multiple drafts of this dissertation and providing the support needed to conduct my research over the past five years. Mark was extremely helpful and supportive in helping me to conduct field research, truly a master of spearfishing. Through failed experiments, fish dying, hard drives crashing and field work hiccups, Mark has been there through it all. Thank you to Callum Ross for always being there when I needed help. I appreciate all the support and advice given to me throughout the years. Thank you to Mike Coates for the insightful comments and always having stimulating conversations about anything and everything. Thank you to Beth Brainerd for being my committee member and giving me incredibly helpful advice.

Thank you to the Westneat Lab (Andrew George, Lily Hughes, Chloe Nash, Linnea Lungstrom, and Katie Whitlow) for always being willing to talk with me about research and helping my form the ideas behind this dissertation over the years. I wouldn't be where I am today without the help of my lab members. A special thanks to Katie Whitlow for being there whenever I needed her. I truly would not have made it to the end of my PhD without her. She always provided help and advice when needed.

Thank you to the Ross Lab for giving me a second home at the University of Chicago. I have had so much fun hanging out over the years with Alec Wilken, Peishu Li, Hannah Farrell, Kelsey Stilson, Kaleb Sellers, Felipe Prado, JD Laurence-Chasen, and Michael Granatosky. You guys have given me incredible advice I use to this day.

I want to give a special thanks to the Shubin lab for always being willing to help me when I needed it. Thank you to Emily Hillan, Melvin Bonilla, Shiri Kult, Nelima Sharma Sam Norris,

Gayani Senevirathne, Vishruth Venkataraman, and Yara Haridy for helping me learn histology and helping me with other fishy stuff.

Thank you to all my friends including Will Koval, Paula Fernandez-Begne, Laura Hunter, Hope Anderson, Peishu Li, Hannah Farrell, Katie Whitlow, Maddie Kelley, Kelsey Stilson, Kaleb Sellers, Vishruth Venkataraman, Emily Hillan, Melvin Bonilla, JD Laurence-Chasen, Stephanie Baumgart, Linnea Lungstrom and anyone I may have missed for always being willing to hear me talk about fish and my research ideas. A special thanks to Stephanie Baumgart for keeping me sane and always being willing to drink wine and watch the Bachelor/Bachelorette with me. I am especially grateful to all the graduate students in the Darwin Cluster who have helped me in various ways get through the five years of graduate school and I look forward to collaborating in the future with many of the students.

I want to thank all the people who supported me who could not be here today in person, my grandma and my godmother. Grandma, you always supported me and my fish even though you hated water. I love you and I promise to say “no” a little bit less in life. Dawn, I’m so sorry you’re not able to see me grow older. I wanted you to see my dissertation as I know you’d be proud of me. I love you and I promise to keep rebelling and I’ll watch over my mom for you.

Finally, I want to thank my family. Mom, you’ve always been there for me throughout everything. You’ve been my biggest supporter and I hope I have made you proud. Anneliese, you are the best sister a girl can have. Even when we don’t get along, you’re still my cheerleader and supporter. Corey, you’re the best brother and debater I could want. I always enjoy talking and debating science with you and I wouldn’t have it any other way. Dad, you’re maybe my biggest cheerleader, besides mom. You always know how to make me smile and I’m lucky to be your daughter. Erica, words cannot describe how much I appreciate you. I love you all.

ABSTRACT

Biomechanical systems such as feeding or locomotor morphologies are usually composed of a complex network of traits and applying the concepts of modularity and integration to these systems may be particularly informative. Fish skulls are a complex skeletal structure composed of up to 30 different bony elements, many of which are connected to other bones through ligaments or muscle via tendons. These soft tissues create essential connections in the skull that allow for force transmission through the skull and concurrently permit the bones to move as a cohesive unit during feeding. Several cranial ligaments have previously been shown to be important for high performance feeding behavior, however the structure and function of connective tissues in fishes has received relatively little attention. In this doctoral dissertation, I aim to understand how the linkage systems created by skeletal elements and connected by ligaments contribute to the diversity of skull shape, to assess the relative importance of various ligament properties to the mobility of the skull, and to explore how ligaments transmit force and control the movement of the skull during feeding using the wrasses (family Labridae). The fish family Labridae is a monophyletic group of over 600 species of coral reef fishes with a large diversity in diet, skull shape, and cranial mobility. By integrating morphometrics, tissue biomechanics, and histology with a well resolved phylogeny this dissertation research advances our understanding of skull diversity in reef fishes through three major aims. First, 3D geometric morphometric data were collected in a 205 species of labrids, and modularity and integration techniques were used to understand how linkages evolve in the wrasse skull. Second, mechanical and structural properties of three cranial ligaments were measured to understand the relative importance of these traits to cranial kinesis and force transmission in the skull. Third, this research program examined the patterns of ligament property evolution across a wide range of

feeding behaviors. Overall, this thesis helps to better understand how ligaments and linkages have evolved and function in the skull and allows for better predictions of the influence of ligamentous properties on cranial movement. This research will make significant advances at the level of tissue biomechanics and add to the knowledge of skull mechanics in a complex functional system in one of the major evolutionary radiations of marine fishes.

CHAPTER 1: INTRODUCTION

Teleost skulls are among the most highly complex structures in vertebrates, composed of multiple bony elements connected by soft tissues that move the bones in an organized and cohesive way to successfully capture prey (Liem 1970; Anker 1974; Barel 1982; Lauder 1982; Westneat 2006) through either suction feeding (Liem 1970; Lauder 1979; Durie and Turingan 2004) or biting. These coordinated movements are accomplished by integrating muscles, bones, and ligaments in the perciform skull to form three linkage systems where muscle forces are added through the input link, transferred through the coupler link, and then amplified and released through the output link. Through these transmission systems fishes can transfer force rapidly produced by the body muscles to power extreme expansions of the cranium during suction feeding (Camp and Brainerd 2014; Camp et al. 2015). High force transmission at somewhat lower velocity is also beneficial for biting species with ligaments transmitting forces through repetitive biting behaviors as well as rapid peak forces during strong bites (Wainwright 1987; Alfaro and Westneat 1999; Grubich et al. 2008, 2012).

Although linkage systems have been studied in some detail from the perspective of morphology, function, and evolution (Gregory 1933; Gosline 1971; Anker 1974; Winterbottom 1974; Muller 1989; Westneat 1990; Wainwright et al. 2004), important questions remain to be addressed regarding evolutionary patterns of shape diversification and linkage geometry in the skull. The concepts of anatomical modularity and integration provide a useful framework for exploring skull evolution in the teleost fishes, addressing important questions of functional modularity and diversification rates of linkage modules in this system. Collagenous soft tissues connect these linkages and transfer forces in between systems to power feeding which raises the question of how these ligaments respond under load due to their intrinsic mechanical properties.

The mechanical properties of ligaments include breaking stress, breaking strain, Young's Modulus, resilience, and other variables measured from the cyclical and failure stress-strain curves. These properties help to determine the function of the ligaments and the amount of time force is transferred through the ligament. Stress is the force per unit area in a material when an external force is applied, while strain is the deformation in the material when an external force is applied. Stress-strain curves can help to further inform the mechanical properties of the material. Young's Modulus is defined as the slope of the stress-strain curve and is a measure of stiffness. This variable quantifies the amount of force required to deform a material (i.e., a stiff ligament would require more force to deform the material). Resilience is the amount of energy returned by a tissue during the loading-unloading cycles (stress-strain curve) and is measured by taking the difference between the areas under each curve. Variables at failure include the stress-strain values, when the fibers in the ligaments undergo plastic deformation, and toughness, the work per volume for work of extension until fracture (Vogel 2013). Failure tests simulate a response to a sudden overload event and help understand the limitations of the force transmission capacity.

A central aim of this thesis is to explore the complex lever and linkage systems in the teleost fish skulls using 3D morphometric techniques and mechanical property testing. Mechanical properties define the stiffness and force transmission capability of cranial ligaments in teleost fishes. In this doctoral dissertation, we have three main hypotheses 1) linkages are tightly integrated and evolve at faster rates of shape diversification 2) stiff ligaments transmit forces faster, with little elastic stretch, functioning as a rope or wire connecting bony elements and 3) compliant ligaments allow for more mobility in the joint, providing elastic stretch capabilities between bony elements, potentially functioning in shock absorption and damping of forces, acting as a spring. This thesis aims to answer the questions 1) "How do the linkages in the fish

skull evolve?" and 2) "What are the roles of cranial ligaments in the fish skull?". Answers to these questions and tests of these hypotheses will provide new insight into the evolution of skull linkages in fishes and increase our understanding of the role of soft collagenous tissues in the function of vertebrate feeding mechanisms.

Phylogenetic Context

This thesis explores the shape of linkage systems and the mechanical properties of cranial ligaments in the wrasses and parrotfishes (fish family Labridae), so it is important to understand the phylogeny of this large group of coral and rocky reef-associated fishes. Figure 1.1 shows the recently resolved phylogeny for fishes in the Eupercaria based on exon-capture phylogenomic analysis (Hughes et al. 2022) illustrating the phylogenetic placement of the Labridae. The Labridae (wrasses and parrotfishes) are most closely related to the Centrogenyidae (false scorpion fish). They fit into the larger fish phylogeny by being a part of the percomorph fishes, specifically Eupercaria which includes over 6000 species from 161 families (Betancur et al. 2017). The recent phylogenomic analysis of 203 species of wrasses (Hughes et al. 2022) illustrates the broad pattern of labrid evolutionary relationships with the different tribes highlighted (Fig. 1.2). This phylogenomic tree topology is largely congruent with large phylogenetic studies using Sanger-sequence datasets incorporating a dozen loci and up to 410 species (Westneat and Alfaro 2005; Aiello et al. 2017; Larouche et al. 2022). In this research, the most recent, updated phylogeny from Larouche et al. 2022 is used as a framework for exploration of patterns in character state evolution of linkage structure and material properties, to understand how the shape of linkages and mechanical properties of cranial ligaments have evolved over time.

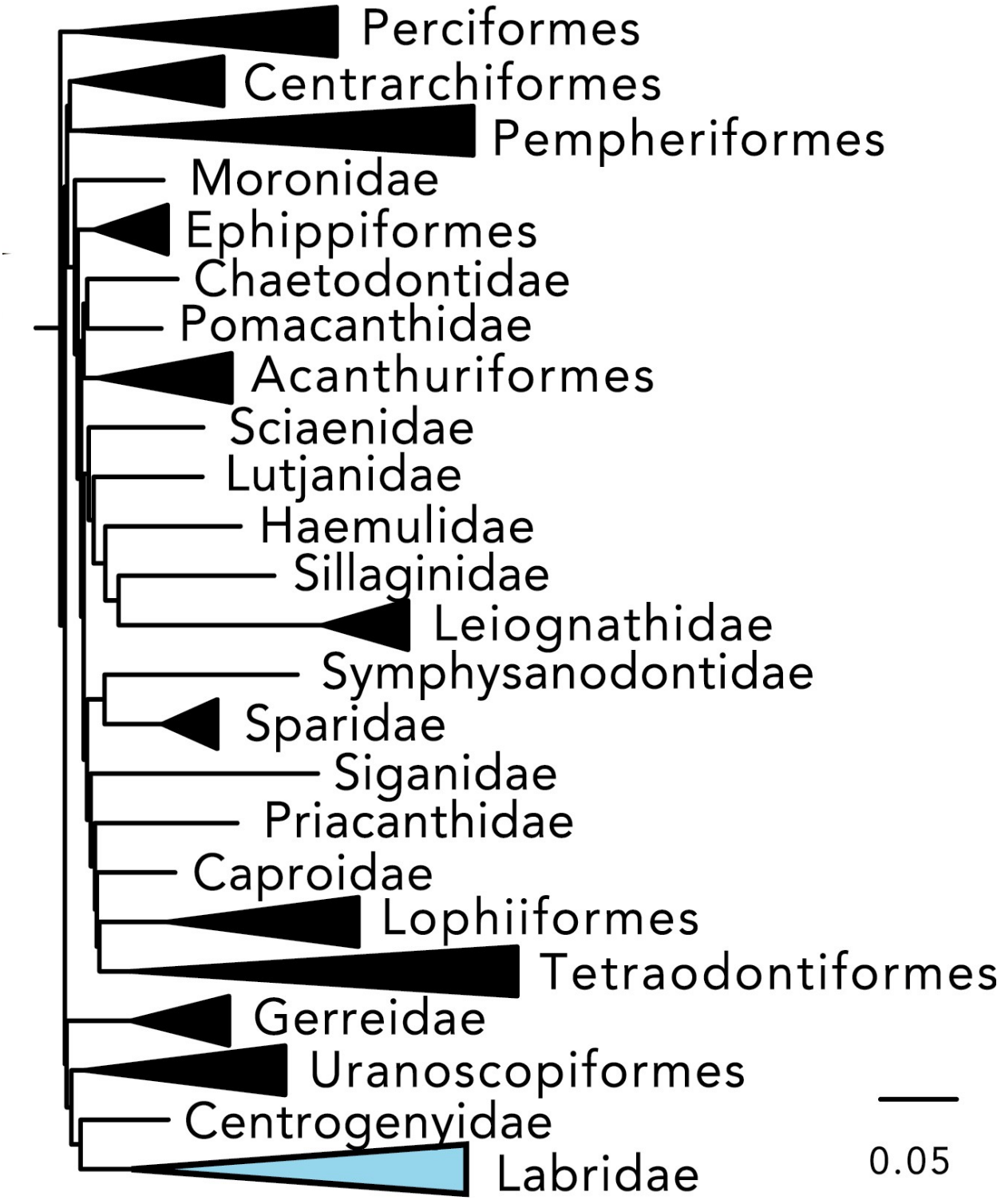

Figure 1. 1: Relationships among fish families within the Eupercaria from Hughes et al. 2022.

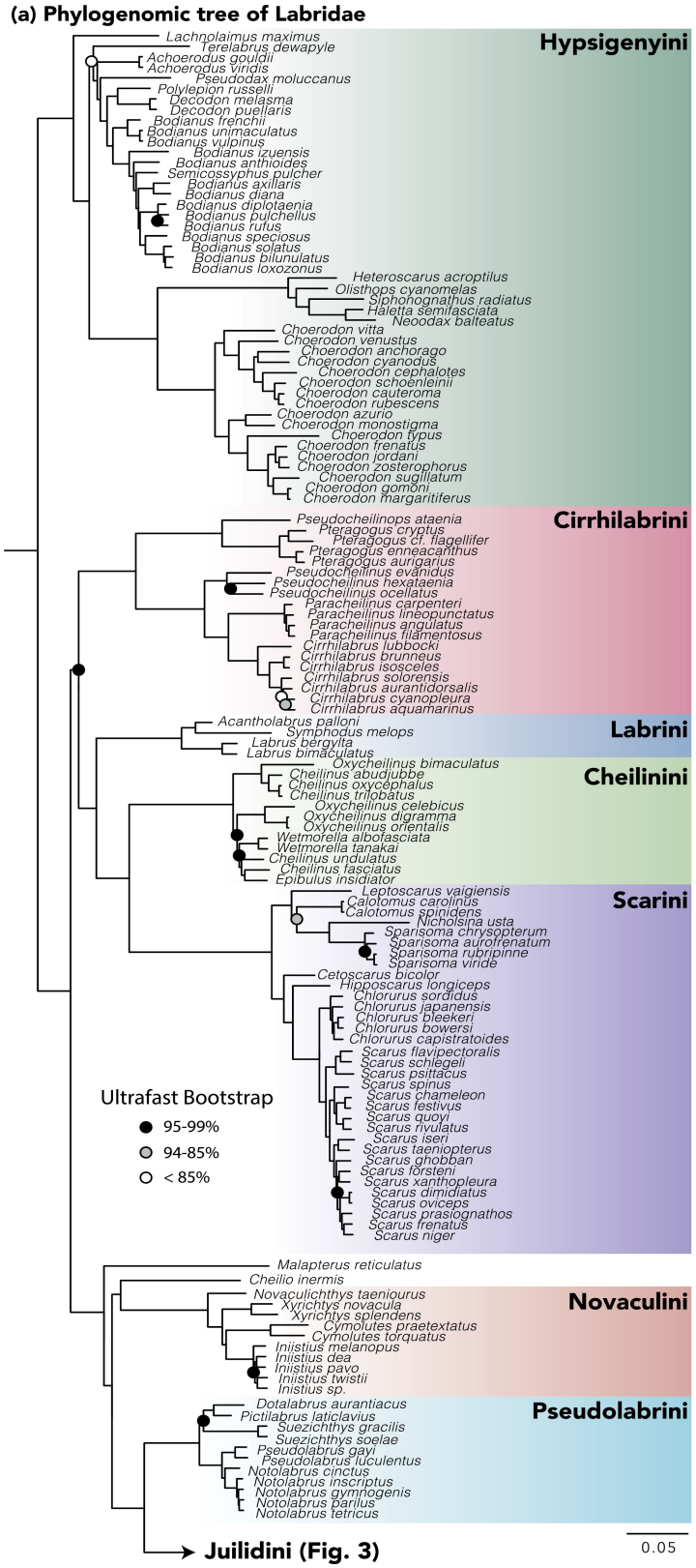

Figure 1. 2: Internal relationships within Labridae (crown Julidini group not shown) based on exon capture phylogenomics of 203 labrid species showing major tribal designations from Hughes et al. 2022.

Modularity and Integration

Morphological, biomechanical, developmental, and physiological traits define a species' ability to persist in their habitat. These traits consist of recognizable structural and functional features with varying levels of interrelationships with other traits that can reflect the independence of a structure. Research often shows that the independence of a trait in a system is variable, with some features coevolving as tightly associated units or modules (Wagner 1996). The variation in independence and coordination between the parts is analyzed using the concepts of modularity and integration. Integration is the pattern of trait covariation which can help to understand on a macroevolutionary level how phenotypes evolved. Modularity takes these patterns of trait covariation and reveals the covariation between blocks, or modules, of traits.

Decades of modularity research have shown patterns of covariation to be unevenly distributed in a system, where some variables show higher correlation with others showing higher independence in a structure (Cheverud 1982, 1995; Olson and Miller 1999; Albertson et al. 2005; Klingenberg 2008; Goswami and Polly 2010; Parsons et al. 2011, 2012; Goswami et al. 2019). These patterns of modularity could result in sets of semi-independent traits that can evolve at different evolutionary rates or respond to evolutionary or biomechanical variables differently, and thus lead to new functional or structural novelties. Identifying these patterns over a large phylogenetic sample can hint at the functional or environmental influences driving the evolution of a system, whereas in ontogenetic samples the developmental or genetic influences are elucidated (Cheverud 1982, 1995; Olson and Miller 1999; Albertson et al. 2005; Klingenberg 2008; Parsons et al. 2011, 2012; Larouche et al. 2018; Adams and Collyer 2019; Bardua et al. 2019; Churchill et al. 2019; Goswami et al. 2019).

Modularity and integration occur on several levels of organization: developmental, genetic, functional, and evolutionary. These different levels occur within an individual, population, or lineage (Zelditch and Goswami 2021). Developmental modularity is defined by modules, or sets of genes, that interact to form parts of a structure while genetic modularity uses sets of genes to define the effects traits have on the interaction of the development of a structure (Klingenberg 2008). Functional modularity refers to the patterns of traits that perform one or more functions while evolutionary modularity involves understanding clade specific patterns of trait evolution (Klingenberg 2008). The interaction between different levels of modularity helps to inform the developmental and evolutionary diversity in and across individuals. For example, research into BMP4's developmental pathway for the out-lever and opening in-lever of the lower jaw in cichlids, helps to understand the genotype-phenotype pattern of this system and reveals the importance of the mechanical forces and tradeoffs in the lower jaw influencing the different shapes and modularity of cichlid mandibles (Albertson et al. 2005; Parsons et al. 2011, 2012). This research shows the interactions between the levels of modularity and how these levels affect the function and development of a complex musculoskeletal structure(s).

Using this framework, the first main contribution of this thesis research is an exploration of modularity and integration in the skull of labrid fishes. We seek to show covariation of bone shape as a signal of the functional modularity of the linkage systems, potentially revealing they are functionally transforming together. Using a large three-dimensional dataset of geometric morphometrics of 200 species of wrasses and parrotfishes, this work sets out to specifically test levels of functional modularity among components of the labrid skull involved in the linkage mechanics of the feeding mechanisms in this diverse group of fishes.

Mechanisms of Fish Feeding

Teleost fish feeding systems display among the most diverse morphological and kinetic structures in vertebrates. The teleost skull, in particular, is a highly complex structure that can have up to 80 different skeletal elements all connected by soft tissues, like ligaments, tendons, muscle, skin, fascia, etc. (Liem 1970; Anker 1974; Winterbottom 1974; Barel 1982; Lauder 1982; Westneat 2006). Together the soft tissue and skeletal elements function in a way that cohesively moves the skull for different behaviors (i.e., feeding, breathing, social communication, etc.). High force transmission is thought to be important for suction feeding that is mediated through the cranial ligaments. The ligaments in a fish skull have been shown to have a significant effect on the ability for the fish to cohesively move the skull during suction feeding and breathing behaviors (Liem 1970; Lauder 1979; Durie and Turingan 2004). The relatively small muscles in the teleost skull alongside the ligaments are able to redirect the high force produced by the body muscles through the skull to produce the extreme expansion of the cranium in suction feeders (Camp and Brainerd 2014, 2015). The configuration of muscles, skeletal elements, and ligamentous connections in the skull typically forms three linkage systems in the percomorph skull (e.g., tunas, wrasse, cichlids, perches) that together transfer movement through the skull that lead to organized patterns of motion.

The three major linkage systems in the percomorph skull are the anterior jaws linkage, the opercular linkage, and the hyoid linkage system (Fig. 1.3). These linkages have been modeled as four-bar linkage systems from mechanical engineering principles (Westneat 1990;

Olsen et al. 2017), where the movement of three mobile links connected by rotating joints has computationally defined motions relative to a fourth fixed link.

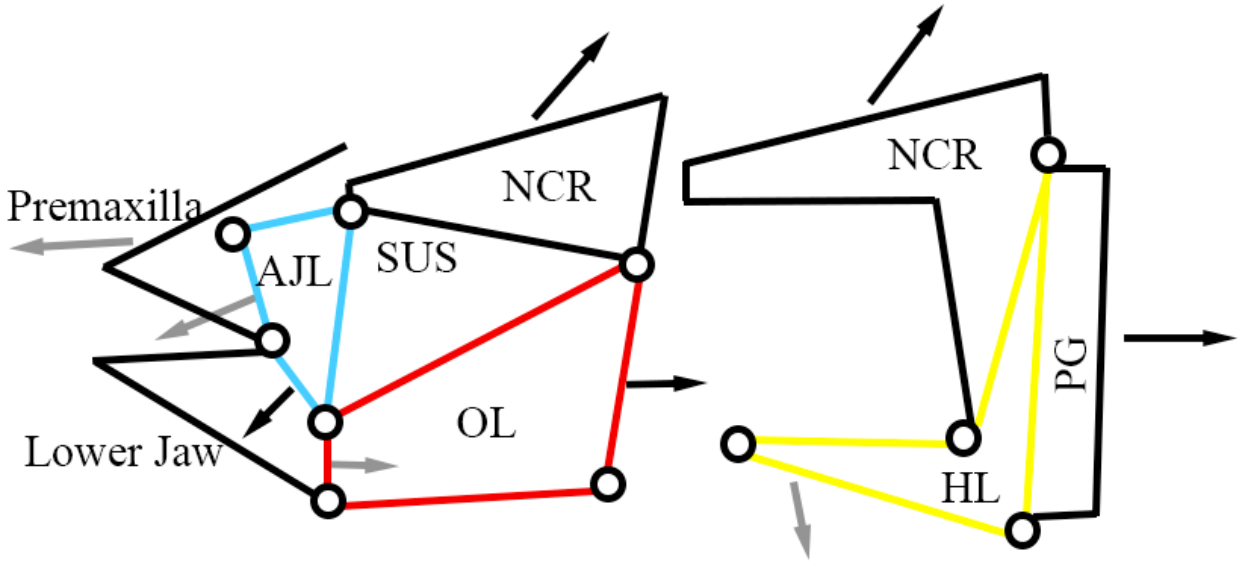

Figure 1. 3: Mechanical diagram of the three four-bar linkage systems. Anterior jaws linkage (AJL) is highlighted in blue, the opercular linkage (OL) is highlighted in red, and the hyoid linkage (HL) is highlighted in yellow. Black arrows represent input forces and grey arrows represent output forces. Abbreviations: NCR-neurocranium, SUS-suspensorium, PG-pectoral girdle. Adapted from Westneat 1990.

Movement of the anterior jaws four-bar linkage involves the depression of the lower jaw and results in anterior rotation of the maxilla which leads to the protrusion of the premaxilla in some species of fishes (Westneat 1990, 1991, 1994, 2006). Movement in the opercular four-bar linkage system contributes to lower jaw depression through the retraction of the operculum and transmission of force to the posteroventral lower jaw through the interopercle link (Anker 1974; Westneat 1994; Olsen et al. 2017). Additionally, the opercular linkage system leads to lateral expansion of the posterior skull region through the abduction of the operculum (Olsen et al. 2017). The final four-bar linkage system is the hyoid system that has two sources of input force (Muller 1989; Westneat 1990). The first input is cranial elevation leading to the rotation at the hyomandibula-interhyal joint and the second input is the contraction of the sternohyoideus

muscle pulling on the posterior part of the ceratohyal (Muller 1989; Camp and Brainerd 2014). The main input link is the link between the neurocranium and interhyal whereas the coupler link follows the sternohyoideus muscle. When force is applied to this system the hyoid apparatus is depressed and retracted and the buccal cavity is expanded ventrally and laterally. Lower jaw depression is also coupled to movement transferred through this system through retraction of the sternohyoideus (Muller 1989; Westneat 1990; Camp and Brainerd 2014; Olsen and Westneat 2016).

These linkage systems have been demonstrated to be essential for cranial movement through ligament removal and transection experiments. Liem (1970) conducted some of the first ligament cutting experiments that systematically removed ligaments and studied the behavioral effects, using three species of leaf fish (family Nanidae) that rely on suction feeding to capture prey. One example transection was the removal of the interoperculomandibular ligament affecting the suction feeding behavior by not allowing the individuals to fully open the jaws. Cutting this ligament interrupted the opercular linkage system and did not allow for the movement of the operculum to be transmitted to the lower jaw, leading to maximum depression. However, since the hyoid linkage and anterior jaws linkage system was uninterrupted, the lower jaw could still depress slightly, but prey were never successfully captured (Liem 1970). Systematic ligament cutting and removal experiments have also been conducted by Lauder (1979) and Durie and Turingan (2004), where both found similar results to those by Liem (1970). Ligament transection studies have not been conducted on species that use biting behaviors to capture prey, but similar results are expected.

Overall, this prior research shows that ligaments are essential for transmitting motion through the skull to allow for synchronous and high performance movement that produces an

expansion of the skull, which only happens when all three linkage systems work concurrently. These ligament transection papers reveal the importance of ligaments to facilitating motion in the teleost skull. However, to further our understanding of the role of skull ligaments in force transmission or energy storage, it is necessary to perform test of mechanical properties of the ligaments, such as stiffness. The role of soft tissue mechanical properties in the biomechanics of fish feeding systems is a largely unexplored area of inquiry.

Teleost skulls have been studied in depth over multiple decades and the few studies on the mechanical properties of connective tissues in fish have been restricted to the tendons in the caudal region in tuna (Shadwick 1990; Shadwick et al. 2002), the hagfish tongue retractor tendon (Summers et al. 2002), and the tendon of the jaw adductor muscles in a durophagous stingray (Summers et al. 2003). Together, these studies found the tendons of fish to have similar stiffness values to mammals and have high resilience values that may be efficient for energy storage (Shadwick 1990; Shadwick et al. 2002; Summers et al. 2002, 2003). Tendons connect muscle to bone, and therefore have more of an influence on the mechanical forces moving through the skull (Alexander 1989; Summers et al. 2002; Roberts and Azizi 2011). The stiffness of tendons may need to remain consistently high due to this function. However, ligaments connect bone to bone and function to mainly hold bones together and act in force transmission and damping of large forces (Alexander 1989), indicating these soft tissues may be able to vary their mechanical properties based on environmental influences.

The secondary aim of this thesis is to explore the material properties of cranial ligaments in labrid fish feeding systems. Analysis of stress-strain properties in teleost cranial ligaments is limited to a single preliminary study of strain to breaking in a set of specimens from the Red Sea (Grubich et al. 2014). This study suggested differences in the mechanical properties of ligaments

across different feeding guilds, and across diverse fish families, including wrasses and parrotfishes. Due to the differences in stiffness and strain of a single ligament, these findings hint at possible novel innovations in fish ligaments that may be important factors in skull mechanics and a source of previously unexplored functional variability. This thesis thirdly aims to test the properties of important cranial ligaments and their functional role at multiple levels within the labrid phylogeny.

Thesis Synopsis and Aims

This Ph.D. thesis seeks to understand the morphometric and biomechanical evolutionary patterns of the labrid skull across a spectrum of cranial mobility. First, I examine the complex three-dimensional morphometrics of the labrid fishes in a phylogenetic context using the three-dimensionality of linkage system shape. Second, I explore the mechanical properties of three skull ligaments in six species of labrid fishes in the closely related tribes Cheilini and Scarini to test the idea that ligament compliance is an important factor in feeding mechanisms. Third, I examine the question of ligament properties more broadly among the labrid fishes to test the idea that ligament properties are associated with the feeding habits and ecomorphology of wrasses and parrotfishes. These questions are addressed using the wrasses (Family: Labridae); a group of coral reef fishes with a wide diversity in skull shape and function (Westneat et al. 2005) and have a well-resolved phylogeny (Aiello et al. 2017; Larouche et al. 2022). This research provides an opportunity to investigate the family-wide and tribe-specific evolutionary influences on the skeletal and ligamentous composition of the skull and provides new insights into the diverse roles of collagenous soft tissues in vertebrate function.

Chapter 2: Evolutionary patterns of modularity in the linkage systems of the skull in wrasses and parrotfishes

Overview: With chapter 2, I aim to answer three main questions. 1) How do the shapes of four-bar linkages evolve in wrasses? 2) Do the linkages evolve at faster rates compared to the remainder of the skull? and 3) How three-dimensional are the four-bar linkage systems in the skull of wrasses? Using three-dimensional geometric morphometric techniques on μCT scanned labrid skulls, I explore how the linkages created by the skeletal system contribute to the morphological and functional diversity in skull shape in the wrasses (family Labridae). Previous work shows some clades of wrasses have greater diversity than others in lever and linkage design (Westneat et al. 2005). Thus, a main prediction of this work is that some labrid tribes will show high amounts of structural and functional diversity, whereas others may be more limited or constrained in skull disparity.

The central aim of this work is to examine the wide diversity in wrasse skull evolution and determine potential biomechanical and ecological drivers of the disparity in skull shape. Assessing the integration structure, how the regions of the skull covary with each other, helps to elucidate how the skull structure is evolving across a wide variety of species among wrasses. Additionally, using the pattern of modularity to test rates of evolution helps to understand the rate at which skull shape and linkage shapes between tribes and in the entire family has evolved.

Significance: This project makes significant advances in understanding the level of evolutionary diversification in a complex functional system. It describes new ways in which the structural and functional changes in the skull of wrasses and parrotfishes can be interpreted in the context of functional modularity versus integration. These results help pinpoint which regions of the skull

are most strongly influencing the direction of evolutionary change across different modules of the labrid skull and among the highly divergent taxonomic tribes in the labrid phylogeny.

Chapter 3: Elastic skull ligaments and the biomechanics of the parrotfish bite (Family: Labridae)

Overview: With chapter 3 I aim to answer two main questions. First, I will seek to understand how the mechanical properties (i.e., resilience, breaking strain, Young's Modulus) vary with feeding behavior in closely related species in the cheiline and scarine labrids. Second, I will describe how the ligaments function in the labrid fish skull. I mechanically tested three cranial ligaments across six labrid species: the coronomaxillary (CM), interoperculomandibular (IOPM), and interoperculohyoid (IOPH). The material properties (Young's modulus, resilience, and breaking strain) and the structural properties (length and cross-sectional area) of three cranial ligaments were quantified to assess the relative stiffness vs. compliance in cheilines and scarines. I also tested whether all three cranial ligaments exhibit similar properties or if the ligaments display region specific patterns. The central result of this work is that parrotfishes have extremely compliant ligaments, with strains up to 60% in some tissues. The IOPM is stiffer in the cheilines, suction feeders on evasive prey, compared to the parrotfishes, which bite on hard substrates. The CM is more compliant in the cheilines and the parrotfishes. From this data, we hypothesize the CM in the mixed feeding species, *Bodianus rufus* and *Lachnolaimus maximus,* function as force transmission structures whereas in biting species, the parrotfishes, and the suction feeding cheilines, the CM ligament functions to provide force damping and shock absorption and allow for more mobility in the oral jaws.

Significance: This research aim reveals a significant new source of functional variability to models of fish feeding systems in general and helps to better understand the diversity and function of tissue biomechanics in the skulls of labrid fishes. Parrotfish cranial ligaments show highly elastic properties, with high strain, among the most compliant ligamentous structures ever discovered among vertebrates. Examining the properties of the cranial ligaments provides a new axis of functional traits to better understand the skull diversity in wrasses. Understanding the structural and material properties of the cranial ligaments helps to quantify the contribution of these soft tissue structures to the movement and force transmission in the fish skull during feeding and reveals how these tissues have been tuned over evolutionary time. The variability in the ligament properties point to soft tissues allowing for new functional abilities of the skull to evolve which has broad functional implications in teleosts.

Chapter 4: Mechanical properties of cranial ligaments across a variety of feeding behaviors and phylogenetic relatedness (Family: Labridae)

Overview: With chapter 4, I aim to answer two main questions 1) How do the mechanical properties of cranial ligaments vary over feeding behavior and phylogenetic relatedness and 2) how do the structural properties of ligaments vary across feeding guilds and phylogenetic relationships? I expand on chapter 3 by including more phylogenetically disparate species, *Lachnolaimus maximus* and *Bodianus rufus* and assess the structural variables, using tissue histology, alongside mechanical properties. I test the mechanical property differences across the phylogeny and across feeding behaviors. The interoperculomandibular (IOPM) ligament in suction feeders have a high Young's modulus. This indicates a stiff IOPM to be the likely ancestral state of wrasses. On the other hand, the CM is stiff for the hypsigenyine wrasses, *Bodianus rufus* and *Lachnolaimus maximus*, but not for the cheilines or parrotfishes, indicating

the ancestral state of the CM to potentially be a more compliant tissue. The IOPM ligament has the strongest ecomorphological relationship and its function is to control the movement of the opercular linkage system.

Significance: This chapter expands on previous knowledge of mechanical properties of cranial ligaments in wrasses. We sought to understand how phylogeny and the ecological feeding guild (suction feeding vs. biting) affects the relationships between the ligament type and mechanical and structural properties. This chapter makes significant advances on tissue biomechanics in wrasses, increasing our understanding of the ways in which phylogenetic relatedness and ecomorphology affects the role of mechanical properties of the two main ligaments in the labrid skull.

Conclusion/Synthesis:

From this thesis emerges a better understanding of the three-dimensional morphometrics and modularity of linkage mechanisms in labrid fishes, and the evolution and function of cranial ligaments and their role in force transmission in one of the largest groups of marine fishes on coral reefs worldwide. This thesis seeks to comprehend the two roles the ligaments seem to play in the skull: restricting and constraining movement, while allowing for variability in cranial kinesis, leading to new functional abilities. Additionally, the macroevolutionary processes influencing the evolution of the skull in wrasse are better understood. First, the macroevolutionary processes that shape the skull and linkage systems in the cranium are elucidated to understand the influences of the linkage structures on the wrasse skull shape. Second, which of the cranial ligament properties influence the skull performance and mobility is uncovered using closely related species. Lastly, how the ligaments evolve across the labrid phylogeny and with feeding behavior is explored. The future implications of this thesis research

include the ability is to synthesize the ligament property data and with developing 3D computer models for the biomechanics of the teleost skull. Another goal of the integration of this data in 3D models is to produce more accurate predictions of fish skull movement to understand further biomechanical limitations to this complex and diverse system.

CHAPTER 2: EVOLUTIONARY PATTERNS OF MODULARITY IN THE LINKAGE SYSTEMS OF THE SKULL IN WRASSES AND PARROTFISHES.

ABSTRACT

The concept of modularity is fundamental for understanding the evolvability of morphological structures and is considered a central framework for the exploration of functionally and developmentally related subsets of anatomical traits. In this study, we explored evolutionary patterns of modularity and integration in the four-bar linkage biomechanical system of the skull in the fish family Labridae (wrasses and parrotfishes). We measured evolutionary modularity and rates of shape diversification of the skull partitions of three biomechanical four-bar linkage systems using 205 species of wrasses (Family: Labridae) and a three-dimensional geometric morphometrics data set of 200 coordinates. We found support for a two-module hypothesis on the family level that identifies the bones associated with the three linkages as being a module independent from a module formed by the remainder of the skull (neurocranium, nasals, premaxilla, pharyngeal jaws). We tested the patterns of skull modularity for four tribes in wrasses: hypsigenyines, julidines, cheilines and scarines. The hypsigenyine and julidine groups showed the same two-module hypothesis for Labridae, whereas cheilines supported a four-module hypothesis with the three linkages as independent modules relative to the remainder of the skull. Scarines showed increased modularization of skull elements where each bone is its own module. Diversification rates of modules show that linkage modules have evolved at a faster net rate of shape change than the remainder of the skull, with cheilines and scarines exhibiting the highest rate of evolutionary shape change. We developed a metric of linkage planarity and found the oral jaw linkage system to exhibit high planarity while the rest position of the hyoid linkage system exhibited increased three-dimensionality. This study shows a strong link between

phenotypic evolution and biomechanical systems, with modularity influencing rates of shape change in the evolution of the wrasse skull.

INTRODUCTION

Morphological and biomechanical traits often have varying levels of interrelationships with other such traits that can reflect their level of evolutionary independence or their tendency to coevolve as tightly associated units or modules (Wagner 1996). The variation in independence and arrangement between traits can be analyzed using the concepts of modularity and integration. Prior modularity research has often shown patterns of covariation to be unevenly distributed in a system, where some traits show higher correlation whereas others show higher independence (Cheverud 1982, 1995; Olson and Miller 1999; Albertson et al. 2005; Klingenberg 2008; Goswami and Polly 2010; Parsons et al. 2011, 2012; Goswami et al. 2019). These patterns of modularity can result in sets of semi-independent traits that can evolve at different evolutionary rates or respond to evolutionary or biomechanical forces differently, potentially leading to new functional or structural innovations (i.e., mosaic evolution). Identifying these patterns over a large phylogenetic sample can hint at the developmental, functional or environmental influences driving the evolution of a system (Cheverud 1982, 1995; Olson and Miller 1999; Klingenberg 2008; Larouche et al. 2018; Adams and Collyer 2019; Bardua et al. 2019; Churchill et al. 2019; Goswami et al. 2019). Modularity analyses applied to complex anatomical systems in a large and diverse group of species can reveal macroevolutionary patterns in a group and help understand the impacts of change in complex functional systems.

Fish feeding systems are among the most diverse morphological and kinetic structures in vertebrates. The teleost fish skull is a highly complex structure composed of multiple bony

elements connected by soft tissues that function in a diversity of ways to successfully feed on prey (Liem 1970; Anker 1974; Barel 1982; Lauder 1982; Muller 1989; Westneat 2006). The functional systems of the skull in most teleost fishes operate as biomechanical levers and linkages that control the movements of bones and co-evolve with the morphological structures. The three major four-bar linkage systems in the perciform skull are the anterior jaws linkage, the opercular linkage, and the hyoid linkage (Westneat, 1990). These linkages have been modeled as a four-bar linkage system using mechanical engineering principles (Anker 1974; Muller 1989; Westneat 1990; Olsen and Westneat 2016), where the movement of three mobile links connected by rotating joints have computationally defined motions relative to a fourth fixed link (Fig. 2.1).

The linked nature of these mechanical systems suggests the hypothesis that each linkage may be tightly integrated, and that the three linkages may show a high level of integration with one another. Alternatively, it has been shown that there is a frequent phylogenetic divergence among close relatives in these systems, leading to a broader pattern of convergence across groups (Westneat et al. 2005), suggesting the alternative hypothesis that functional diversity may be driven by independent evolution of linkage systems.

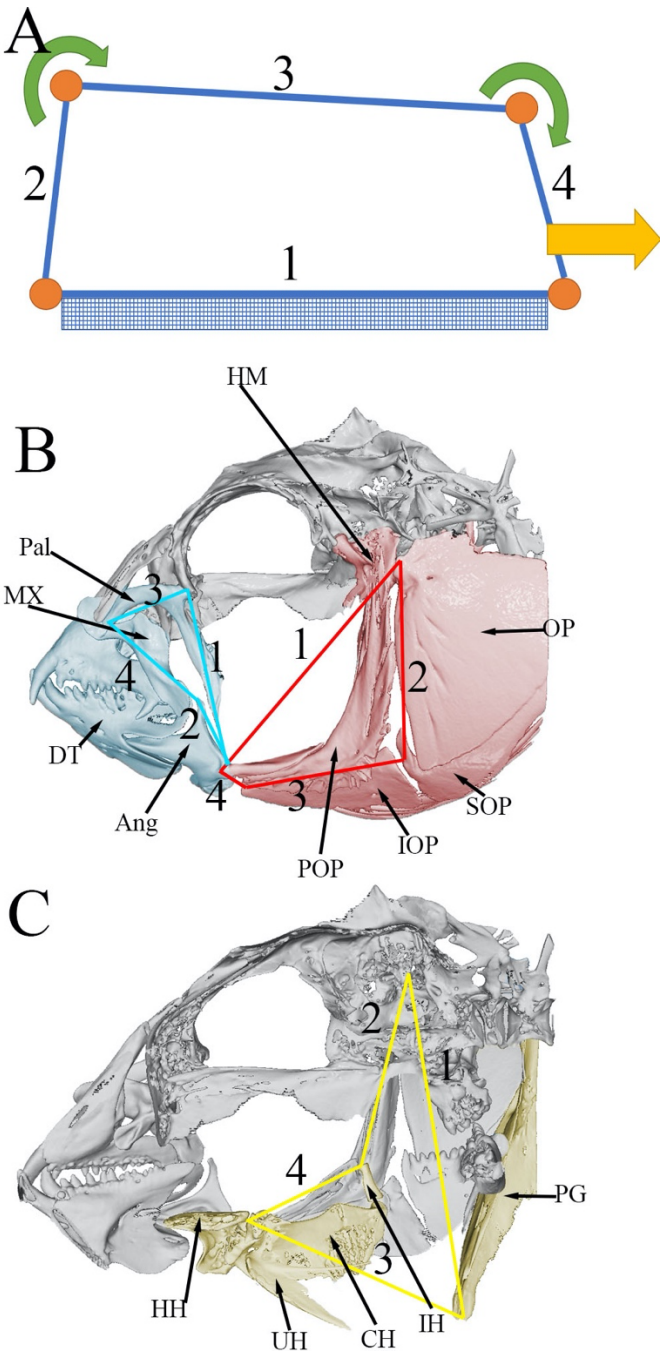

Figure 2.1: A) Basic schematic of the four-bar linkage. 1 represents the fixed link, 2 input link, 3, coupler link, 4 output link. These letterings correspond to B) and C). B) Lateral view of *Halichoeres argus* with the anterior jaw (blue) linkage with the associated bones highlighted in blue and opercular (red) linkage with the associated bones highlighted in red. C) lateral view of the inside of *H. argus* with the hyoid (yellow) linkage with the bones involved with the linkage system highlighted in yellow. Abbreviations: Pal – palatine; PX—premaxilla; DT—dentary; Ang—angular; POP—preoperculum; OP—operculum; SOP—suboperculum; IOP—interoperculum; IH—interhyal; PG—pectoral girdle; CH—ceratohyal; UH—urohyal; HH—hypohyal; HM—hyomandibula.

Teleost skulls have been the subject of multiple modularity studies (Evans et al. 2017, 2019, 2022; Ornelas-García et al. 2017; Baumgart and Anderson 2018; Larouche et al. 2018, 2022). Recent work in the labrid fishes (Larouche et al. 2022) found functional hypotheses compared to developmental hypotheses to be more strongly supported in a modularity analysis of the skull. This work also found that the best-fitting functional hypotheses exhibited patterns in which traits with similar functions (i.e., the oral jaws and pharyngeal jaws) were more tightly integrated than traits that share developmental origins (i.e., maxilla and premaxilla). Recent studies have revealed patterns of modularity based on developmental and functional systems in the teleost skull, yet a central question remaining is the degree to which the biomechanical linkage systems of the skull are tightly integrated as modules. The linkage systems all share a similar function in that they help to move the skull during different behaviors (i.e., feeding, breathing, social communication, etc.). Mainly, the anterior jaws linkage system functions to move the oral jaws, the opercular linkage system moves the opercular series and the lower jaw, and the hyoid linkage system moves the hyoid apparatus and the lower jaw (Fig. 2.1). This leads to the question of does having a shared function lead to higher covariation among traits? Are the 4-bar linkage systems modular at an evolutionary level? In other words, do the skulls parse out into modules described by the 4-bar linkage systems across lineages. Here, we further investigate the functional trends that govern the modularity and integration of the fish skull, testing the level of integration in and among the modules defined by the biomechanical four-bar linkages of the teleost skull. We try to further understand whether covariation of bone shape is a signal of the functional modularity of the linkage systems (e.g., whether the linkage systems are functionally transforming together).

Wrasses and parrotfishes (Family: Labridae) are a group of coral reef fishes with a wide diversity in skull shape and have a well-resolved phylogeny (Aiello et al. 2017; Larouche et al.

2022). This group of fishes represents the second largest marine fish family and has been shown to have a wide diversity in skull shape and function, with the amount of diversity in each tribe showing divergence in lever and linkage mechanisms (Wainwright et al. 2004; Westneat et al. 2005). These findings provide an opportunity to investigate the family-wide and tribe-specific evolutionary influences on the skull and associated skeletal elements. Using this diversity, we seek to quantify the relationship between the four-bar linkage systems and skull morphology over evolutionary time. Thus, the main objectives of this study were to investigate the modularity patterns seen across wrasse linkage systems and in four main wrasse tribes, (hypsigenyines, julidines, cheilines, and scarines) and to test whether the best-fitting hypotheses of modularity led to differences in phylogenetic rates of linkage diversification. In addition, because four-bar linkages are typically modeled as planar transmission systems, we set out to quantify the three-dimensionality of the linkage systems by developing a metric of linkage planarity to understand if modularity is affected by the relative planarity versus three-dimensionality of these mechanical systems.

METHODS

Phylogeny

To provide a framework for modularity testing, we used a recently published phylogenetic analysis of 410 species of labrid fishes (Larouche et al. 2022) (Fig. 2.2). This tree provides an updated topology and time-tree branch lengths for the family, used in our prior work to explore the tempo and mode of skull modules. The phylogeny was built as a subset of a larger in-progress study of 550 species using a set of 12 genes, both mitochondrial and nuclear, accumulated by a series of recent studies (Westneat and Alfaro 2005; Smith et al. 2008; Aiello et

al. 2017) and analyzed in BEAST using the same fossil calibration framework as the recent phylogenomic analysis of the Labridae (Hughes et al. 2022). The resulting time-calibrated Bayesian inference tree was then pruned down to the 205 taxa for which we collected morphometric data using the *drop.tip* function in the R-package *ape* (Paradis et al. 2004).

Geometric morphometrics

We quantified three-dimensional (3D) skull shape across 205 labrid species using micro-computed tomography (μCT) scans (previously detailed in Larouche et al. 2022 and Evans et al. 2022). We scanned one individual for each species. Specimens scanned were all adults and free of any sex-specific morphologies (e.g., the hump on the male Napoleon wrasse). Specimens were selected in an appropriate size range for scanning and with jaws closed when available. The specimens were primarily from the ichthyology collection from the Field Museum of Natural History (FMNH), Chicago, IL. Additional specimens came from the Academy of Natural Sciences of Drexel University (ANSP), the American Museum of Natural History (AMNH), the

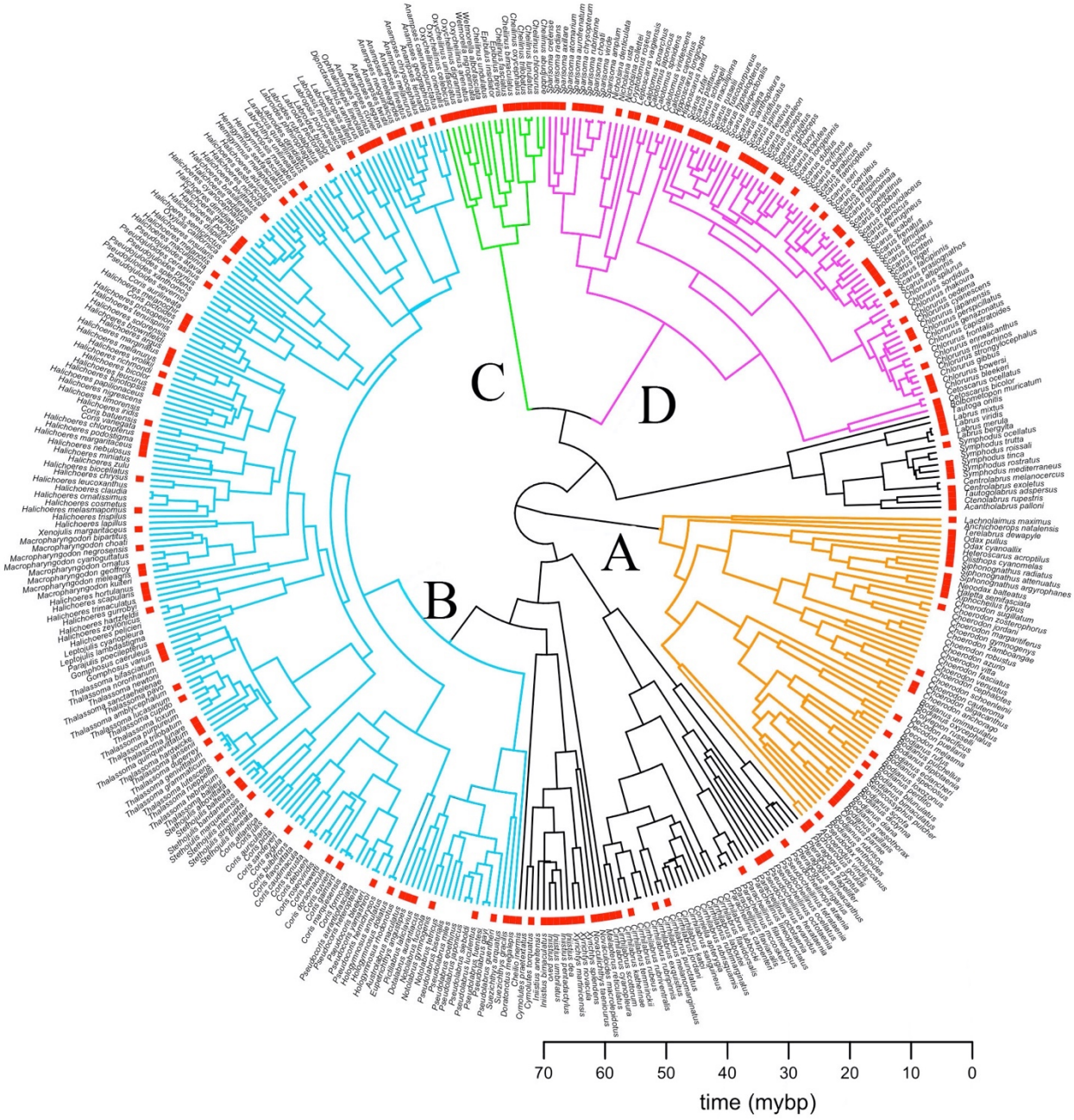

Figure 2.2: Time calibrated tree of the Labridae (410 species) from Larouche et al. 2022 with red bars indicating presence of the 205 wrasse species in our data set while red arrows point to the tribes we analyzed further in the modularity study: A) hypsigenyines highlighted in orange, B) julidines highlighted in blue, C) cheilines highlighted in green, and D) scarines highlighted in pink. A scale bar is provided on the bottom right in million years per before present (mybp).

Australian Museum (AM), the Bell Museum of Natural History (JFBM), the Bernice Pauahi Bishop Museum (BPBM), the Burke Museum of Natural History and Culture (UWFC), the National Museum of Natural History (USNM), and the Natural History Museum (BMNH) (Appendix A Table 1). Specimens were scanned at the University of Chicago, University of Minnesota, and University of Washington, Friday Harbor Laboratory as a part of the scanAllFishes and oVert initiatives.

Scans were segmented in Amira v. 2.0.0 (Thermo Fisher Scientific, Waltham, MA) to isolate the skull and remove scales and debris. We followed the landmarking methods described in Larouche et al. (2022). However, we added three landmarks that describe points along the pectoral girdle (Appendix A Table 2). Briefly, the isolated skulls were converted into 3D meshes and imported into Checkpoint (Stratovan, Davis, CA). Shape variation was described by 200 3D points: 83 landmarks and 117 semi-landmarks (Appendix B Fig. 2.1) that adequately sampled the pharyngeal jaws, oral jaws, neurocranium, nasals, hyomandibula, operculum, hyoid apparatus, and pectoral girdle (Appendix Table 2 for descriptions of each landmark). Points were solely placed on the left side of the skull.

Due to our interest on the linkage systems, and their essential reliance on positioning, we used a General Procrustes Analysis (GPA) (Fig. 2.2) of the entire composition where the landmark configurations are first centered at their origin (i.e., the centroid), then scaled to unit centroid size, and finally, they are optimally rotated using an iterative process to minimize the summed squared distances between homologous landmarks (Rohlf and Slice 1990; Zelditch et al. 2012). For the semi-landmarks, the positions were optimized using the criterion of minimizing the Procrustes chord-distance between the reference and target specimens. We chose this method

due to the alternative criterion of minimum bending energy being shown to potentially introduce spurious spatial autocorrelations among sliding semi-landmarks (Cardini et al. 2019).

Phylomorphospace

To explore the phylogenetic patterns of 3D skull morphometrics, and to identify regions of interest, we used a phylomorphospace approach (Sidlauskas 2008). Principal components analysis (PCA) was used as an exploratory method to describe major axes of variation in the skull of the Labridae. Major axes of shape variation were visualized by plotting shape changes between the species with the most extreme scores along each PC axis that captured the most shape variation. We visualized the phylomorphospace using R (RStudio 2012) in the package *phytools* using the function *phylomorphospace* (Revell 2012). We plotted the entire Labridae family (Fig. 2.3) as well as the tribes of interest (Fig. 2.4) to visualize the geometric patterns of change along the phylogeny in and across tribes.

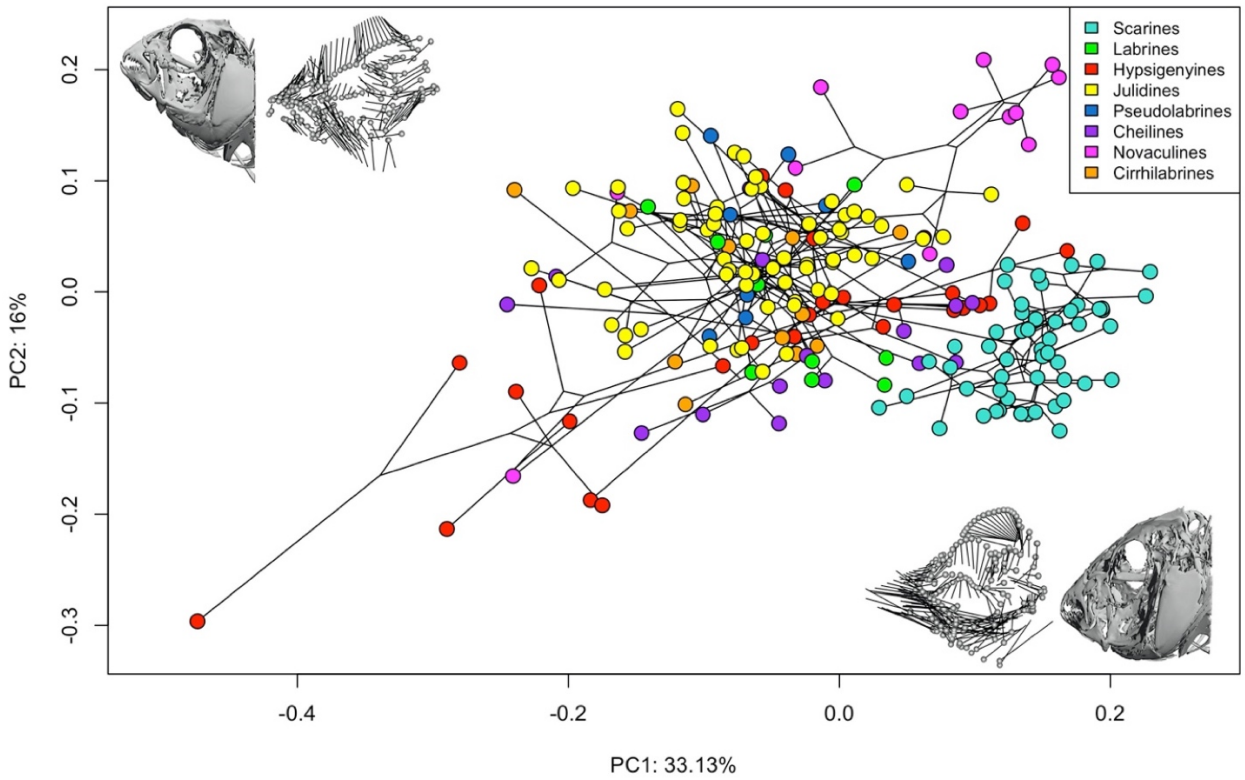

Figure 2.3: Phylomorphospace with the first two PCs from a principal components analysis of 205 wrasse specimens. 3D mesh insets illustrate changes in landmark positions between the species with the minimum and maximum values along both axes. Ball-and-stick insets illustrate changes in landmark positions between the species with the mean (grey dots) and highest (tips of vectors) along both axes.

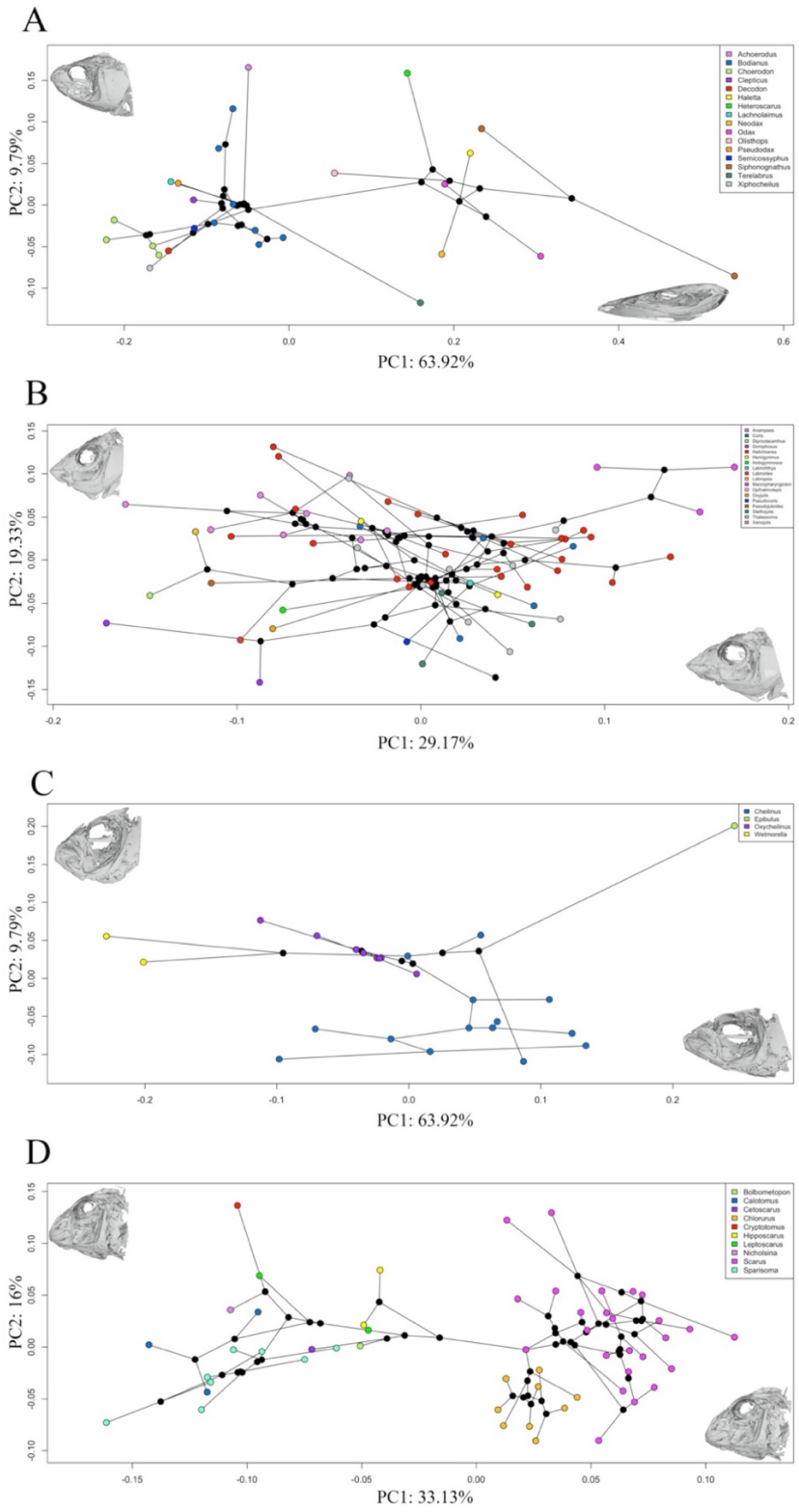

Figure 2. 4: Phylomorphospaces of four Labrid tribes: A) Hypsigenyines, B) Julidines, C) Cheilines, D) Scarines. 3D mesh insets illustrate changes in landmark positions between the species with the lowest and highest variation along both axes.

Modularity Tests

Thirteen modularity hypotheses were created and tested, determined by the bones directly connected in the four-bar linkage systems (Table 2.1).

Table 2. 1: Description of all thirteen hypotheses tested with the number of modules each hypothesis is testing. Parentheses designate separate modules, plus signs represent separate modules, * represents covariation between modules.

Hypothesis	Description of Modules	Number of Modules
H1	Premaxilla + maxilla + dentary + articular + neurocranium + nasals + upper pharyngeal jaw + lower pharyngeal jaw + ceratohyal + urohyal + hyomandibula + opercular series + palatine + pectoral girdle + hypohyal + suspensorium	14
H2	(Angular * dentary * ceratohyal * opercular series * palatine * maxilla * suspensorium * pectoral girdle * hypohyal * urohyal * hyomandibula * premaxilla) + (nasals * neurocranium * upper pharyngeal jaw * lower pharyngeal jaw)	2
H3	(Angular * dentary * ceratohyal * opercular series * palatine * maxilla * suspensorium * pectoral girdle * hypohyal * urohyal * hyomandibula) + (premaxilla * nasals * neurocranium * upper pharyngeal jaw * lower pharyngeal jaw)	2
H4	(angular * dentary * palatine * maxilla * premaxilla) + (ceratohyal * hypohyal * urohyal * pectoral girdle) + (opercular series * suspensorium * hyomandibula) + (nasals * neurocranium * upper pharyngeal jaws * lower pharyngeal jaws)	4
H5	(angular * dentary * palatine * maxilla) + (ceratohyal * hypohyal * urohyal * pectoral girdle) + (opercular series * suspensorium * hyomandibula) + (premaxilla * nasals * neurocranium * upper pharyngeal jaws * lower pharyngeal jaws)	4
H6	(Angular * dentary * ceratohyal * opercular series * palatine * maxilla * suspensorium * pectoral girdle * hypohyal * urohyal * hyomandibula * premaxilla) + nasals + neurocranium + upper pharyngeal jaw + lower pharyngeal jaw)	4
H7	(Angular * dentary * ceratohyal * opercular series * palatine * maxilla * suspensorium * pectoral girdle * hypohyal * urohyal * hyomandibula) + premaxilla + nasals + neurocranium + upper pharyngeal jaw + lower pharyngeal jaw	5
H8	(angular * dentary * palatine * maxilla * premaxilla) + (ceratohyal * hypohyal * urohyal * pectoral girdle) + (opercular series * suspensorium * hyomandibula) + nasals + neurocranium + upper pharyngeal jaws + lower pharyngeal jaws	7

Table 2.1, continued

H9	(angular * dentary * palatine * maxilla) + (ceratohyal * hypohyal * urohyal * pectoral girdle) + (opercular series * suspensorium * hyomandibula) + premaxilla + nasals + neurocranium + upper pharyngeal jaws + lower pharyngeal jaws	8
H10	(Angular * dentary * ceratohyal * opercular series * palatine * maxilla * suspensorium * pectoral girdle * hypohyal * urohyal * hyomandibula * premaxilla) + (nasals * neurocranium) + (upper pharyngeal jaw * lower pharyngeal jaw)	3
H11	(Angular * dentary * ceratohyal * opercular series * palatine * maxilla * suspensorium * pectoral girdle * hypohyal * urohyal * hyomandibula) + premaxilla + (nasals * neurocranium) + (upper pharyngeal jaw * lower pharyngeal jaw)	4
H12	(angular * dentary * palatine * maxilla * premaxilla) + (ceratohyal * hypohyal * urohyal * pectoral girdle) + (opercular series * suspensorium * hyomandibula) + (nasals * neurocranium) + (upper pharyngeal jaws * lower pharyngeal jaws)	5
H13	(angular * dentary * palatine * maxilla) + (ceratohyal * hypohyal * urohyal * pectoral girdle) + (opercular series * suspensorium * hyomandibula) + premaxilla + (nasals * neurocranium) * (upper pharyngeal jaws * lower pharyngeal jaws)	6

We tested whether the linkage systems were three separate modules due to them affecting different parts of the skull, or one module due to having a shared function of skull movement for the entire family Labridae. The linkages were separated by the bones they interact with the most with the anterior jaw system including the maxilla, premaxilla, dentary, angular, and palatine, the opercular system included the opercular series, suspensorium, and hyomandibula, and the hyoid system included the hypohyal, ceratohyal, urohyal, and pectoral girdle. The first hypothesis was a control which treated each bone as a separate module to test if there is a pattern of modularity and integration in the system. Half of the hypotheses treat the premaxilla as a part of the anterior jaw linkage system while the other half of the hypotheses treat the premaxilla as a separate module from the linkage system due to the premaxilla not being directly associated with the links, despite its motion being directly attributed to the anterior jaw linkage system. The hypotheses also varied in how many modules remained after the linkage systems were placed in

modules (See Table 2.1 for details). We recognize that the opercular four-bar linkage system has a point on the lower jaw, however, because the lower jaw is more influenced by the anterior jaw four-bar linkage, we included the lower jaw in the anterior jaw linkage module only.

To test patterns of modularity in the tribes, we repeated our analyses of modularity in four tribes that had a large enough sample size of species. The tribes included were hypsigenyines (hogfishes, tuskfishes, and relatives), julidines (crown tribe of many genera), cheilines (maori wrasses), and scarines (parrotfishes).

Hypotheses of evolutionary modularity were compared using the effect size of the covariance ratio (CR), one of the most widely used methods to analyze modularity. The CR is a measure of the relative strengths of associations among partitions of landmarks versus associations in these subsets (Adams and Collyer 2019). CRs were computed with the function *phylo.modularity* , and the effect sizes were compared using the *compare.CR* function, both functions are implemented in the R package *geomorph* (Adams et al. 2022).

We also analyzed the modularity hypotheses using the distance matrix method, which produces a correlation matrix between the shape partitions of landmark subsets by calculating pairwise Procrustes distances between each specimen for each shape partitions, and then computing matrix correlations between the pairwise distance matrices (Monteiro et al. 2005). The resulting correlation matrices were analyzed and visualized using graphical modeling. Graphical modeling uses the assumption of conditional independence between the partitions of shape and the hypotheses can be ranked using the Deviance Information Criterion (DIC). Correlation matrices were produced using a Rscript developed by Adam Roundtree [available as supplementary material from Zelditch et al. 2012] and edited for its application with three-dimensional landmark data and controlling for phylogeny (Larouche et al. 2022; available on

Dryad). Graphical modeling was performed using the function *fitConGraph* from the R package *ggm* (Marchetti 2006).

The best-supported modularity hypothesis may differ between the covariance ratio method and the distance matrix approach. These methods use different metrics and test modularity in conceptually different ways. The covariance method uses the relative strengths of association in modules versus across modules and shows the pattern of integration across partitions of shape. Here, we defined the best-fitting hypothesis for the CR ratio as the lowest effect size. The distance matrix approach takes conditional independence into consideration and emphasizes aspects of modularity that are quasi-independent (i.e., consequential for evolvability). We defined the best-fitting hypothesis as the one with the lowest deviance information criterion (DIC) score. Together, these methods can help elucidate broad scale modularity patterns by looking at the commonalities between the results.

Evolutionary Rates Analyses

We used the rate ratio method (Denton and Adams 2015) to investigate whether the best-fitting modularity hypothesis for each tribe was paralleled by differences in phenotypic rates across modules. We ran these analyses on the best fitting hypotheses from the two modularity analyses described above. The rate ratio method assumes a Brownian motion (BM) evolutionary model for each module, estimates per-module rates, and then calculates a ratio between the highest and lowest of these rates. These rate comparisons use the function *compare.evol.rates* for group-wise (i.e., across tribes) comparisons of the same landmark configurations, and *compare.multi.evol.*rates for comparisons among subsets of landmarks belonging to these configurations, both implemented in the R package *geomorph* (Adams et al. 2022). We recognize

that some of the modules may not evolve in BM, however, at this time there is no method we can use to overcome this assumption. But recent analyses suggests the trends of the results are minimally influenced even if some partitions are not evolving under BM (Larouche et al. 2022).

Linkage Planarity Metrics

To test the idea that linkage modularity may vary with the three-dimensionality of linkage structure, we developed a metric of linkage planarity. Computational four-bar linkage mechanics typically assumes that linkages are planar, with deviations from planarity resulting in some models being rejected as appropriate constructs for function, highlighting the need for three-dimensional modeling (Westneat 1994, Olsen and Westneat 2016). The three-dimensional coordinates of each four-bar linkage were used to develop a metric of planarity to assess the degree to which the four rotational joints were positioned in the same plane in their rest positions. The fixed link (involving two joints) plus one mobile joint was aligned in the XY plane (with Z at zero), with the fourth joint retaining its Z axis value, and the 3D area of the linkage was computed. Then the fourth joint was projected onto the XY plane, and the projected planar area recalculated. 3D area was always greater than projected area, so the ratio of projected area to 3D area was used as a metric (ranging from 0 to 1.0) of the planarity of each of the three linkages across all 205 specimens.

RESULTS

The main results from our study are 1) the general pattern of modularity across the family Labridae is the three linkage systems are highly integrated with each other, but are separate modules from the neurocranium, nasals, premaxilla, and pharyngeal jaws; 2) linkage systems are

conditionally independent in scarines and cheilines and evolve at faster diversification rates than in hypsigenyines and julidines; 3) the module containing all three linkage systems evolved faster than the remainder of the skull and 4) the planarity of the linkages in their rest position is high in the anterior jaws linkage and opercular linkage, but lower in the hyoid linkage.

Phylomorphospace

We constructed multiple phylomorphospaces based on the shape data from the whole skull and for each individual tribe. For the whole skull phylomorphospace, PC1 explains the variation in rostral-caudal length (36.61% of the variation) of the skull. In addition, PC1 captures variation in urohyal length and positioning of the pectoral girdle (Fig. 2.3). PC2 explains the variation in dorsal-ventral length (15.26% of the variation) across the skull shapes. Additionally, PC2 captures variation in the supraoccipital crest and positioning of the pharyngeal jaws (Fig. 2.3). These two axes explain over half (51.87%) of the variation in wrasses.

Hypsigenyines' first two axes of the phylomorphospace explain over half the variation in this tribe (67.18%). PC1 explains changes in rostral-caudal length as well as changes in the orbit which accounts for 55.64% of the variation in this clade (Fig. 2.4). There is a strong stratified pattern along PC1 that is dominated by the species, *Siphonognathus argyrophanes.* This species is an outlier among all wrasses and is characterized by an elongated skull with long premaxilla and dentary bones. PC2 captures 11.54% of the variation and describes changes in dorso-ventral length and in urohyal length. Additionally, changes to the dorsal-ventral positioning of the hyoid apparatus, specifically the ceratohyal, are captured by PC2 (Fig. 2.4), indicating PC2 captures the changes in the hyoid linkage system as well.

The julidine phylomorphospace shows PC1 containing 28.42% of shape change relating to the posterior region of the skull. More specifically PC1 captures changes in shape of the operculum and pectoral girdle (Fig. 2.4). PC1 also captures the frontal-caudal length changes to the hyoid apparatus. PC1 therefore is capturing changes to the opercular and hyoid linkage systems. On the other hand, PC2 captures 16.30% of variation and is dominated by variations in premaxilla, supraoccipital, and urohyal morphologies, indicating PC2 captures some changes to the anterior jaw linkage system. Interestingly, there were no genera related groupings in this tribe.

The cheiline phylomorphospace exhibits a PC1 and PC2 that capture a majority of variation in this tribe's skull (56.78%; Fig. 2.4). PC1 captures 39.28% variation while PC2 captures 17.50%. The variation in PC1 is related to length changes in the lower jaw and urohyal while PC2 captures variation in dorsal-ventral length. PC1 additionally, captures rostral-caudal displacement of the nasals. Therefore, PC1 captures changes to the anterior jaw and hyoid linkage system while PC2 captures changes in the opercular linkage system on the dorsal-ventral axis. *Oxycheilinus* mainly varies along PC1 while *Cheilinus* has most of its variation along PC2.

For the scarine phylomorphospace, shape change is captured by the primary axis of variation (PC1) which contains 26.46% of the overall variation and is dominated by changes in premaxilla angle and length and rostro-caudal length (Fig. 2.4). PC1 also mainly captures the placement of the lower pharyngeal jaw. In contrast, the next largest shape axis (PC2) contains 12.67% of the overall variation and explains differences in toothed versus beaked species. This indicates both PC1 and PC2 captures changes to the anterior jaw linkage system. Additionally, PC2 captures dorsal-ventral variation, mainly with the hyoid linkage system. Several of the remaining axes of variation are related to the hyoid apparatus, pectoral girdle, and other aspects

of the skull. About four PCs describe half the variation in scarines. We additionally see a stratified pattern along PC1 between the beaked and non-beaked parrotfish (Fig. 2.4).

Modularity Tests

Modularity analysis across the entire family Labridae supports several of the hypotheses of modularity. The CR ratio test supports hypothesis 3, showing integration between all the linkages and placing the premaxilla in the remainder of the skull module (i.e., nasals, neurocranium, premaxilla and pharyngeal jaws; Appendix A Table 3). Graphical modeling supports hypothesis 2 in both tests (Appendix A Table 4), which indicates that the premaxilla is integrated with the linkages. The support for these hypotheses indicates integration of the three linkages with one another is the main pattern of modularity throughout wrasses. Furthermore, these linkages are decoupled from the remainder of the skull, including the upper and lower pharyngeal jaws (Fig. 2.5).

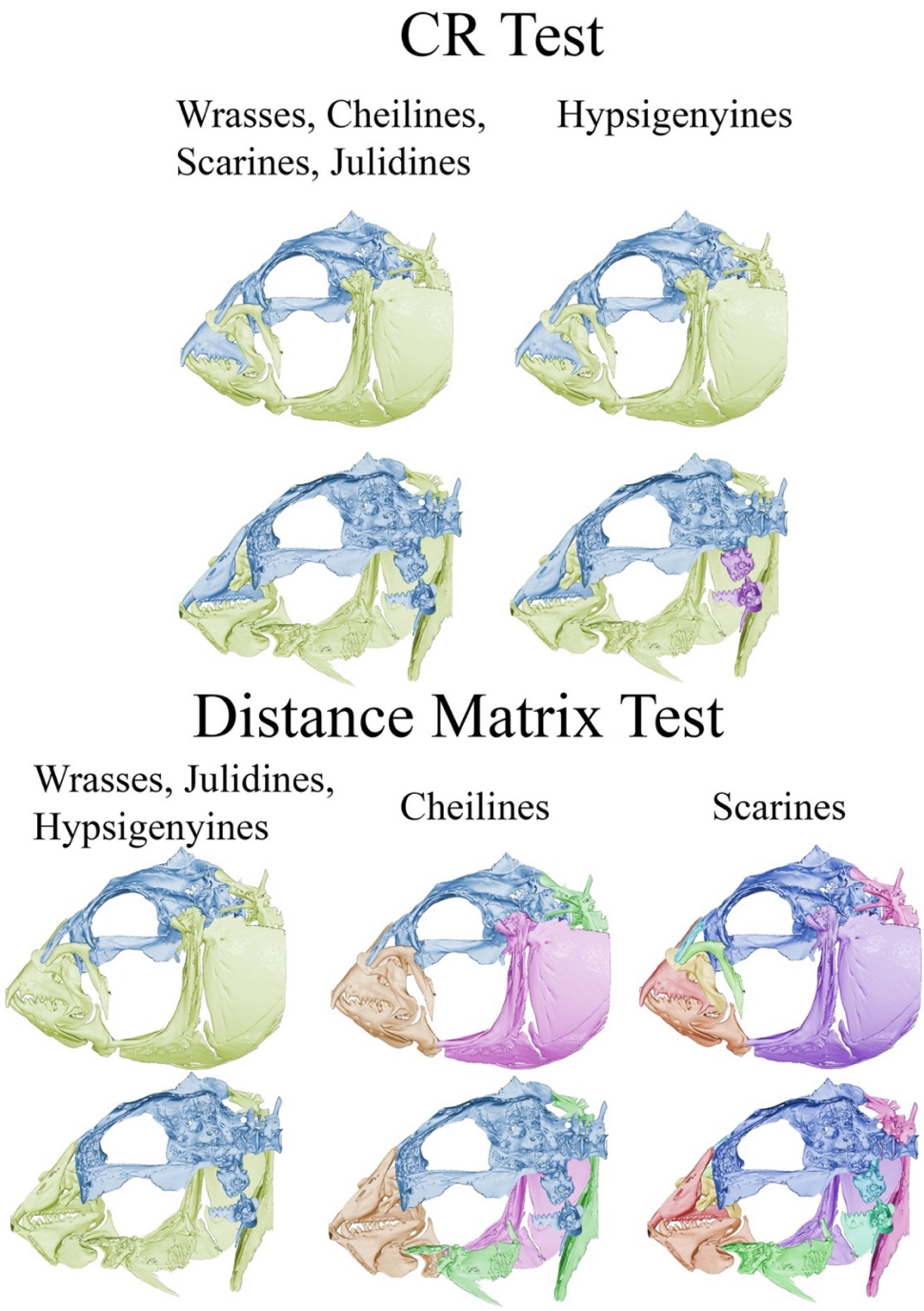

Figure 2. 5: Modularity results represented on Halichoeres argus from the covariance ratio and distance matrix method modularity tests. Each color represents a different module where green is the three linkage module, blue is the remainder of the bones (neurocranium, nasals, pharyngeal jaws, premaxilla). In the CR test results, Wrasses, Cheilines, Scarines and Julidines are being represented by hypothesis 3 while Hypsigenyines are representing hypothesis 10. In the Distance Matrix test, Wrasses, Julidines, and Hypsigenyines are representing hypothesis 2, Cheilines are representing hypothesis 8, and Scarines are representing hypothesis 1. All these hypotheses were the best supported in the corresponding tests.

Table 2. 2: Modularity hypothesis support for the CR and GM methods.

Tribe	Test	hypothesis supported	p-value	effect size	DIC score
Hypsigenyines	CR	10	0.001	-10.54	N/a
	GM	3	N/a	N/a	-37.652346
	GM	5	N/a	N/a	-76.026436
Julidines	CR	2	0.001	-20.000761	N/a
	GM	2	N/a	N/a	2.45716529
	GM	4	N/a	N/a	-19.694909
Cheilines	CR	2	0.001	-17.36	N/a
	GM	8	N/a	N/a	-80.949597
	GM	9	N/a	N/a	-126.36137
Scarines	CR	3	0.001	-10.52	N/a
	GM	12	N/a	N/a	-96.073491
	GM	1	N/a	N/a	-183.58255

Analysis of the hypsigenyines supported three hypotheses of modularity (Table 2.2). The CR test supports hypothesis 10 (Appendix A Table 5), a three-module hypothesis with all the linkages integrated into one module, with the nasals and neurocranium making a second and the pharyngeal jaws making a third module. The graphical modeling supported hypotheses 3 and 5 (Appendix A Table 6). Hypothesis 3 is a two-module hypothesis and partitions the data into the linkage bones (e.g., the bones that compose the four-bar linkage systems) and the remainder of the skull. This hypothesis is supported by the graphical modeling test that preserves relative positions and sizes in the data. Hypothesis 5 is a four-module hypothesis in which the three linkages compose three modules with the premaxilla, and the remainder of the bones are in the 4th module. This hypothesis is supported by the graphical modeling test that only considers variation in shapes of landmark positions. We reran our analyses without the outlier *Siphonognathus argyrophanes* and found similar results in that the hypotheses supported grouped the linkages together as one module. These hypotheses indicate that in hypsigenyines

the linkages are integrated in all variables except shape where the linkages are more modular. This indicates the bones involved with each linkage are able to vary in shape but are linked to each other in position and size.

The julidine data supports two modularity hypotheses. The CR test supports hypothesis 2 (Appendix A Table 7) while graphical modeling supports hypotheses 2 and 4 (Table 2.2; Appendix A Table 8). Hypothesis 2 has two distinct modules with the premaxilla being treated as a part of the linkage systems. Hypothesis 4 has four distinct modules and splits the linkage systems into three with the remainder of the bones, including the premaxilla, as the fourth module. The GM method that emphasizes shape variation supports hypothesis 4 (Supplementary Table 2.8), suggesting strong covariation in shape *in* linkage systems, whereas covariation in position and size is predominant *between* the linkage systems. Julidines have a similar pattern to the hypsigenyines in that the bones involved in linkages are able to vary in shape more independently but are linked in all other variables.

Cheilines support three hypotheses of modularity: hypotheses 2, 8, and 9 (Table 2.2). The CR test supports hypothesis 2 (Appendix A Table 9) while GM supports hypotheses 8 and 9 (Appendix A Table 10). Hypothesis 2 is a two-module hypothesis with the premaxilla being treated as a part of the linkage module. Hypotheses 8 and 9 both demarcate the linkage systems as their own modules. These two hypotheses indicate the linkages are conditionally independent when position and shape are considered. However, there is still strong covariation across the linkages compared to the bones not involved in the linkages based on the CR test supporting hypothesis 2. We reran our analyses without the outlier, *Epibulus insidiator,* and found similar results that splits the linkages into three different modules. The support for these three

hypotheses indicates cheilines deviate from the pattern of modularity at the family level. Cheilines' linkages have become more modular and more independent from each other.

Finally, the scarine data support three modularity hypotheses (Table 2.2). The CR test supports hypothesis 3 (Appendix A Table 11). This hypothesis has the three linkages covarying but independent from the remainder of the skull with the premaxilla. The graphical modeling method supports hypotheses 1 and 12 (Appendix A Table 12). Hypothesis 1 separates each bone into its own module whereas in hypothesis 12 there are five modules with each linkage system being a separate module, alongside a fourth module including the neurocranium and nasals and a fifth module including the pharyngeal jaws. This indicates that there may be increased modularization across scarines due to the majority of the tests supporting hypotheses that treat the linkages as separate modules and the remainder of the skull parsing into two more additional modules.

Evolutionary Rates of Change in Skull Shape

We calculated the net rate of shape evolution for the whole skull and across all labrid tribes. Additionally, we computed the rate of shape evolution for each four-bar linkage system across Labridae, represented as the bones connected in the linkage system. The cheilines have the highest rate of evolution for every shape tested (Table 2.3).

Table 2. 3: Comparison of the whole skull and three linkage systems across the four tribes analyzed.

Tribe	Structure	Evolutionary Rate
Cheilines	Whole Skull	9.85 E -05
Hypsigenyines	Whole Skull	2.69 E -06
Julidines	Whole Skull	3.32 E -06
Scarines	Whole Skull	4.13 E -06
Cheilines	Anterior Linkage	6.45 E -05
Hypsigenyines	Anterior Linkage	2.69 E -06
Julidines	Anterior Linkage	2.44 E -06
Scarines	Anterior Linkage	3.03 E -06
Cheilines	Opercular Linkage	6.47 E -05
Hypsigenyines	Opercular Linkage	1.88 E -06
Julidines	Opercular Linkage	2.09 E -06
Scarines	Opercular Linkage	2.54 E -06
Cheilines	Hyoid Linkage	3.31 E -04
Hypsigenyines	Hyoid Linkage	4.25 E -06
Julidines	Hyoid Linkage	7.41 E -06
Scarines	Hyoid Linkage	7.94 E -06

We additionally calculated the shape change for the bones associated with the linkages. We found a trend in which the hyoid module is the fastest evolving system, followed by the anterior jaws module, opercular module, and the neurocranium module (Table 2.4).

Table 2. 4: Evolutionary rates for shape across all 205 species. Remainder of the skull includes the neurocranium, nasals, premaxilla, and pharyngeal jaws.

Structure	Evolutionary Rate
Anterior Jaw Linkage	1.12E-05
Opercular Linkage	9.70E-06
Hyoid Linkage	4.06E-05
Remainder of the skull	8.87E-06
Linkage module	2.01E-05

Additionally, the linkages having a higher rate of evolution than the remainder of the bones, held true when rates were estimated and compared between a linkage module (i.e., all linkages are included in a single module) and a second module comprising the remainder of the bones (Table 2.4).

We analyzed the four tribes independently and found that the hypsigenyine and julidine pattern of modularity supports integration between linkages. The evolutionary rates of the overall hypsigenyine and julidine trend are the linkage module evolves at a faster rate than the neurocranium (Table 2.5).

Cheilines show a pattern of modularity in which the three linkage systems are independent modules. The net change of shape for the bones associated with the anterior linkage system was the lowest followed by the opercular and hyoid linkage systems. The upper pharyngeal jaw has diversification rate that is higher than the lower pharyngeal jaws (Table 5). Scarines show a pattern of modularity that indicates each bone to be its own module. The net shape diversification rates of each bone from lowest to highest rate were nasals, hyomandibula, premaxilla, dentary, maxilla, neurocranium, articular, operculum, palatine, pectoral girdle, upper pharyngeal jaws, lower pharyngeal, ceratohyal, urohyal. Overall, in the intra-tribe analyses the bones associated with the linkages are mostly evolving at faster rates compared to the remainder of the bones in the skull.

Table 2. 5: Evolutionary rates of shape for the modularity hypotheses supported by graphical modeling and covariance ratio.

Tribe	Modularity Hypothesis	Module	Evolutionary Rate
Hypsigenyines	3	linkage	3.23E-06
		remainder of skull	2.24E-06
	5	anterior jaw	3.17E-06
		opercular	1.75E-06
		hyoid	4.24E-06
		remainder of skull	2.23E-06
	10	linkage	2.99E-06
		neurocranium and nasals	2.28E-06
		pharyngeal jaws	2.22E-06
Scarines	1	palatine	4.81E-06
		premaxilla	2.64E-06
		dentary	2.83E-06
		articular	3.79E-06
		nasal	1.44E-06
		neurocranium	3.31E-06
		lower pharyngeal jaw	5.78E-06
		upper pharyngeal jaw	4.97E-06
		maxilla	2.85E-06
		hyomandibula	1.91E-06
		urohyal	1.05E-05
		ceratohyal	6.42E-06
		operculum	4.38E-06
		pectoral girdle	4.95E-06
	12	anterior jaw	3.02E-06
		opercular	7.89E-06
		hyoid	2.47E-06
		pharyngeal jaws	5.56E-06
		neurocranium and nasals	3.01E-06
	3	linkage	4.93E-06
		remainder of skull	3.44E-06
Julidines	2	linkage	3.88E-06
		remainder of skull	2.55E-06

Table 2.5, continued

	4	anterior jaw	2.44E-06
		opercular	1.90E-06
		hyoid	7.41E-06
		remainder of skull	2.55E-06
Cheilines	8	anterior jaw	6.44E-05
		hyoid	0.000331381
		opercular	4.55E-05
		upper pharyngeal jaw	3.38E-05
		lower pharyngeal jaw	3.34E-05
		nasal	1.23E-05
		neurocranium	4.20E-05
	9	anterior jaw	9.64E-05
		hyoid	0.000331381
		opercular	4.55E-05
		upper pharyngeal jaw	3.38E-05
		lower pharyngeal jaw	3.34E-05
		nasal	1.23E-05
		neurocranium	4.20E-05
		premaxilla	2.77E-05
	3	linkage	0.000177413
		remainder of skull	3.40E-05

Linkage Planarity

The anterior jaws linkage and opercular linkage were highly planar in their rest positions, with a mean planarity value of about 0.9 for both systems, and often ranging up to 1.0, indicating that the four linkage joints occupy the same plane (Appendix A Table 13). The maximum planarity for the anterior jaw linkage system was 1.0 in *Pseudolabrus guentheri* with the minimum in *Ctenolabrus rupestris* at 0.62. Similarly, the planarity for the opercular linkage system ranged from a maximum of 1.0 in *Chlorurus microrhinos* down to 0.41 in *Epibulus insidiator.* In contrast, the most rapidly evolving linkage, the hyoid linkage, was typically less

planar, with a mean planarity of 0.72, ranging from 0.96 in *Labropsis australis* to 0.52 in *Leptoscarus vaigiensis.*

DISCUSSION

An important question at the interface of phylogenetics and biomechanics is the degree to which important musculoskeletal systems, such as the forelimbs in tetrapods or the skulls of teleost fishes, coevolve in an integrated way or evolve relatively independently of one another. Here we reveal a strong pattern of modularity across the reef fish family Labridae in which the four-bar linkage systems are often integrated as a unit, vary across groups in whether they coevolve with each other, and evolve independently from the remainder of the skull. Hypsigenyines and julidines generally supported a model of integration across the linkage systems, similar to the family-wide patterns. Cheilines are an anatomical and functional hotspot of linkage evolution, as the three linkage systems are all separate modules, and they have the fastest rates of linkage evolution in the family. The parrotfishes (scarine wrasses) are also extreme, showing a pattern of increased modularization of the skull. Among the linkages, the hyoid is the fastest evolving linkage system, and the least planar in its rest position, with the anterior jaws and opercular system showing somewhat lower evolutionary rates of change in shape and a mostly planar geometry. We conclude that the biomechanical systems in the labrid skull affect the modularity and integration of the bones in the skull and that the trade-off of integration versus modularity of biomechanical systems influences the tempo of skull evolutionary shape change in the labrid fishes.

Labrid phylomorphospace and the modularity of four-bar linkage systems

The central conclusion of this study is that biomechanical four-bar linkages in the skull of labrid fishes show a strong pattern of evolutionary modularity across the family, with labrid subclades showing different levels of integration and evolutionary rates among linkage modules. Recent work exploring this three-dimensional morphometric data set on the skull of labrid fishes has highlighted the independent modular evolution of the neurocranium and pharyngeal jaws (Evans et al. 2019), revealed the morphometric constraints in the skull shape related to burrowing behavior in wrasses (Evans et al. 2022), and discovered significant functional modularity and mosaic patterns of evolution in the labrid skull (Larouche et al. 2022). Here we extend the analysis of these data to specifically test evolutionary modularity in the four-bar linkage mechanisms that function in the feeding apparatuses of this diverse group.

Hypsigenyines and julidines have similar linkage modularity patterns to each other and the family Labridae. Most tests in hypsigenyines support a single linkage module with the remainder of the skull being one or two modules. The support for a three-module hypothesis may indicate a small release of integration in this tribe. This may explain why there is a wide spread in the phylomorphospace (Fig. 2.4) reflecting a high diversity in feeding ecologies and deep-water forms in this tribe. The release in constraint may have also allowed the extreme variation in *Siphonognathus argyrophanes* to evolve as an extreme morphology in the phylomorphospace of wrasses (Fig. 2.3).

Similarly, in julidines the linkage systems form a single module, and this is supported in all the modularity tests conducted. This pattern may indicate some constraint on the julidines' skull, although this tribe is a catch-all assemblage of many genera forming the diverse crown of the phylogeny (Hughes et al. 2022), some of which are paraphyletic, which may confound the

results. The skull of julidines appears to have radiated in shape to fill most of the phylomorphospace (Fig. 2.4) and there are many convergences between julidine taxa and other genera among wrasses in the phylomorphospace (Fig. 2.3). The integration of the three linkage systems may have spurred the evolution of specialty feeding behaviors (i.e., cleaners) not found in the other tribes and may have driven patterns of convergent morphology in the phylomorphospace. Further investigations into individual species patterns of modularity should be conducted to determine the effect of constraint on the morphology of the skull. Additional investigations into the phylomorphospace of julidine subgroups with increased sampling, such as the multiple radiations of *Halichoeres*, might further reveal constraint on the morphology of the julidine skull.

Two hotspots of skull and linkage evolution in the family Labridae identified here are the tribes Cheilini and Scarini, the labrid groups with the most independent linkage modules, the least integrated skull components, and the highest rates of shape change. The independence of the linkage systems may have enabled morphological innovations to evolve in these two groups.

Cheiline wrasses are morphologically and ecologically diverse, including piscivores and hard-shelled molluscivores, with size ranging from the smallest wrasse *Wetmorella nigropinnata* to the largest, *Cheilinus undulatus* (Westneat 1993). Research on the cheilines wrasse genera (*Cheilinus, Epibulus,* and *Oxycheilinus*) reveal the actions of planar four-bar linkage models which have been directly tested and supported with live animal feeding kinematics (Westneat 1990, 1991, 1994). In cheilines, morphological innovations have evolved in the four-bar linkage systems with linkage modifications for biting and piscivory. This includes the highly modified six-bar anterior jaw linkage system in the sling-jaw wrasses, *Epibulus* (Westneat 1991). The increased modularization of the three linkage systems may have allowed for more independent

evolution between the linkage systems in cheilines associated with their ecomorphological diversification, restructured functional traits, and elevated levels of linkage modularity and rates of shape change. It is interesting that the quasi-independence of the three linkage systems gave way to a general pattern of mobility in cheilines which may point to cranial kinesis' ability to reorganize and restructure functional traits and can result in differences in modularity and rates of diversification.

In scarines, a model of increased modularization is supported compared to the hypsigenyines and julidines. The Scarini is composed of the parrotfishes which vary in jaw morphology from the partially fused teeth of *Sparisoma* to the fully fused beak of the genus *Scarus*. In addition to changes in tooth morphology, some scarines also exhibit a mobile intramandibular joint in their lower jaw (i.e., anterior jaw linkage system; Price et al. 2010). Previous research on parrotfishes has shown moderate diversity in their skull shape (Wainwright et al. 2004) and high partitioning in their feeding habits (Nicholson and Clements 2020), leading these fishes to occupy a largely separate region of the labrid phylomorphospace (Fig. 2.3) This divergence of the scarines has been previously found in analyses of linear measures and muscle metrics (Wainwright et al. 2004) as well as 3D geometric morphometrics of the labrid skull (Larouche et al. 2022). Additionally, parrotfishes have elevated diversification rates, with most *Scarus* and *Chlorurus* species diversifying in just the past 5-10 million years (Smith et al. 2008; Hughes et al. 2022) with elevated rates of morphological evolution associated with rapid diversification (Price et al. 2010), which may further drive the diversity in these fishes.

Overall family trends show more independence of the linkages which allows for more variability in the linkage systems, providing more evidence that modularity can lead to innovative morphologies (Wagner and Altenberg 1996; Tokita et al. 2007; Hansen and Houle

2008; Clune et al. 2013). New morphologies in the anterior four-bar linkage system evolved in the cheilines and scarines which show patterns of increased modularization, indicating a tight relationship between the four-bar linkage systems and the morphology and shape of the skull in wrasses. It is intriguing that hypsigenyines and julidines show similar modularity patterns, while they are distantly related to one another. The ancestral state of modularity patterns appears to be an integrated skull with the linkages and the remainder of the skull as separate modules, shown in most hogfishes and tuskfishes. Future studies should investigate the other tribes (labrines, cirrhilabrines, pseudolabrines, and novaculines) to understand if there is convergent evolution in modularity patterns of the skull. Furthermore, this points to function and the corresponding mechanical systems potentially being more of a proximal driver of evolutionary modularity than development.

Modularity related to evolutionary rates of shape

Four-bar linkage systems in the skull of labrid fishes show elevated rates of evolutionary shape diversification relative to the rest of the skull (neurocranium, nasals, pharyngeal jaws, and premaxilla; Table 5). We conclude that elevated rates of linkage change are an expression of the diversity of feeding mechanisms enabling the global ecological diversification of this iconic reef fish family.

Several recent studies have explored the relationship between integration and rates of diversification, quantifying phenotypic and evolutionary modularity to determine how they relate to these variables in various species and clades and providing evidence for a relationship in which more modular structures have either higher or lower evolutionary rates (Goswami and Polly 2010; Claverie and Patek 2013; Larouche et al. 2018; Bardua et al. 2019; Evans et al.

2019). However, some studies have found no relationship between these variables (Bardua et al. 2019, 2020; Bon et al. 2020), indicating a relationship that is complex. In our study, we found a relationship between modularity and the evolutionary rates of skull shape across the labrid phylogeny with the more modular structures showing higher rates of evolution (Table 2.5) and the linkage system module evolving at a faster rate of shape diversification than the neurocranium, nasals, premaxilla, and pharyngeal jaws (Table 2.5).

The concept of evolvability has been used to assess the potential for evolutionary change and has been used to examine anatomical modularity and evolutionary rates of change (Wagner et al. 2007; Pigliucci 2008; Clune et al. 2013). The four-bar linkage systems evolve at about double the rate of the neurocranium, nasals, premaxilla, and pharyngeal jaws (Table 2.4). These differences in evolutionary shape change among skull modules signify elevated evolvability in these systems, likely related to the strong pattern of ecomorphological diversification of labrid fishes (Wainwright et al. 2004) that is accompanied by rapid divergence in feeding biomechanics among closely related lineages (Westneat et al. 2005).The linkage modules directly influence the performance and success of prey capture, which may be driving the evolvability of these regions. The evolvability of the linkage systems may have allowed for new morphologies to evolve and thus tribes, like scarines and cheilines, moved into new niches and habitats. However, being modular can confer only so much of a benefit to the species where if it is also accompanied by rate differences in the modules, further influence of modularity could affect the evolution of a structure. The spectacular ecomorphological diversity of the labrid fishes across reef systems is associated with different levels of modularity in the skull and elevated rates of shape change in the configuration of the complex skull levers and linkages involved in feeding mechanisms.

Planarity vs. three-dimensionality of linkage systems

An important finding of our three-dimensional linkage analysis is that the anterior jaws and opercular linkages are highly planar, with all four rotational joints aligned close to a plane. A key conclusion from this result is that the most three-dimensional linkage system, the hyoid, is the fastest evolving in shape. Additionally, kinematic analyses and computational modeling studies that start from an assumption of planar linkage positioning are supported, at least for the initial starting position. The four-bar linkage systems have been modeled as two-dimensional structures (Westneat 1990) and as three-dimensional structures (Olsen et al. 2017). Moving forward researchers need to especially treat the hyoid linkage system as a three-dimensional structure. This allows more precise measurements to be taken from this system. This also leads to a question of why the hyoid linkage system is so three-dimensional compared to the other systems? And why is this system the fastest evolving?

The three dimensionality of the hyoid linkage system is clearly related to complex three-dimensional hyoid kinematics in many fish groups (Van Wassenbergh et al. 2007; Camp and Brainerd 2014, 2015). The main motions of the hyoid linkage system are depression and retraction. The retraction drives some lower jaw depression, while the depression influences the lateral expansion of the skull during feeding and hyoid depression. A more three-dimensional linkage system would allow greater lateral and ventral expansion of the skull (Olsen et al. 2017; Gartner et al. 2022; Whitlow et al. 2022). Furthermore, changes to this system occur faster due to the high rate of shape change in the hyoid linkage system. This lateral movement may be why the hyoid system is so three-dimensional compared to the anterior jaw and opercular linkage systems. More lateral movement would increase the oral cavity volume and would increase the pressure differential created during suction feeding (Lauder 1983). This would also benefit biting

species as it would draw the prey further into the oral cavity bringing the food to the pharyngeal jaws to be broken down.

CONCLUSION

In summary, we find the shapes of the bones associated with the linkage systems to be evolving more independently and faster than the remainder of the skull shape (i.e., neurocranium, nasals, pharyngeal jaws, and premaxilla) in the family Labridae. An analysis of family-wide and tribe-wide modularity patterns show evolution of different modularity patterns across the tree where the scarines and cheilines show evolution of increased modularization of the skull and faster rates of shape evolution, relative to other clades in the family. We conclude that variable modularity and elevated rates of shape evolution contribute to the morphological and functional novelties in the anterior jaws linkage system and drive patterns of shape evolution in wrasses. The planar positions of the jaws and opercular linkages, and the high level of three-dimensionality of the hyoid linkage system also helps to inform future computational analyses on these linkage systems in wrasses.

CHAPTER 3: ELASTIC SKULL LIGAMENTS AND THE BIOMECHANICS OF THE PARROTFISH BITE (FAMILY LABRIDAE).

ABSTRACT

Connective tissues, like skin, ligaments, tendons, are critical to musculoskeletal function, yet the material properties of collagenous tissues are not often studied in fish feeding systems in which the skull is a complex, mobile system connected by connective tissues. Here, we aim to test the mechanical properties of cranial ligaments and characterize them histologically in the closely related parrotfishes and cheiline wrasses to explore their function. We investigated the mechanical properties of three cranial ligaments (coronomaxillary (CM), interoperculohyoid (IOPH), and interoperculomandibular (IOPM)) across 6 species of parrotfishes and 2 cheiline wrasses, using tensile tests to measure ligament breaking strain, resilience, and elastic (Young's) modulus (E). Results show that suction feeding wrasses have stiffer IOPM ligaments than biting parrotfishes, which possess highly compliant IOPM ligaments. Extensibility (breaking strain) is higher in the parrotfish compared to the cheilines, *Oxycheilinus unifasciatus* and *Epibulus insidiator.* The parrotfishes and cheilines have highly compliant CM ligaments, indicating a damping of forces in these systems. Young's Modulus (E) in parrotfishes is low, reflecting the extensibility of connective tissues involved in transmitting forces during feeding. Biomechanical resilience in all three ligaments in parrotfishes and wrasses is high (85-95%) suggesting substantial energy return. Percentage of collagen in the IOPM is high (70%) in *Epibulus insidiator* but just 40% in *Scarus guacamaia*, with a high percentage of collagen yielding stiffer ligaments. Parrotfishes appear to have a unique feeding system by having compliant and stretchy ligaments in their skulls, which can help to damp repetitive biting forces, absorb peak forces from hard bites and store energy repetitive biting over many cycles per day. These data suggest ligamentous springs in fish skull linkages, like elastic tissue mechanisms more broadly among

vertebrates, play a key role in the biomechanics of cyclic as well as rapid explosive events during vertebrate feeding.

INTRODUCTION

Vertebrate ligaments are fibrous connective tissues that originate and insert on bones or cartilages, connecting skeletal elements, stabilizing joints, and functioning in transmission of forces and motions in musculoskeletal systems. Ligaments function in tension, with the material properties determined by the collagen and elastin composition of the ligament, and the size and orientation of ligamentous fibers in relation to a loading regime. The tensile properties of vertebrate ligaments have mainly been studied in humans, mammals, and various tetrapods where researchers have found a wide range of material properties. The majority of ligaments have relatively high Young's Modulus, a measure of stiffness measured from the slope of the stress-strain curve, ranging from around 100 MPa up to over 1000 MPa in mammalian knee ligaments (Alexander 1989; Danto and Woo 1993; Stäubli et al. 1999; Moon et al. 2006; Souza et al. 2010). This research has found that ligaments with high stiffness function in joint stabilization or rapid force transfer and act in tension similar to a relatively inextensible rope or wire. Other studies on more compliant ligaments like the small periodontal ligaments that surround teeth (Mandel et al. 1986; Fill et al. 2011) or the stretchy nuchal ligament of large mammals (William Fielding et al. 1976; Gellman and Bertram 2002a) have revealed low stiffness around 1MPa or lower. These elastic ligaments can store energy which can help reduce costs associated with certain behaviors, like feeding or locomotion (Biewener 2008) and function to reduce the susceptibility to damage, especially in ligaments that are subjected to constant loading cycles during an individual's lifetime (Thornton et al. 2007; Biewener 2008). Compliant

ligaments can be modeled as springs, and this modeling can reveal the basic mechanics of energy absorption and force damping in these tissues.

The ligaments in the skulls of teleost fishes experience sudden force transmission load during behaviors such as suction feeding, and more extended yet potentially high loads during slower behaviors such as biting or scraping. The stiffness versus compliance of ligaments in the teleost skull may therefore be a relatively unexplored axis of important variation in these complex structures undergoing variable stress-strain regimes. Modeling ligaments as ropes or springs can reveal the theoretical function and performance of these tensile tissues. The mass, damping, and stiffness are elemental properties of a mechanical system when modeling a structure (Cross 2008) affecting the reaction forces and response when an object, such as a jaw, experiences sudden suction forces or contacts a hard substrate. Stiffness affects force transmission and the amount of stretch in the tissue as forces are experienced at contact. Damping, a loss of energy, can be either active or passive, with viscoelastic materials, like a ligament, exhibiting mainly passive damping (Johnson 1995). Ligaments that are compliant can be considered as embedded dampers that function to dissipate high forces or strains from a specific system or area and may influence the contact time when the system contacts a hard surface (Cross 2008). Therefore, a central prediction of the present study is that ligaments will vary in their stiffness versus compliance, possibly indicating the functional roles of rapid force transmission by stiffer tissues, or functional roles in elastic recoil or damping in more compliant tissues. In addition, other material properties, like the efficiency of energy return in a ligament (resilience) and the overall work to failure for a tissue (toughness) may further elucidate the function of teleost cranial ligaments on an organismal level whereas information on histological properties helps to understand connective tissue fiber composition at a tissue structural level.

The function of ligaments can be further understood through the characterization of the ligament's tissue level properties. Collagen is the main building block in ligaments that receive tensile loads while elastin provides elasticity to many ligaments. Stiff ligaments have a higher concentration of collagen and have fibers oriented more parallel to each other compared to more compliant ligaments where the orientation of fibers is more mixed (Biewener 2008). The orientation of fibers is hypothesized to determine how much shear and multiaxial loading a ligament can incur before rupture (Biewener 2008). Therefore, a second aim of this work is to explore the histological fiber composition of fish cranial ligaments, as investigation into the fiber orientation of ligaments and concentration of collagen is key to fully understanding the function of the ligaments in complex musculoskeletal systems. This study explores the histological structure of the interoperculomandibular (IOPM) ligament in two different species, *Epibulus insidiator* and *Scarus guacamaia*, to understand the significance of the histological properties with function. By exploring the mechanistic and tissue properties of ligaments, we gain a better understanding of the function of the cranial ligaments in these fishes.

The skull of teleost fishes is a highly complex musculoskeletal system, composed of up to 80 different bony elements that all cohesively move together to capture prey (Lauder 1982). The levers and linkages that play a role in force transmission during biting, and in rapid movements during suction feeding have been studied in depth and many of the mobile elements are connected through soft tissues (Anker 1974; Muller 1989; Westneat 1990; Olsen et al. 2017). Although research on the material properties of soft tissues in the feeding mechanics of fishes is relatively unexplored, *in vivo* experiments that remove or cut (transect) cranial ligaments have been crucial to studying the function of ligaments. Experimentally cutting prominent cranial ligaments (e.g., the interoperculomandibular ligament) prevented the jaws from fully opening in

a wide range of suction-feeding fishes such as leaf-fish (Liem, 1970), trout and wolf fish (Lauder, 1979), and tilapia (Durie and Turingan, 2004). Ligament transection studies have not been conducted on species that use biting behaviors to capture prey, however, similar results are expected. Overall, these experiments concluded ligaments are essential for transmitting motion through the skull to allow for synchronous, fast, and powerful movements that rapidly expand the skull to create the negative pressure needed for suction feeding. Previous work found that linkage systems promote diversification in wrasses by evolving at higher rates than the other skeletal elements (Gartner et al. *in review*) but phylogenetic comparisons of the functional morphology and biomechanics of cranial ligaments would fill a major gap in understanding the morphological and functional diversification of fishes.

The present study aims to understand the use of ligaments in the fish skull using wrasses and parrotfishes; a diverse group of coral reef fishes that have a wide diversity in feeding behavior and morphology (Wainwright et al. 2004; Westneat et al. 2005). To test these ideas, we analyzed the mechanical properties (Young's Modulus (E), breaking strain, and resilience) under tensile loads of three key cranial ligaments, the coronomaxillary (CM), interoperculomandibular (IOPM), and the interoperculohyoid (IOPH) ligaments (Fig. 3.1), in four species of parrotfishes and two species of cheilines (*Chlorurus spilurus, Epibulus insidiator, Oxycheilinus unifasciatus, Scarus guacamaia, Scarus globiceps,* and *Scarus taeniopterus*).

Parrotfishes browse and excavate live or dead coral surfaces by ramming their heads into the coral and biting chunks off the reef or scraping seaweed, sponges, algae, and bacterial film from coral surfaces (Nicholson and Clements 2020). Parrotfishes have hard beaks and are feeding upon hard coral substrates often biting thousands of times a day and up to 40 bites per minute (Bonaldo et al. 2006; Smith 2008; Ong and Holland 2010; Afeworki et al. 2013).

However, compared to a suction feeding species, parrotfishes bite very slowly. We hypothesize the parrotfishes have compliant ligaments in their skulls to damp high forces and increase the amount of time the beak interacts with the hard substrate. On the other side of the feeding spectrum, cheiline wrasses mainly suction feed upon other fishes and evasive shrimps and crabs, with some species having a mix of suction and biting (Westneat 1990, 1994). Based on preliminary data on material properties of cranial ligaments from several Red Sea species (Grubich et al. 2014), we hypothesize that suction feeding species will have stiffer ligaments while biting species will have more compliant ligaments. Stiff ligaments are predicted to be beneficial to suction feeders because force can be transferred faster through the tissue during the burst movements involved with a suction event. Compliant ligaments may be beneficial to biters as elastic ligaments may allow for shock absorption, damping, and increased flexion between the bones during the rhythmic and cyclic movements incurred by biting species. Furthermore, we hypothesize that resilience and the potential for energy storage and damping may be variable between stiff ligaments for suction feeding and more elastic ligaments for biting.

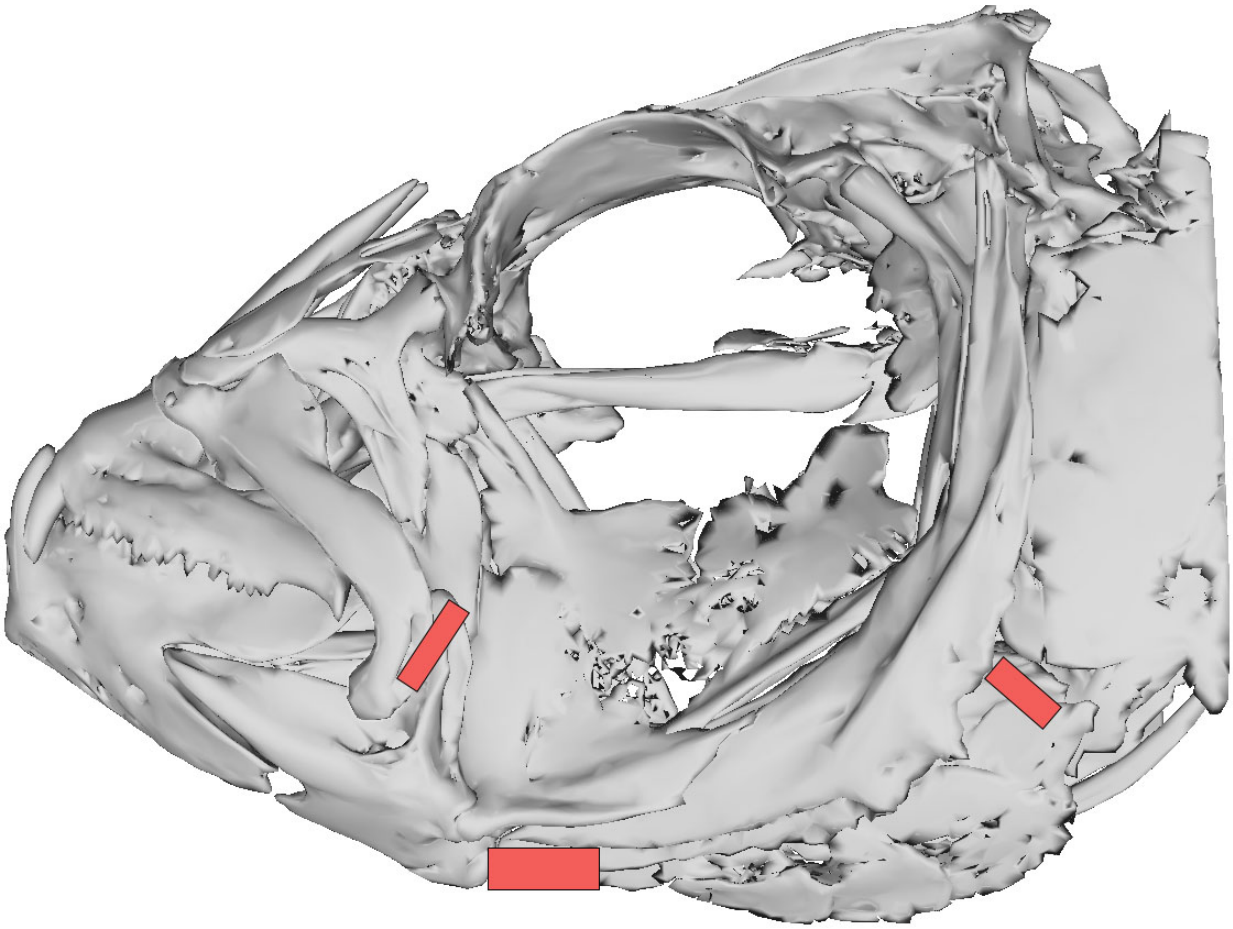

Figure 3. 1: Model of Oxycheilinus unifasciatus with the three ligaments highlighted in red. From anterior to posterior the ligaments are coronomaxillary, interoperculomandibular, and interoperculohyoid. The maxilla and interopercle are transparent to indicate the ligaments are located behind these bones.

METHODS

Specimen collection and preparation

We collected four species of parrotfishes and two species of cheilines wrasses from the Florida Keys, Florida and Mo'orea, French Polynesia using spear on SCUBA (Permit: SAL-22-2331-SR and French Polynesia permit #MCE/DRM 6019) and purchased from local fishermen. The species collected for ligament testing include 3-6 specimens each of *Chlorurus spilurus, S. globiceps, S. guacamaia, S. taeniopterus, Epibulus insidiator,* and *Oxycheilinus unifasciatus*.

After collection, specimens were immediately put on ice and subsequently were refrigerated for up to 48 hours after collection. If 48 hours was reached and the specimen wasn't processed, it was frozen. Frozen specimens were wrapped in wet paper towels and sealed in an airtight container following standard protocols to prevent dehydration and freezer burn (Moon et al. 2006). To harvest ligaments for analysis, one side of the head was dissected and the CM, IOPM, and IOPH were dissected out still attached to the bone at both ends. Once as much extraneous tissue as possible was removed from the ligaments, geometric measurements were taken (e.g., height, length, and width). Dissection and measurements were made at room temperature, and the ligament surface was kept wet through spray or submersion in water intermittently. Once ligament tests were conducted, we measured the cross-sectional area (CSA) of the ligaments through photos via a Wild M3Z microscope. Average CSA was measured at the attachment site using two different images.

Testing Apparatus

We used a Mark-10 or Lloyd LS1 testing machine to measure the force (N) and displacement (mm) of each ligament in repetitive tensile tests. Clamps held the bone fragment at each end of the ligament with a load cell at the upper clamp measuring the tensile forces and the testing machine recording distance traveled, both of which were stored on a laptop computer with a 50 Hz sample rate. Parameters were based on pilot and previous studies (Grubich et al. 2014). To study the effect of cyclical loading, we carried out tests with different strain conditions based on the starting length of the ligament. The cyclical tests involved sequential trials of 5% strain, 10%, 20%, 30%, etc. in 10% strain increments until the ligament reached failure. Each cyclical trial consisted of 10 loading and unloading cycles at 50 mm/min. Tests were determined to start when

the load began increasing above 0.1 N in order to avoid long toe regions with slack in the ligament. A monotonic failure test was performed for each ligament as a single loading curve past the yield point to breaking strength with subsequent decline in force.

Ligament Analysis and Statistics

Ligament tensile tests yielded raw data on force-displacement curves that were used to measure Young's Modulus (E), resilience, and breaking strain. Force-displacement curves were converted into stress-strain curves by dividing the force by the cross-sectional area (CSA; stress) and the displacement or ligament stretch was divided by the initial resting ligament length, to yield engineering strain. CSA was determined by photographing the cut cross-section of each ligament with a scale bar, using a dissecting scope and camera, and computing CSA using the *slice geometry* function in BoneJ found in ImageJ. Failure was defined at the maximum stress-strain point at which a non-plastic deformation occurred on the force-displacement curve. Young's modulus (E) was the highest linear slope of the stress-strain curve. The linear region was calculated as follows. The data was split into thirds and the slope was taken from each section of the data. The highest slope was taken as the E for that trial for the ligament. Resilience was measured as the area under the loading curve minus the area under the relaxation curve.

All data is presented as mean ± standard error. Intergroup differences were analyzed using a pANOVA to account for phylogenetic relatedness. We further ran Tukey tests to find the means that were statistically different from each other. Data analysis was significant at $p<0.05$.

Histological Analyses

To test the hypothesis that the proportions of collagen and elastin are different at the extremes of high and low modulus fish ligaments, tissue specimens were analyzed from *Scarus guacamaia* and *Epibulus insidiator* of the IOPM. Each of the specimens was separated from the bone at the bone-ligament interface. The ligament tissue was cut into smaller slices to be prepped for the embedding process. Specimens were fixed in 10% formalin. After fixation, specimens were embedded in paraffin through the University of Chicago Human Tissue Resource Center. Sections were made with a microtome and were stained with Picro Sirius Red. This stain under polarized light is specific for identifying collagen and elastin. These sections were examined using a Zeiss Axioscope compound microscope under polarized light. Analysis of percent collagen and elastin content was conducted using ImageJ. We first split the image into red, green, and blue wavelengths and chose the red image to analyze, since this provided the highest contrast in coloration. *Threshold* was used in the analysis, and we changed the threshold until only the collagen was highlighted. We then applied the threshold leaving only the particles from the collagen and used *analyze particles* to analyze what percent of the histological slide contained collagen. Elastin was calculated as the remaining percentage.

RESULTS

The central result of this study is that cranial ligaments in wrasses and parrotfishes are highly variable in their mechanical properties between species, and also may vary between tissues within species. The ligaments in the skull of parrotfishes are highly compliant, with low modulus and showing high strains up to 60% of rest length. Ligaments in suction feeding cheiline species showed higher stiffness, with the highest elastic modulus found in the interoperculomandibular

(IOPM) ligaments of the sling-jaw wrasse, *Epibulus insidiator.* Tissue histology results indicate that ligament stiffness versus compliance is associated with the proportion of collagen versus elastin in the IOPM tissue. Results generally showed that tissue mechanical properties are associated with predicted biomechanical traits required for suction feeding and biting strategies.

Ligament Analysis

Tensile testing of cranial ligaments in six species of labrid fishes shows that fish ligaments generally have low stiffness and are variable across species. Qualitative analysis of the stress-strain curves during cyclical tensile testing indicates differences in the toe region, linear region, and failure point (Fig. 3.2 & 3.3). In parrotfishes the toe region appears to be longer, and the slope is not as steep as the suction feeding fishes, *Oxycheilinus unifasciatus* and *Epibulus insidiator*, in the IOPM (Fig. 3.3). The parrotfish's ligaments are also able to be stretched further than the cheilines, indicating parrotfish to have higher strain values in the IOPM compared to the suction feeding fishes (Table 3.1). Monotonic failure tests were also analyzed for strain at failure.

Cyclic loading tests were analyzed for Young's Modulus (modulus in the linear region of the stress-strain curve) and resilience. Parrotfish's ligaments (*Scarus*, and *Chlorurus*) have low Young's Moduli compared to the sling-jaw wrasse (*Epibulus insidiator*) and the lined maori wrasse (*Oxycheilinus unifasciatus*) (Fig. 3.4 & 3.5). Average E for parrotfishes is 3.52 MPa for CM, 12.55 MPa for IOPM, and 1.68 MPa for IOPH. Parrotfish have an average E that was not significantly different from each species across the three ligaments (Fig. 3.4; Appendix B Table 1-3). Average E for *E. insidiator* is 2.16 MPa for CM, 70.90 MPa for IOPM, and 1.39 MPa for IOPH and *O. unifasciatus* average E is 7.85 MPa for CM, 35.16 MPa for IOPM, and 4.23 MPa

for IOPH. For the CM and IOPM ligaments, *E. insidiator* and *O. unifasciatus* are significantly different from the majority of parrotfishes (Appendix B Table 1 - 2).

Parrotfish have highly elastic cranial ligaments, with high strains of 30-50% before failure, compared to the cheilines (Table 3.1). Average strain for parrotfishes was for CM 33.97%, for IOPM 32.50%, and for IOPH 41.03%. *E. insidiator* has an average strain for the CM of 28.14%, for the IOPM of 4.90%, and for the IOPH of 44.95%. *O. unifasciatus* has an average strain for CM of 31.78% for IOPM of 27.16%, and for IOPH of 46.12%. Across all species tested, the IOPM consistently had the highest stiffness and the lowest breaking strains among the three ligaments.

Resilience was high for all three ligaments in parrotfishes (Table 1). Parrotfishes had resilience for CM of 76.43%, for IOPM of 80.37%, and for IOPH of 82.28%. For *E. insidiator* resilience was for CM 91.16%, for IOPM 89.94%, and for IOPH 93.64%. For *O. unifasciatus* was for CM 95.59%, for IOPM 100.00%, and for IOPH 93.72%. Resilience stayed constant through the cycles, with few outliers (Table 3.1), and ecomorphological relationships were not supported for resilience in the species tested. From the phylogenetically corrected ANOVAs, we found mechanical properties of the cranial ligaments have significant differences in Young's Modulus based on feeding ecology (Appendix B Table 1 - 3).

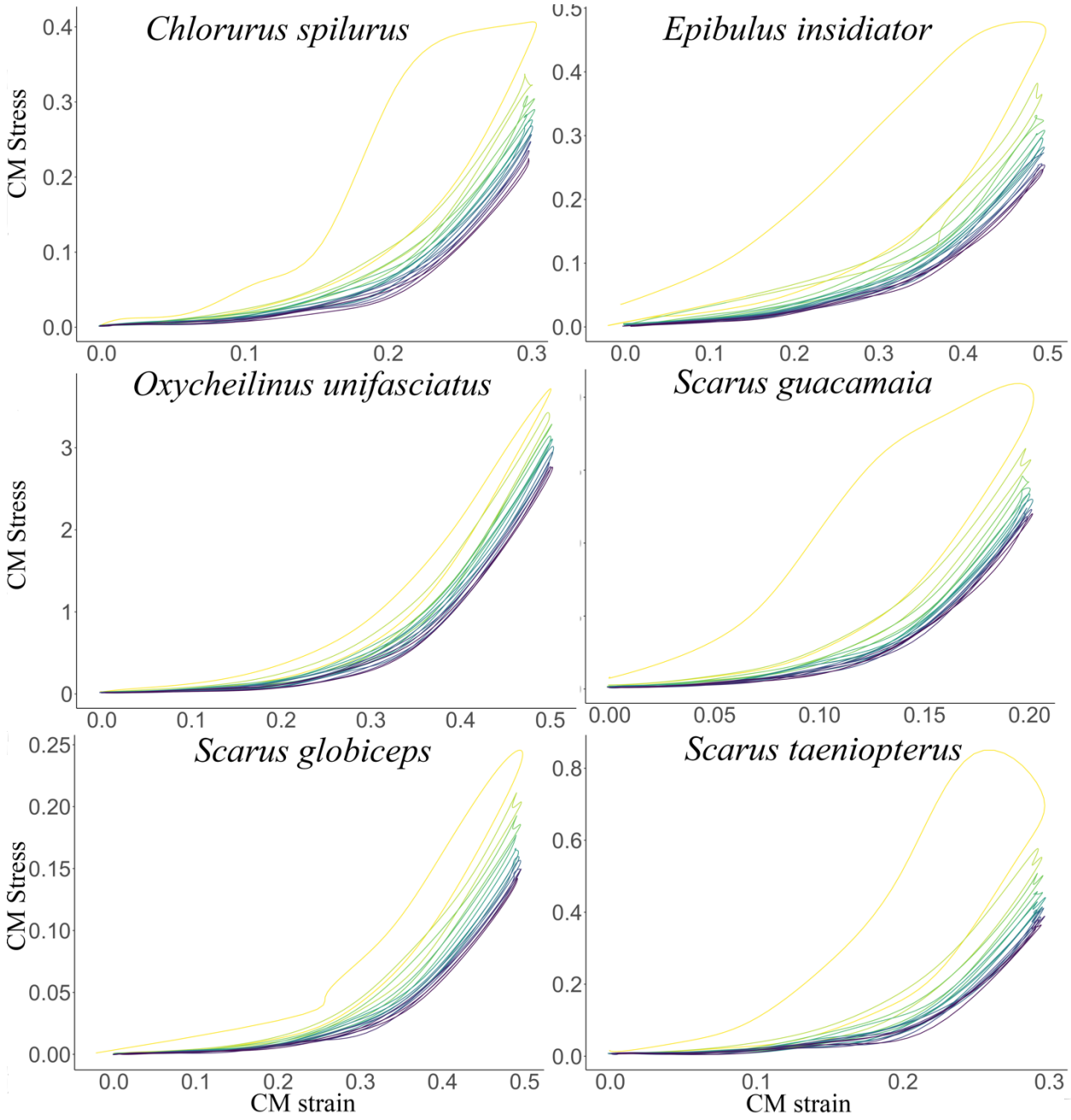

Figure 3. 2: Representative stress-strain curves of the coronomaxillary (CM) ligament for each species in the study. Each trial has 10 loading-unloading cycles at 50mm-min. The colors represent each cycle during a trial with cycle 1 being the lightest color and cycle 10 being the darkest.

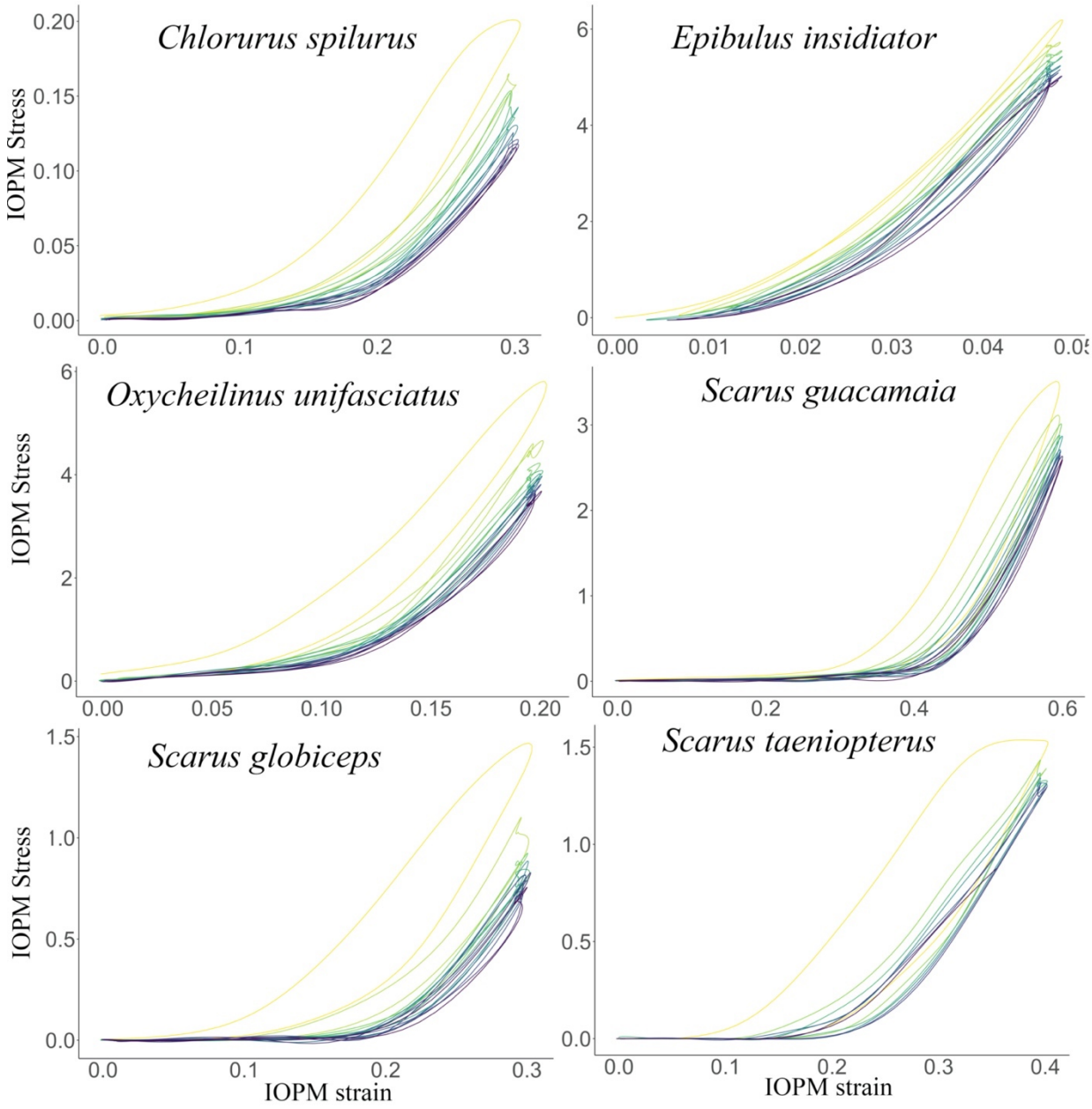

Figure 3. 3: Representative stress-strain curves of the interoperculomandibular (IOPM) ligament for each species in the study. Each trial has 10 loading-unloading cycles at 50mm-min. The colors represent each cycle during a trial with cycle 1 being the lightest color and cycle 10 being the darkest.

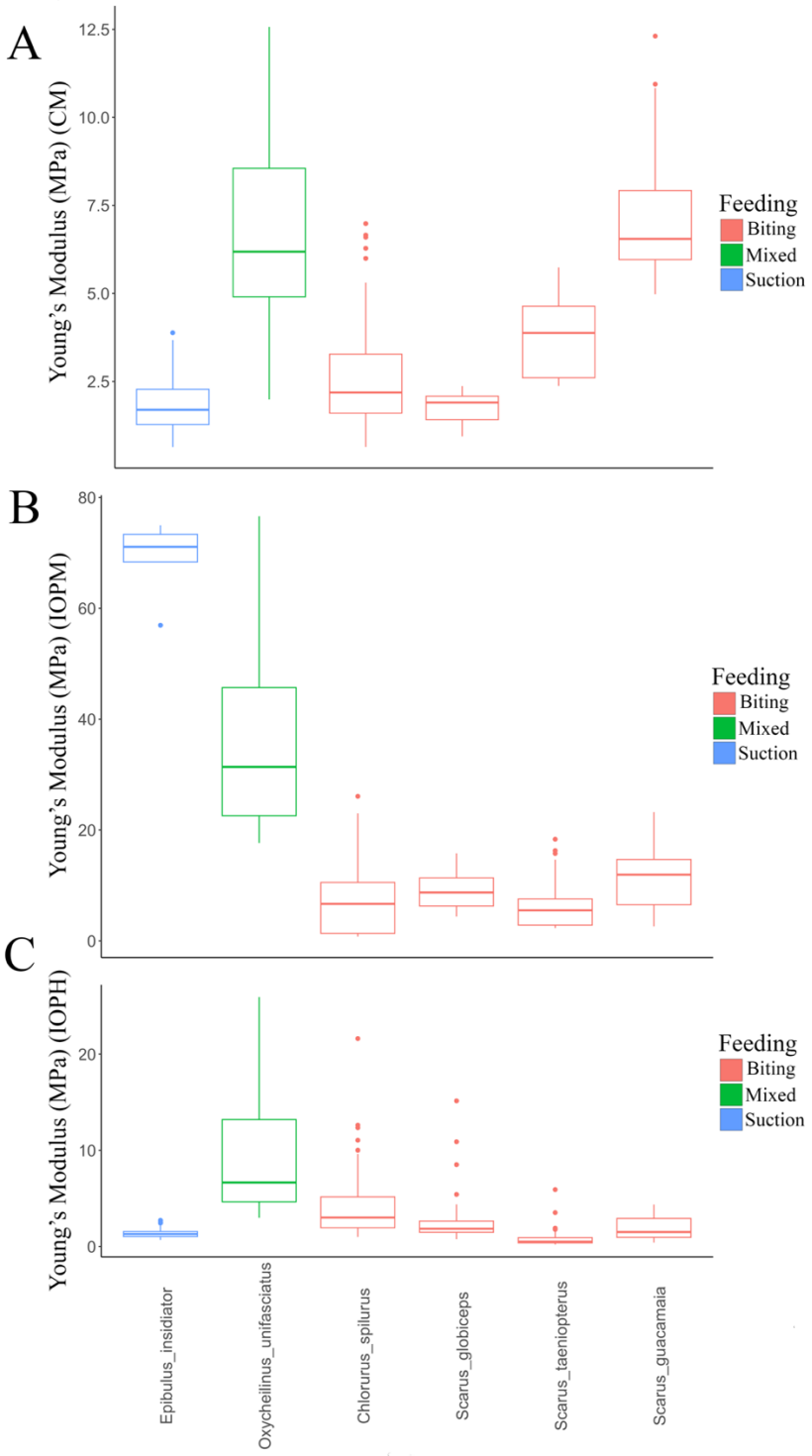

Figure 3. 4: Boxplots of the species vs. Young's Modulus in MPa. A) Represents the Young's Modulus for the coronomaxillary ligament, B) shows the Young's Modulus for the interoperculomandibular ligament and C) represents the Young's Modulus for interoperculohyoid ligament. The line through the boxplot represents the mean with the outliers being represented as dots. The lines from the boxplot represent the values in a 95% confidence interval.

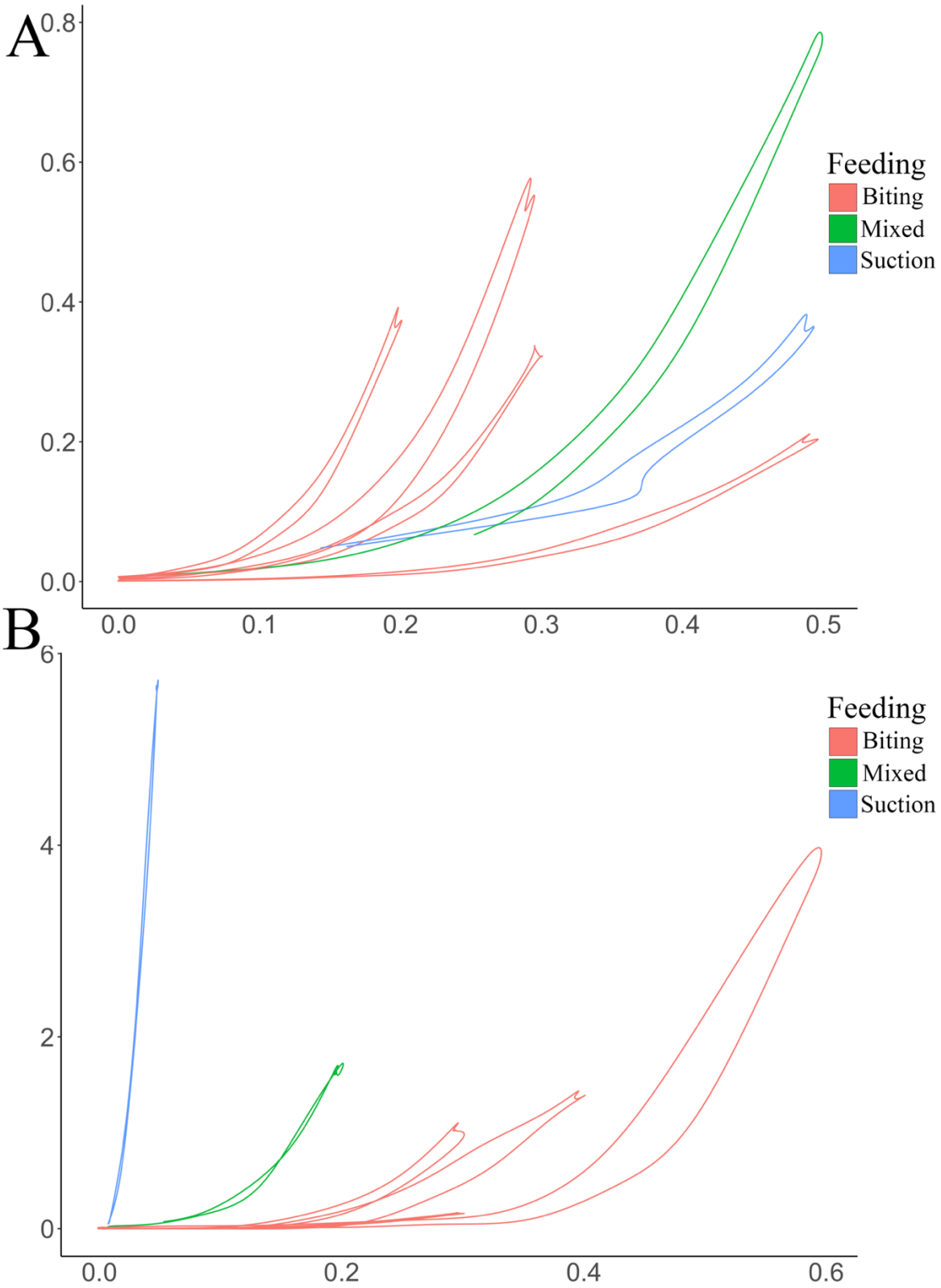

Figure 3. 5: Stress-strain curves of coronomaxillary (A) and interoperculomandibular (B) ligaments for biting species in red (parrotfish), mixed feeding species in green (Oxycheilinus unifasciatus), and suction feeding species in blue (Epibulus insidiator).

Table 3. 1: Values of the average Young's Modulus (E), resilience, and breaking strain from the species analyzed.

Species	Ligament Type	E (Mpa)	Resilience (%)	Breaking Strain (%)
Chlorurus spilurus	CM	2.72	98.11	29.50
Chlorurus spilurus	IOPM	4.56	95.74	39.33
Chlorurus spilurus	IOPH	3.70	97.00	59.00
Scarus globiceps	CM	1.63	94.41	48.67
Scarus globiceps	IOPM	10.25	95.42	29.33
Scarus globiceps	IOPH	1.84	97.27	39.00
Scarus gucamaia	CM	7.71	95.18	19.67
Scarus gucamaia	IOPM	13.48	87.59	59.00
Scarus gucamaia	IOPH	2.17	95.81	59.00
Scarus taeniopterus	CM	3.91	87.39	59.00
Scarus taeniopterus	IOPM	5.06	85.65	44.00
Scarus taeniopterus	IOPH	0.82	87.08	76.00
Oxycheilinus unifasciatus	CM	7.10	95.59	31.78
Oxycheilinus unifasciatus	IOPM	42.87	100.00	27.16
Oxycheilinus unifasciatus	IOPH	9.27	93.72	46.12
Epibulus insidiator	CM	2.13	91.16	28.14
Epibulus insidiator	IOPM	70.9	89.94	4.90
Epibulus insidiator	IOPH	1.47	93.64	44.95

Histological Analyses

The elastic and collagen fibers ran parallel in the IOPM in a craniocaudal direction (Fig. 3.6). Collagen and elastin were found in different concentrations in the IOPMs from *Epibulus insidiator* and *Scarus guacamaia*. The collagen content was higher in the IOPM of *E. insidiator* at 70.34% of the total area in the histological slide. In contrast the IOPM of *Scarus guacamaia* has a collagen concentration of 40.71% of total area (Fig. 3.6).

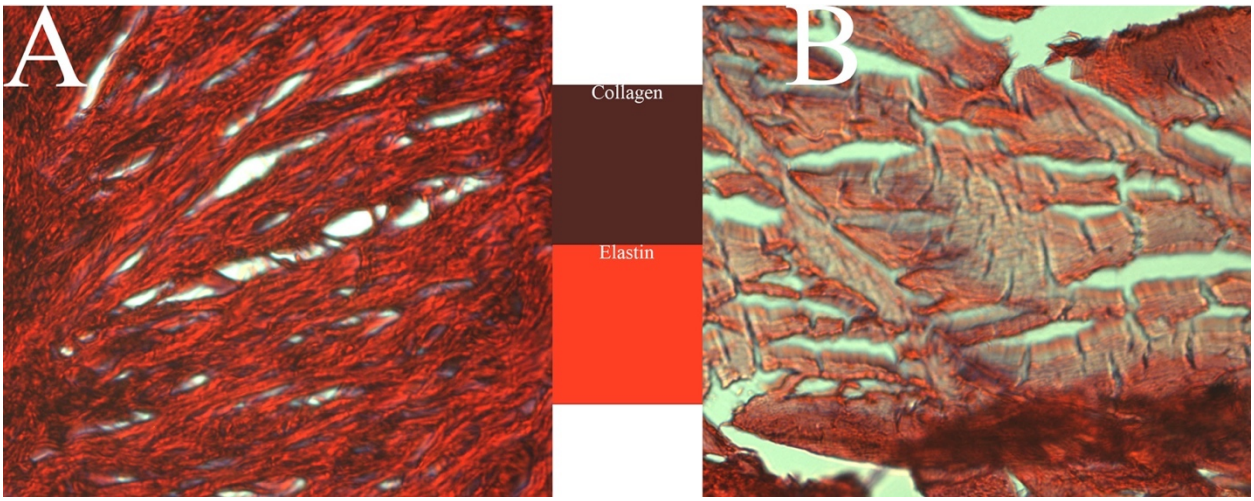

Figure 3. 6: Histological slides at 20x stained with picro sirius red stain under polarized light. A) IOPM ligament of *Scarus guacamaia* to highlight the elastin: collagen content. Elastin is stained bright red whereas collagen is dark red. B) IOPM ligament of *Epibulus insidiator* to highlight the small amount of elastin in the ligament. Insets of the collagen and elastin color are in the middle of the figure.

DISCUSSION

The properties of soft collagenous tissues in transmitting tensile forces are critical in many musculoskeletal systems, with a central paradigm of this research being that ligament stiffness versus compliance is a key tradeoff in fish feeding systems. The main conclusion of this study is that parrotfishes have ligaments in their skull that are among the most compliant in vertebrates, reflecting their function in energy efficiency and damping large forces during repetitive biting behavior. In contrast, the IOPMs of the closely related piscivorous cheilines wrasses have a higher elastic modulus for rapid force transfer. We conclude that variation in the material properties of ligaments in fish skulls is a central missing component of our understanding of force transmission and energy return in teleost feeding mechanisms. We explore the role of ligament stiffness and compliance in the mechanical design of feeding

mechanisms of labrid fishes, and consider the multiple roles of force transmission, motion transfer, and damping that these tissues provide to the dynamic feeding behaviors of these fishes.

Comparative Mechanical Properties

Parrotfishes exhibit viscoelastic properties, similar to other ligaments that have been studied (Matthews and Ellis 1968; Schatzmann et al. 1998; Moon et al. 2006). However, they exhibit low Young's Modulus (E) which is not typical of most ligaments studied (Fig. 3.7). The anterior cruciate ligament in rabbits (ACL) and patellar ligament in humans exhibit high E and very low strains (Danto and Woo 1993; Jones et al. 1995; Stäubli et al. 1999). This allows force to be quickly transferred through the ligament, but it leads to a higher probability the ligament can break (Nicholls et al. 2018). Ligaments with low E are the nuchal ligament in the back of the neck in horses (0.84 MPa), ligamentum flavum which is located in spinal canal in humans (4.36 MPa), or the periodontal ligament which surrounds tooth roots in mammals (1.4-3 MPa) (Mandel et al. 1986; Gellman and Bertram 2002a; Fill et al. 2011; Mihara et al. 2021).

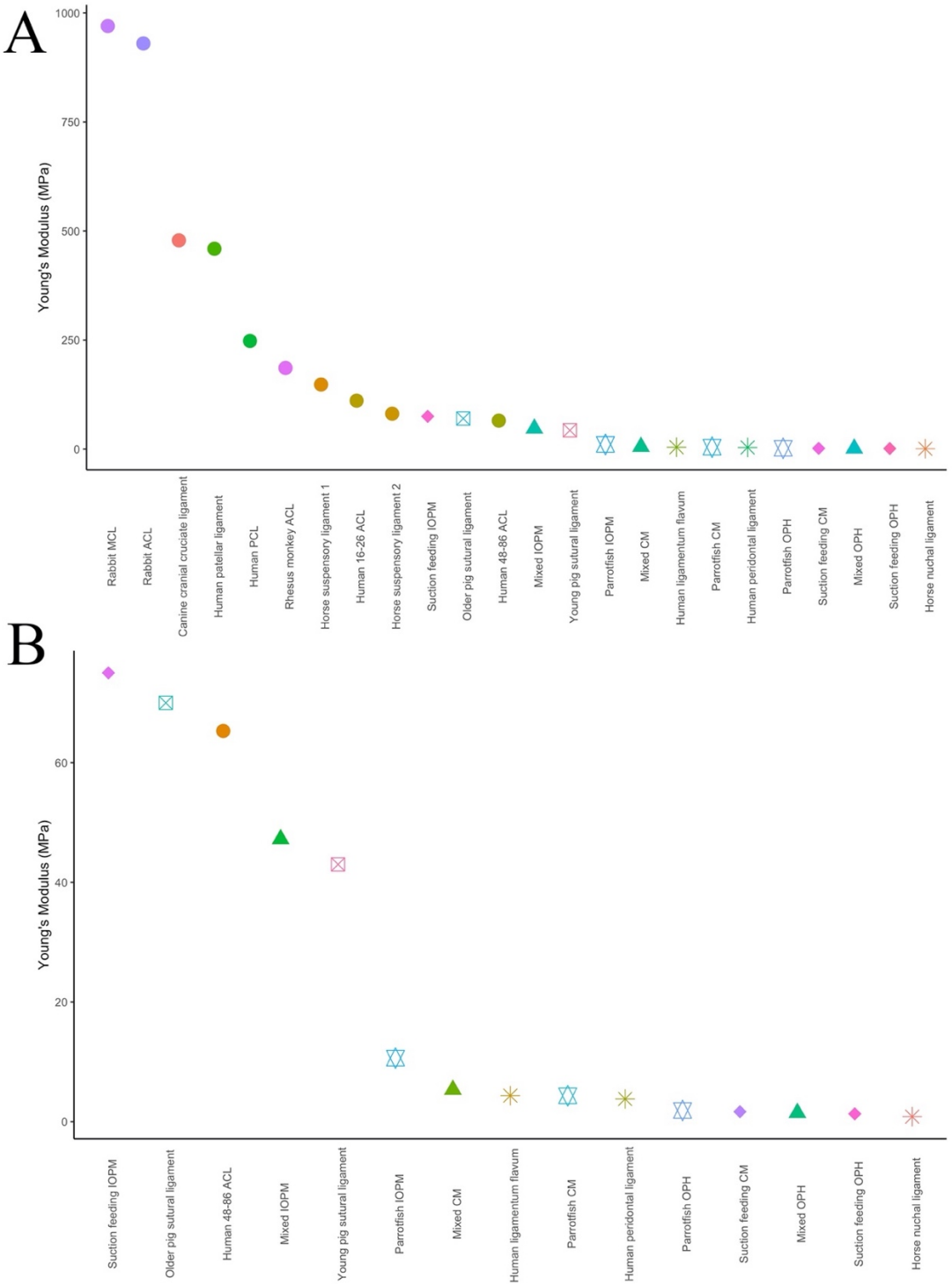

Figure 3. 7: A) Plot of a literature review of the Young's Modulus in MPa of representative ligaments where each color designates a different ligament study. B) A subset from A of the ligaments with the lower stiffness. The different symbols correlate to different groups of ligaments: the star represents the parrotfish, the triangles are the mixed species, the diamonds are suction feeders, and the asterisks are the three compliant ligaments that are not found in fishes. Summary of the literature review can be found in Appendix B Table 4.

A commonality across compliant ligaments is the repetitive use and frequency of stretch cycles in the various musculoskeletal systems in which the compliant ligaments are found. The teeth of humans, vertebral column of humans, and necks of horses receive frequent force transfer through the musculoskeletal system. Humans use their teeth to chew frequently, humans constantly move their spines through the day, and horses repeatedly modulate their heads during walking, trotting, etc. (Gellman and Bertram 2002b). For the periodontal ligament, the compliant ligaments allow the teeth to constantly move in the socket and act as mechanosensors for the teeth (Jiang et al. 2021). With low hysteresis and high resilience, energy is stored and recovered during the loading and unloading cycles of the ligaments (Biewener 2008). In horses this aspect of the nuchal ligament is important for head movement and functioning of the ligament (William Fielding et al. 1976). Additionally, more compliant ligaments are often involved in damping large forces that may get transmitted to musculoskeletal systems. This may indicate the cranial ligaments in parrotfish have energy storing and damping capabilities.

We conclude the same principle of viscoelastic behavior, high ligament strain, and energy return apply to the ligaments of the parrotfish skull. Parrotfishes feed with bouts of repetitive biting and engage in feeding bouts all day during daylight hours (Bonaldo et al. 2006). This repetitive behavior produces cyclic tension on the ligaments in the skull. During these motions energy storage may be occurring, and we predict that sudden high forces experienced by the jaws would be damped by ligament stretch. This may also point to compliant ligaments being necessary for joints and bones to move more repetitively. The compliant ligaments in parrotfishes may be allowing for the constant movement of the jaws involved with prey capture.

In suction feeding fishes, our results indicate that there are different combinations of stiff and compliant ligaments, suggesting a difference in the association of mechanical properties and feeding behavior. In the CM ligament, *Oxycheilinus unifasciatus* has a significantly stiffer E compared to biting species (parrotfish) and the sling-jaw wrasse (*Epibulus insidiator*). This indicates the main role of the CM may be damping of forces. We suggest that when *O. unifasciatus* and *E. insidiator* strikes at prey, the CM may undergo large tensile loads for which energy absorption and damping may be an important mechanical response. Additionally, parrotfish slam their heads into the reefs contributing to a large increase in force to the CM ligament. However, *O. unifasciatus* has a stiffer CM compared to parrotfishes and the sling-jaw wrasse. *O. unifasciatus* is able to suction feed at a greater extent than most other wrasses, but it still bites occasionally (Westneat 1994). This mixture of feeding behavior may indicate a more generalist feeding condition and thus the feeding system does not receive high force input from a specialized feeding behavior, as seen in the sling-jaw wrasse and parrotfishes. Therefore, we hypothesize *O. unifasciatus* does not have a compliant CM because it does not receive high inputs of force to its oral jaws and instead exhibits the generalist condition for the mechanical properties of the CM ligament. Future studies should investigate more species to see if a stiffer ligament is the condition for more generalist feeders.

These relationships change for the IOPM ligament, where the extreme suction feeder, the sling-jaw wrasse (*Epibulus insidiator*), has a significantly higher E compared to biters, and the highest modulus tissue that we found in our sample. It is intriguing to note that the sling-jaw wrasse has a relatively stiff IOPM, with low breaking strain, but has a highly compliant CM ligament. The sling-jaw thus has a rope in the rear that helps to initiate the action of the complex feeding linkage, and a spring in the front to damp high forces that may result from contact with

prey or substrate. In contrast the lined maori wrasse, *Oxycheilinus unifasciatus,* a close relative of the sling-jaw that employs both biting and suction, has a relatively high modulus for both the IOPM and CM ligaments, and is significantly different from the majority of parrotfishes. (Appendix B Table 2).

Considering the roles of ligaments in force and motion transmission vs. compliance and potential force damping, the higher stiffness of the IOPM allows force to be transferred faster through this linkage system and in parrotfishes the ligaments allow for damping of forces and modulation of the oral jaws. The sling-jaw wrasse, *Epibulus insidiator,* and the maori wrasse, *Oxycheilinus unifasciatus,* are able to protrude their jaws during feeding on evasive prey (Westneat and Wainwright 1989; Westneat 1994), but only *E. insidiator* exhibits extreme protrusion. This protrusion necessitates faster transmission of forces through the skull in order to suction feed quickly and successfully. However, with the strike and protrusion *E. insidiator* exhibits, this necessitates damping of forces. On the other hand, parrotfishes essentially have two springs in their heads, one between the interopercle and articular and one between the dentary and maxilla. These springs allow the parrotfish to move its jaws more frequently, compared to the cheilines wrasses, without damaging the ligaments. The influence feeding behavior has on the elastic modulus of the cranial ligaments is thus complex, suggesting that an examination of additional ligaments in these species, and expansion of the species sample may improve our understanding of the role of ligament properties in labrid feeding.

Our results for the interoperculohyoid (IOPH) show a consistently low modulus, with quite high strain capabilities across species. The high strain, low modulus characteristics of the IOPH suggest that this tissue is behaving largely as a spring across all species measured. Due to its low variability, we did not find a relationship between the E of the ligament and the feeding

behavior of the species, likely due to the function of the ligament. The IOPH is involved with transferring forces between the ceratohyal and the interopercle during feeding and breathing. The dual function of this ligament may point to the reason feeding behavior does not have a significant effect on the E of the cranial ligaments. The function of this ligament with high compliance across all species measured also remains to be explored in more detail and suggests that spring-like ligamentous tissues may be widespread in musculoskeletal systems in fishes.

Collagen and Elastin Composition in Labrid Cranial Ligaments

Histological examination of two species, the extreme suction feeder *Epibulus* insidiator and the extreme biter *Scarus guacamaia*, shows there is different ligamentous fiber composition of the IOPM ligament. Results show that there is a higher concentration of collagen in cranial ligaments in the suction feeder *E. insidiator* than in the biting *S. guacamaia* (Fig. 3.6). Qualitatively we also saw more parallel fibers in the IOPM from the suction feeding sling-jaw compared to the parrotfish examined, in which the ligaments had densely packed interlaced collagen fibers (Fig. 3.6). Previous studies have looked at the collagen concentration in ligaments, specifically in the mammal knee ligaments. However, few studies have compared the elastin: collagen relationship in the ligaments via histology (Abe et al. 2013). Here, we quantified how much collagen was in the histological slides collected. It is likely that the remainder of the tissue was elastin due to the contrast of collagen and elastin under the polarized light (Abe et al. 2013), although additional fiber-specific stains are needed to identify the full fiber composition of the tissue.

Ligaments are composed of multiple types of collagens, elastin, and variable proportions of gelatinous, hydrated ground substance (Nakagawa et al. 1994; Souza et al. 2010; Birch et al.

2013). The relationship between compliant and stiff ligaments has been studied in bovids (Eleswarapu et al. 2011), and a wide range of other mammals. In bovine knee ligaments, the patellar ligament was found to be stiffer with higher collagen concentrations compared to the cranial and caudal cruciate ligaments (Eleswarapu et al. 2011). The authors concluded the differences in tissue properties were based on the function of the ligament (i.e., the ligaments with more collagen experience more tensile forces). Thus, they concluded there is a structure-function relationship with the knee ligaments in bovids. We see a similar relationship with the cranial ligaments in labrids.

In our histological analysis, we removed as much of the fascia and peripheral tissue surrounding the ligament as possible, to ensure correct quantification of the elastin: collagen ratio. Higher concentration of collagen leads to stiffer ligaments whereas ligaments with high elastin content tend to be more compliant (Eleswarapu et al. 2011). This relationship is key to understanding how ligaments take loads when in tension. In the parrotfish ligament (*Scarus guacamaia*), we found low levels of collagen and many bundles of elastin in the histological slices (Fig. 3.6A), indicating a more compliant ligament on the tissue level. On the other hand, we found high concentrations of collagen in the ligaments of a suction feeder (*Epibulus insidiator*), indicating a stiffer ligament. This implies that in suction feeding fishes, the ligaments are adapted for transmitting forces faster through the tissue. A productive avenue for future studies may be to investigate the collagen cross-links, how the collagen fibers are aligned in the tissue, in these ligaments to further understand the tissue components of cranial ligaments in wrasses.

Modulation in wrasses and parrotfishes

One of our hypotheses is that parrotfishes have compliant cranial ligaments to modulate the movement of their oral jaws. Modulation is defined here as the ability to vary behavior actively or passively once perturbed. Active modulation might involve a change in muscular control, while passive modulation might be implemented by rate dependent stiffness or compliance of soft tissues. Combined active/passive modulation has been identified in vertebrate systems ranging from fish feeding (Nemeth 1997; Ferry-Graham 1998; Sass and Motta 2002; Whitlow 2022) to running in guinea fowl (Daley et al. 2006). In fishes, active modulation of the oral jaws is common and likely primitive for jawed vertebrates (Whitlow 2022). Bowfin, *Amia calva,* and various shark species show an ability to modulate their feeding systems when they suction feed or bite (Nemeth 1997; Ferry-Graham 1998; Ross et al. 2007; Montuelle et al. 2012; Whitlow 2022). Parrotfishes encounter uneven substrate when they feed, raising the question, do parrotfishes exhibit passive or active modulation in their oral jaws?

We hypothesize parrotfishes show both active and passive modulation of their oral jaws. If a parrotfish were to incur a change in the substrate during feeding, they are likely to be able to alter the pattern of muscle contraction of the adductor mandibulae muscle complex, in order to actively move their beaks to bite the coral more efficiently, and EMG data show this pattern (Alfaro and Westneat 1999). The role of compliant ligaments may be to allow for passive modulation of the feeding bite, in which the contact surface of the jaws with the substrate may be flexible across an uneven surface due solely to ligament stretching, without muscle activity changes.

Parrotfishes feed thousands of times a day (Bonaldo et al. 2006; Smith 2008; Ong and Holland 2010; Afeworki et al. 2013), but they are particular about which corals they will bite and scrape (Nicholson and Clements 2020). Due to the interspecific resource partitioning in parrotfishes, the parrotfish will actively move to the different corals and feed off the variable substrate. This creates more questions, such as how do parrotfishes know how close they are to the substrate? Are they able to passively modulate their jaws if there's a perturbance? Future studies should investigate the ability for parrotfish to change the positioning of their beaks and bodies based on the substrate in order to understand whether parrotfish actively or passively modulate their beaks.

Parrotfishes have evolved a fused beak of the upper and lower jaws several times (Evans et al. 2023) which allows these fishes to bite and scrape the corals. In addition, some parrotfishes possess a mobile intramandibular joint, a joint between the dentary and articular that have evolved to be mobile and allows for a wider gape (Price et al. 2010). This joint enable coral browsing parrotfishes to excavate and take larger chunks of coral from the reef and may enable modulation of the positioning of the lower jaw surface during scraping behaviors. We hypothesize the compliant cranial ligaments help in absorption of forces, with or without the novel intramandibular joint, as our data do not show significant differences between major groups of parrotfishes. Parrotfishes have been shown to be pivotal for the health of coral reefs, as without contact browsing algae takes over coral heads and leads to unhealthy reefs (Lewis 2010; Shantz et al. 2020). The biomechanics of this important behavior is partially determined by the mechanical properties of the ligaments enabling parrotfishes to scrape and excavate in their unique and ecologically important manner.

CHAPTER 4: MECHANICAL PROPERTIES OF CRANIAL LIGAMENTS ACROSS WRASSES AND PARROTFISHES (FAMILY LABRIDAE)

ABSTRACT

Ligaments are soft connective tissues which connect bone to bone and help transfer force through the musculoskeletal system. Cranial ligaments in fishes are severely understudied, limiting our understanding of the biomechanics and evolution of the teleost skull. Here, we expand upon our previous research on cranial ligaments in wrasses and parrotfishes by adding in key species from the hypsigenyines and seagrass clade of the scarines (*Sparisoma* and *Calotomus*). We measured the mechanical and structural properties of two main ligaments in the fish skull: the coronomaxillary (CM) and the interoperculomandibular (IOPM). We ran phylogenetic ANOVAs to understand the phylogenetic influences on the mechanical properties of the cranial ligaments. In the CM, the ligament stiffness (Young's Modulus) evolved to be fairly compliant compared to the IOPM and we found the hypsigenyines to have stiffer CM ligaments than the majority of wrasses and parrotfishes. However, in the IOPM we found an eco-functional relationship with the stiffness of the ligaments being high in species that suction feed. This indicates the evolution towards stiffness evolved multiple times in fish that suction feed due to the species' phylogenetic positioning. Parrotfishes share similar mechanical and structural properties with most ligaments being highly compliant compared to suction feeding species, indicating compliant ligaments evolved once in parrotfishes. Breaking strain, the amount of strain at fracture, was found to be higher in parrotfishes and cheilines compared to the hypsigenyines in the IOPM. Toughness, the amount of energy per unit volume a material can withstand before breaking, was found to be low in suction feeding fish, *Epibulus insidiator, Lachnolaimus maximus,* and *Bodianus rufus* in the IOPM. The cranial ligaments in wrasses

appear to be highly variable, evolving towards specific mechanical properties and not towards similar mechanical properties. These insights help to understand the biomechanics and evolution of the skull among wrasses and further understand which soft tissues are important for 3D modeling of the fish skull.

INTRODUCTION

Ligament mechanical properties (i.e., Young's Modulus, resilience, breaking strain) help in understanding the fundamental material properties of a ligament which can assist in predictions and an insight into the structure-function relationship. Ligament mechanical properties are measured from cyclical or failure stress-strain curves (Fig. 4.1). These variables, like Young's Modulus, breaking strain, resilience, toughness, etc., can help to understand the biomechanics of the ligament in a musculoskeletal system. There are three main parts of a failure stress-strain curve (Fig. 4.1).

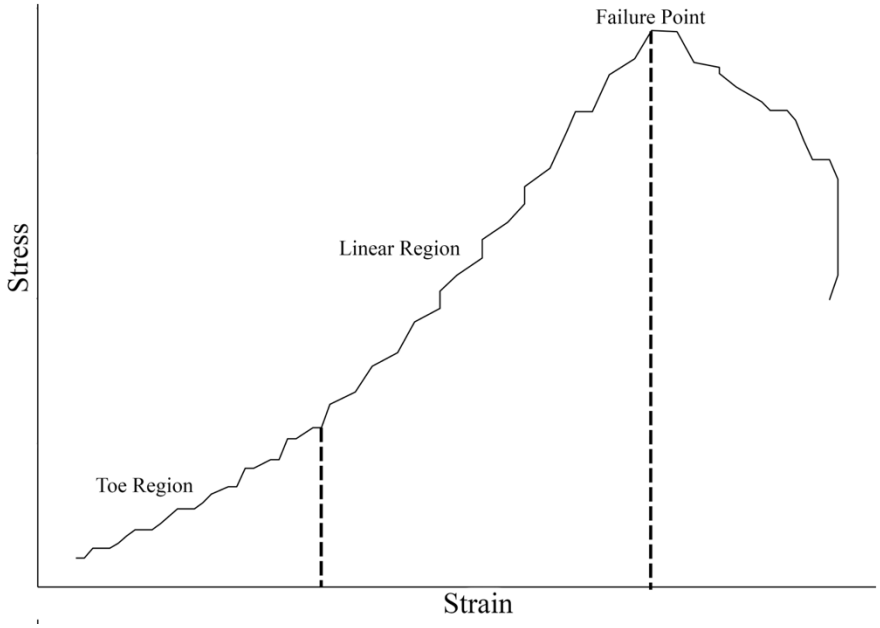

Figure 4. 1: Examples of a typical stress-strain curve. Highlighted are the toe region, where collagen fibers are crimped, the linear region, where collagen fibers are stretched, and the failure point, where collagen fibers first break. Dotted lines demarcate where these regions are delineated.

The first is the toe region in which the collagen and elastin fibers are still crimped and little to no force is being transmitted. Next is the linear region where the fibers are straightening out and

stress is gradually increasing in a linear fashion. Finally, the failure or yield point is where fibers begin to break, and plastic deformation occurs. For cyclical test stress-strain curves, there is no failure region, and the tissue returns to rest position before the next cycle begins. The toe region is typically where the slack of the collagen fibers in the ligament is measured from.

These measurements clarify the material properties of a ligament which can help in understanding the ligament's function. However, understanding the sub-structure of a ligament can also help to understand a ligament's function at the tissue level. Assessing the histological components of a ligament helps elucidate the fiber orientation and the percentage of components (i.e., collagen, elastin, proteoglycans) in the ligament which helps to further understand the function of a ligament. Collagen is the main building block of ligaments followed by elastin, proteoglycans, and extra- and intra-cellular matrices. The concentration of collagen can determine how compliant or how stiff a ligament performs (Eleswarapu et al. 2011). Elastin is thought to be a restorative material in that it brings the material back to its original shape (Ristaniemi et al. 2018), so higher concentrations would affect the length of the toe region and the compliance of the ligament. Additionally, while collagen provides stiffness to the ligament, elastin has a low stiffness but high tolerance for deformation (Buschmann and Meier Bürgisser 2017). These components of a ligament are under tension when force is applied to a musculoskeletal system.

The fish skull is a musculoskeletal system that is highly mobile and is thus particularly susceptible to tension as the skeletal elements expand and separate during suction feeding, the most common feeding behavior in teleost fishes. Fishes are an excellent model to study ligaments as their skulls are composed of many skeletal elements (Lauder 1982) connected by muscles, ligaments, and other soft tissues. There are many ligaments in the skull of percomorph

fishes (e.g., tuna, gobies, wrasse, pufferfish), and in this study we focus on two: the coronomaxillary (CM) and the interoperculomandibular (IOPM) (Datovo and Vari 2013; Gobalet 2017). The CM connects the coronoid process of the lower jaw to the posterior part of the maxilla and the IOPM connects the mandible (lower jaw) with the interopercle. These ligaments not only connect these bones but are involved with the four-bar linkage systems in the fish skull.

The four-bar linkage systems in the percomorph skull help to determine the motion of cranial elements. There are four links, fixed, input, coupler, and output, that function to move force and motion through the system. The CM interacts with the anterior jaws linkage system, which functions to depress the lower jaw, rotate the maxilla, and protrude the premaxilla (Westneat 1990, 1994). When this linkage system receives an input force, the CM will stretch and be in tension when the maxilla rotates away from the coronoid process on the lower jaw. This ligament has been found to be highly compliant and has force damping capabilities (see Chapter 3). The IOPM transfers force from the opercular four-bar linkage system to the lower jaw, in an action that rotates the opercular apparatus and depresses the lower jaw. The force transfer through this system stretches the IOPM when the opercular apparatus rotates. Additionally, the IOPM is a part of the coupler link in the opercular four-bar linkage system, indicating the IOPM acts more like a rope or wire in the posterior region of the skull (see Chapter 3), indicating force is being transferred more efficiently through the IOPM.

Here, we analyze the material properties of these two ligaments, the CM and IOPM in the family Labridae (wrasses and parrotfishes), a group of coral reef fishes with a wide diversity in size, shape, color, and cranial morphology. This study focuses on differences between mechanical properties that may be associated with the feeding behavior, diet, and phylogenetic relatedness in labrids. Previous work on cranial ligaments in labrids has found an

ecomorphological relationship with Young's Modulus in the IOPM ligament (see Chapter 3). We expand upon previous research by adding in pivotal species that represent the basal characteristics of wrasses, members of the hypsigenyine tribe which include hogfishes and tuskfishes, and scarines from the seagrass clade, *Sparisoma* and *Calotomus*. With this increased sample size, we aim to answer several questions. First, what is the basal state of the CM and IOPM mechanical properties in wrasses and parrotfishes? By including hogfishes in our analyses, we are sampling from taxa closer to the root of the phylogenetic tree than in prior analyses. Secondly, how does phylogeny and feeding behavior affect the mechanical properties of ligaments in labrid skulls? With data on eleven species across three major labrid clades, we may be able to characterize the range of ligament properties and assess their functional role in a diversity of skull mechanical designs. The results of this study aid in understanding the differences between the intrinsic material properties and their structure-function relationship, as well as the evolutionary relationship between the material and structural properties across the phylogeny of wrasses.

METHODS

Specimen Collection

We collected seven parrotfishes and four wrasses, two cheilines and two hypsigenyines, using standard collection techniques on SCUBA from the Florida Keys, Florida and Mo'orea, French Polynesia (Permit: SAL-22-2331-SR and French Polynesia permit #MCE/DRM 6019) and purchased from local fishermen. The parrotfish collected were from 3-6 individuals each from the species: *Calotomus carolinus, Chlorurus spilurus, Scarus globiceps, Scarus guacamaia, Scarus psittaus, Scarus taeniopterus,* and *Sparisoma viride.* The wrasses collected were 3-6

individuals and were *Bodianus rufus, Epibulus insidiator, Lachnolaimus maximus,* and *Oxycheilinus unifasciatus.* Once specimens were collected, they were immediately put on ice and processed within 48 hours of collection. Standard measurements were taken from the specimens before dissection. We dissected out the adductor mandibulae complex and the CM and IOPM ligaments. The ligaments were harvested via dissection of one side of the individual and removing the ligament still attached to the bone at both ends. We removed as much extraneous skin and other tissue from the ligaments as possible before testing. The ligaments were immediately tested once dissected out to prevent the tissue from drying out. The cross-sectional area (CSA) was measured from the attachment site after testing was completed using photos via a Wild M3Z microscope. Average CSA was computed from two different photos of the attachment site. Once the specimen was measured, it was wrapped in wet paper towels and frozen according to standard practices to prevent freezer burn (Moon et al. 2006). If a specimen was not processed within 48 hours of collection, the individual was frozen according to standard practices (Moon et al. 2006) and processed at a later time.

Material Testing

We used standard tensile testing to analyze two main ligaments, the CM and IOPM, from the skulls of eleven wrasse species. Standard corrugated grips were used to clamp the bones to the mechanical testing machine. We used a Mark-10 tensometer with a force gauge attached to the top grip. The tensometer measured the force and tensile displacement of the ligaments during both cycle sub-failure and ultimate deformation to failure tests. Parameters were based on prior measurements (see Chapter 3) and previous pilot studies (Grubich et al. 2014). The following steps were taken to measure the mechanical properties of the cranial ligaments. First, the bones

were clamped in the grips of the tensometer and stretched until the ligament was visibly tight and recorded to be in tension, with a force > 0.5 N. Previous length measurements taken before testing were used, and 10% of the ligaments' length was calculated. This number was then used to determine how far the ligament would initially be stretched. Trials were conducted at 5% the initial length, then 10%, and increments of 10% thereafter to stretch 20% initial length, 30% initial length, etc. Ligaments went through 10 cycles of loading-unloading cycles at 50mm-min. Once a break was detected, trials stopped, and the breaking trial was recorded. Stress-strain curves were computed from the raw force-displacements curves by measuring the cross-sectional area of each ligament. Young's Modulus (E), a measure of stiffness, was measured by first subsetting the loading curve into thirds and measuring the slope from each of these subsets. We measured the slope from the toe region and two parts of the linear region resulting in low, medium, and high Young's Moduli. Toughness, the ability for a material to resist deformation in joules per volume, is measured as the area under the failure curve and breaking strain, strain at the failure point, is measured from the failure stress-strain curve. Resilience, a measure of energy retention, is computed as the ratio of total work returned by the tissue during recovery, divided by the total work done by the tissue during stretching from the cyclical stress-strain curves for each of the 10 cycles for each trial.

Histological Analysis

We collected tissue from the IOPM of *Bodianus rufus, Lachnolaimus maximus, Epibulus insidiator, Sparisoma chrysopterum, and Scarus guacamaia.* Tissue was extracted from the ligaments and put into 10% formalin. Once preserved, the tissue was stored in ethanol until the embedding process. Tissue was cut into smaller slices and embedded by the University of

Chicago Human Tissue Resource Center. The embedded tissue was sliced at 10 microns using a microtome and the tissue was placed onto slides for further processing. Slides were stained using Picro Sirius Red which under polarized light show elastin to be bright orange and collagen to be dark red. Slides were examined under a Zeiss Axioscope compound microscope and pictures were taken. Analysis of percent collagen was conducted using ImageJ to isolate the colors of elastin and collagen. First, we split the color channels into the red, blue, green from the pictures of the histological slides. We took the red channel and used the *Threshold* function to isolate the colors of collagen. We analyzed the particles left from the collagen and took the percent as the percent collagen in the histological slides. Elastin was assumed to be the remainder of the particles in the histological slides based on the staining of the slides.

Statistical Analysis

All data are presented as mean ± standard error with significant results at $p < 0.05$. We ran pANOVAs in RStudio (RStudio 2012) to understand intergroup mean differences followed by Tukey tests to find the results that were statistically significant. We used the *contMap* function from the phytools package to graphically reconstruct the values of Young's Modulus with a phylogenetic signal across the phylogeny. *ContMap* estimates the ancestral condition of the internal nodes using maximum likelihood and assuming Brownian motion as the model for trait evolution (Revell 2012).

RESULTS

The central result from this study is that the parrotfishes have extremely compliant ligaments with high strains and high toughness compared to the suction feeding fishes, *Epibulus insidiator,*

Oxycheilinus unifasciatus, Bodianus rufus, and *Lachnolaimus maximus*. Suction feeding fishes have stiffer IOPM ligaments with low strain and low toughness compared to the parrotfishes. The CM was found to be stiff in the hypsigenyines and more compliant in the parrotfishes and the cheilines. Tissue histology of the IOPM results indicate suction feeding species to have more collagen and less elastin in their cranial ligaments compared to the parrotfishes. Results indicate the IOPM to have mechanical properties significantly associated with a species' feeding behavior and dietary habits.

Ligament Analysis

Testing of cranial ligaments in eleven species of wrasses and parrotfishes shows that labrids generally have compliant ligaments and ligament mechanical properties are variable across species. Qualitative analysis of the cyclical stress-strain curves shows high resilience throughout the wrasses and parrotfishes. Suction feeding species have lower breaking strains and lower toughness compared to biting species. Failure tests were analyzed for breaking strain and toughness while cyclical tensile tests were analyzed for Young's Modulus (E) and resilience (Fig. 4.2 & 4.3).

We measured E from three different regions of the loading curve for the CM and IOPM ligaments. In the CM, E is similar in the toe region but then the mixed species have higher E in the linear regions and the parrotfishes and sling-jaw wrasse have lower E (Appendix C Fig. 1). We found the patterns in the ligaments' material properties stay consistent through the loading cycle for the IOPM (i.e., *Epibulus insidiator* always has a higher E compared to the parrotfishes in the IOPM; Appendix C Fig. 2).

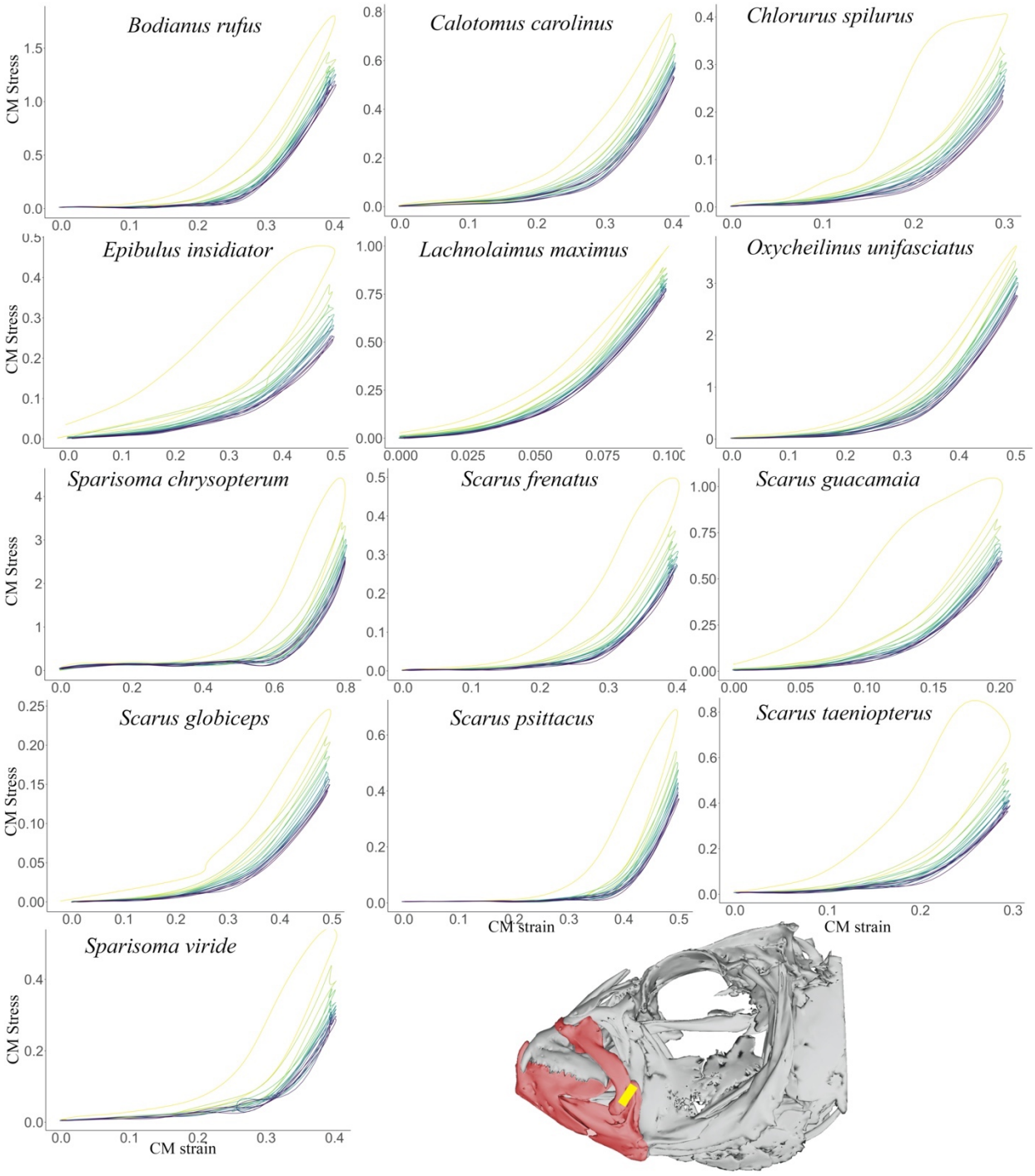

Figure 4. 2: Representative stress-strain curves of the coronomaxillary (CM) ligament for each species analyzed in this manuscript. The model of *Oxycheilinus unifasciatus* highlights the bones associated with the CM and shows the position of the CM ligament. The colors represent each cycle during a trial with cycle 1 being the lightest color and cycle 10 being the darkest.

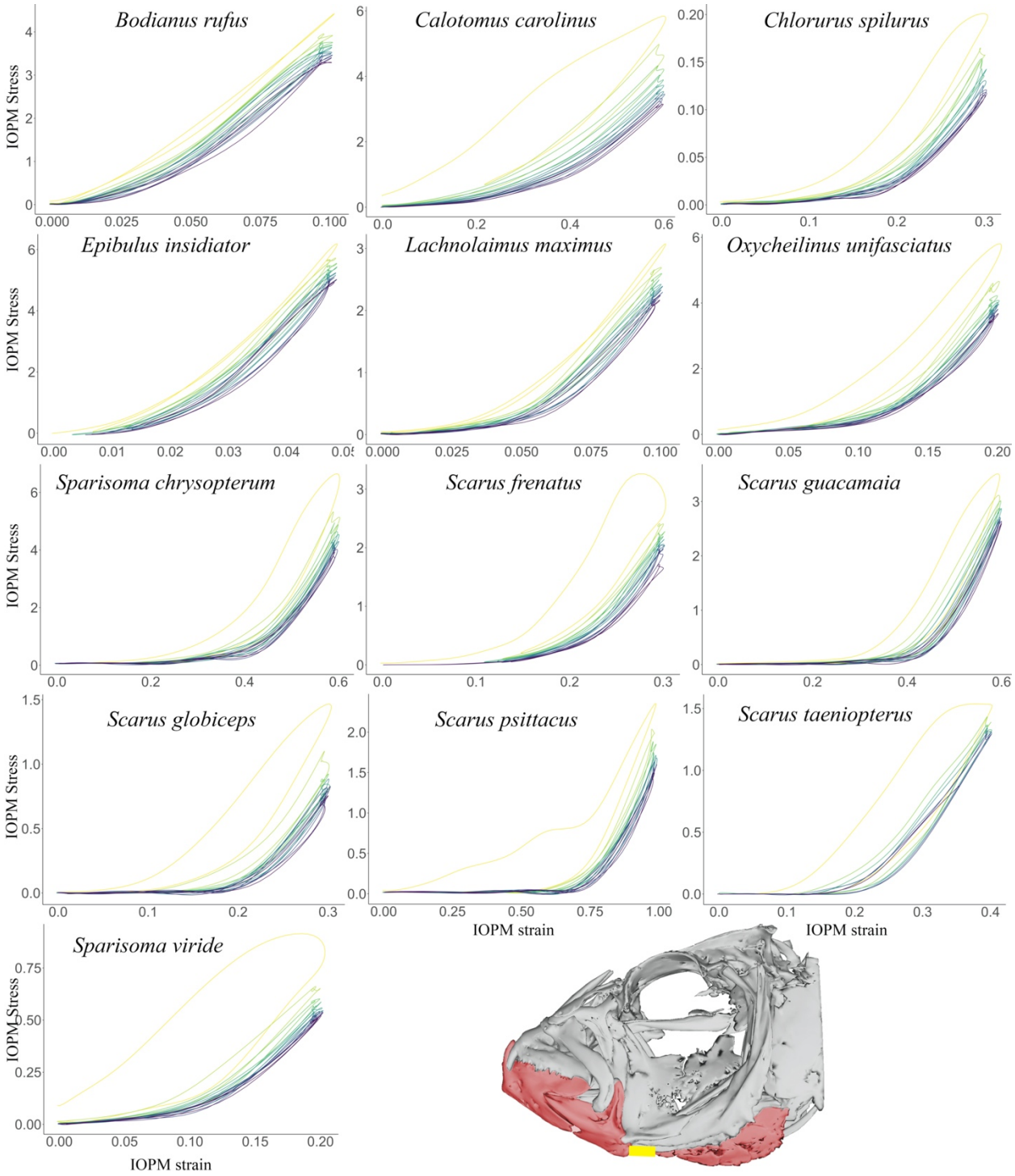

Figure 4. 3: Representative stress-strain curves of the interoperculomandibular (IOPM) ligament for each species analyzed in this manuscript. The model of *Oxycheilinus unifasciatus* highlights the bones associated with the IOPM and the IOPM's position. The colors represent each cycle during a trial with cycle 1 being the lightest color and cycle 10 being the darkest.

The coronomaxillary ligament has a higher E in the hypsigenyines compared to the parrotfishes and cheilines (Fig. 4.4) *Oxycheilinus unifasciatus,* has an average E of the CM of 7.10 MPa while the average E of the CM for *Epibulus insidiator* is 1.82 MPa. The hypsigenyines, *Bodianus rufus* and *Lachnolaimus maximus,* have an average E of 9.03 MPa and 7.33 MPa, respectively, while the scarines have an average E of 3.58 MPa.

We find all scarines to have a low E compared to the hypsigenyines and cheilines for the interoperculomandibular ligament (Fig. 4.4). The scarines, *Scarus spp.* and *Sparisoma spp, Calotomus carolinus,* and *Chlorurus spilurus* have an average E of 12.41 MPa for the IOPM. The hypsigenyines, *Bodianus rufus* and *Lachnolaimus maximus*, have an average E of 39.55 MPa and 36.54 MPa for the IOPM, while the cheilines, *Epibulus insidiator* and *Oxycheilinus unifasciatus,* have an average E of 70.90 MPa and 35.15 MPa for the IOPM.

Resilience was found to range from about 85%-95%. Resilience for the IOPM for *Bodianus rufus* is 100.00%, for *Lachnolaimus maximus* IOPM resilience is 98.70%, for *Epibulus insidiator* IOPM resilience is 90.00%, and for *Oxycheilinus unifasciatus* IOPM resilience is 100.00%. For the parrotfishes, IOPM resilience is 100.00%. The CM resilience for *Bodianus rufus* is 100.00%, for *Lachnolaimus maximus* CM resilience is 91.00%, for *Epibulus insidiator* CM resilience is 83.30%, and for *Oxycheilinus unifasciatus* CM resilience is 95.78%. For parrotfishes, CM resilience is 100.00%.

The breaking strain in the IOPM for *Bodianus rufus* is 16.11%, for *Lachnolaimus maximus* IOPM strain is 12.71%, for *Epibulus insidiator* IOPM strain is 6.12%, and for *Oxycheilinus unifasciatus* IOPM strain is 27.16%. For the parrotfishes, IOPM breaking strain is 37.14%. The CM has lower breaking strain in the hypsigenyines; for *Bodianus rufus* breaking strain for the CM is 21.40% and for *Lachnolaimus maximus* breaking strain for the CM is

11.66%. For the cheilines and scarines breaking strain was significantly higher compared to the hypsigenyines in the CM. For *Epibulus insidiator* breaking strain for the CM was 49.11%, for *Oxycheilinus unifasciatus* breaking strain for the CM is 42.75% and in parrotfishes breaking strain for the CM is 39.67%.

Toughness for the IOPM is significantly greater in the parrotfishes compared to the hypsigenyines and the sling-jaw wrasse. For *Bodianus rufus* toughness in the IOPM is 0.30 $J*m^{-3}$, for *Lachnolaimus maximus* toughness in the IOPM is 0.26 $J*m^{-3}$, for *Epibulus insidiator* toughness in the IOPM is 0.03 $J*m^{-3}$. For the parrotfishes, toughness for the IOPM is 0.52 $J*m^{-3}$. For the CM, toughness is similar across all species, except in *Lachnolaimus maximus* where toughness is significantly lower. For *Bodianus rufus* toughness in the CM is 0.40 $J*m^{-3}$, for *Lachnolaimus maximus* toughness in the CM is 0.03 $J*m^{-3}$, for *Epibulus insidiator* toughness in the CM is 0.17 $J*m^{-3}$. For the parrotfishes, toughness in the CM is 0.21 $J*m^{-3}$.

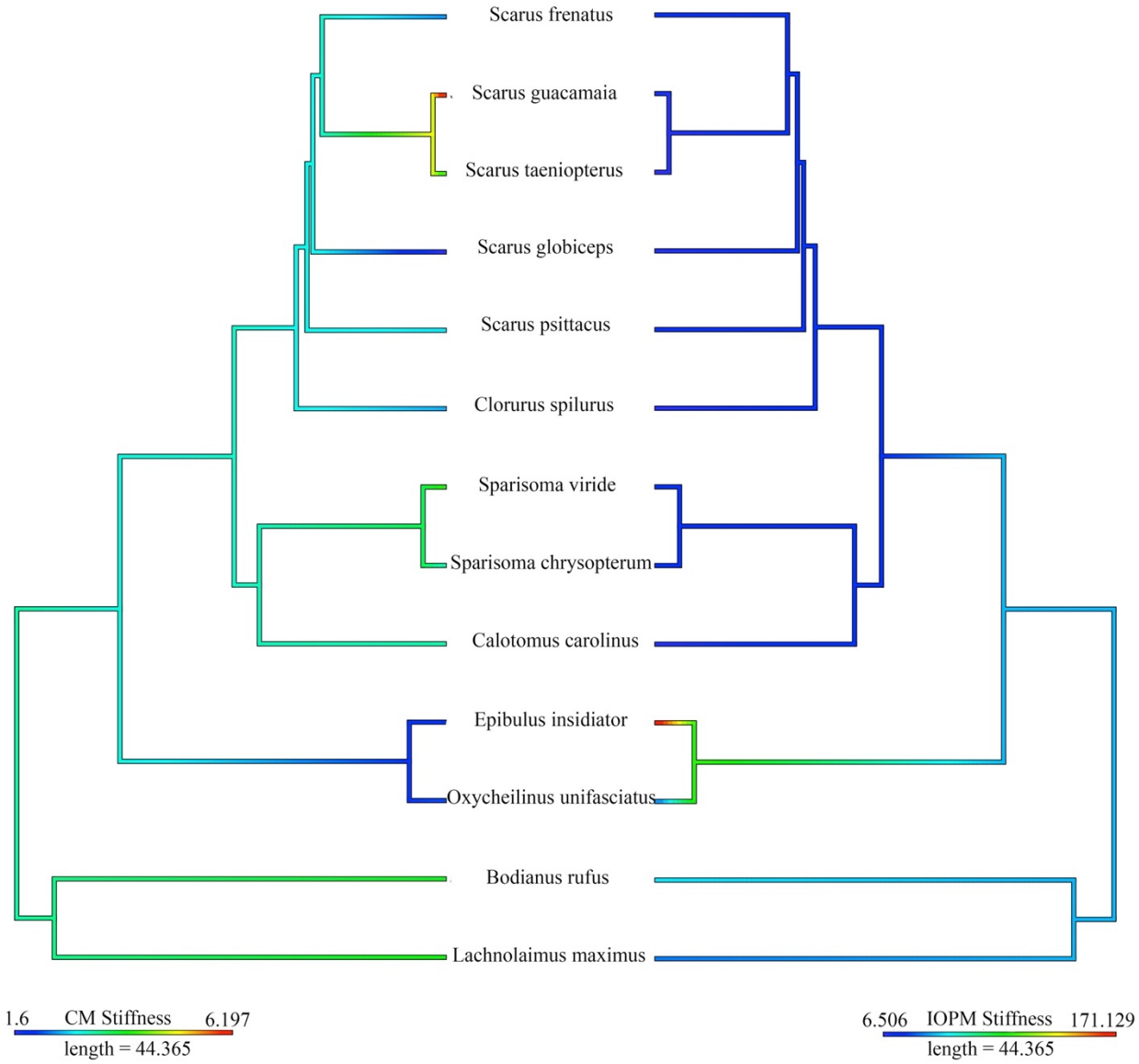

Figure 4. 4: Phylogeny of the thirteen species used in this study. We mapped Young's Modulus (E) using the *contMap* function from the phytools package. The left side shows the values of the E for the coronomaxillary ligament while the right side shows the values for the E of the interoperculomandibular ligament. The length of the legend gives the scale for the branch lengths of the tree, in this case units are millions of years.

Histological Analysis

Collagen and elastin were found in the IOPM of the wrasse and parrotfish species: *Epibulus insidiator, Scarus guacamaia, Lachnolaimus maximus, Bodianus rufus,* and *Sparisoma chrysopterum* (Fig. 4.5). The collagen concentrations were higher in *E. insidiator* (70.34%), *B. rufus* (58.55%), and *L. maximus* (61.51%). *S. guacamaia* has a collagen concentration of 40.71% while *S. chrysopterum* has a collagen concentration of 37.58%. These results show that parrotfishes have less collagen, and presumably more elastin in their IOPM ligaments.

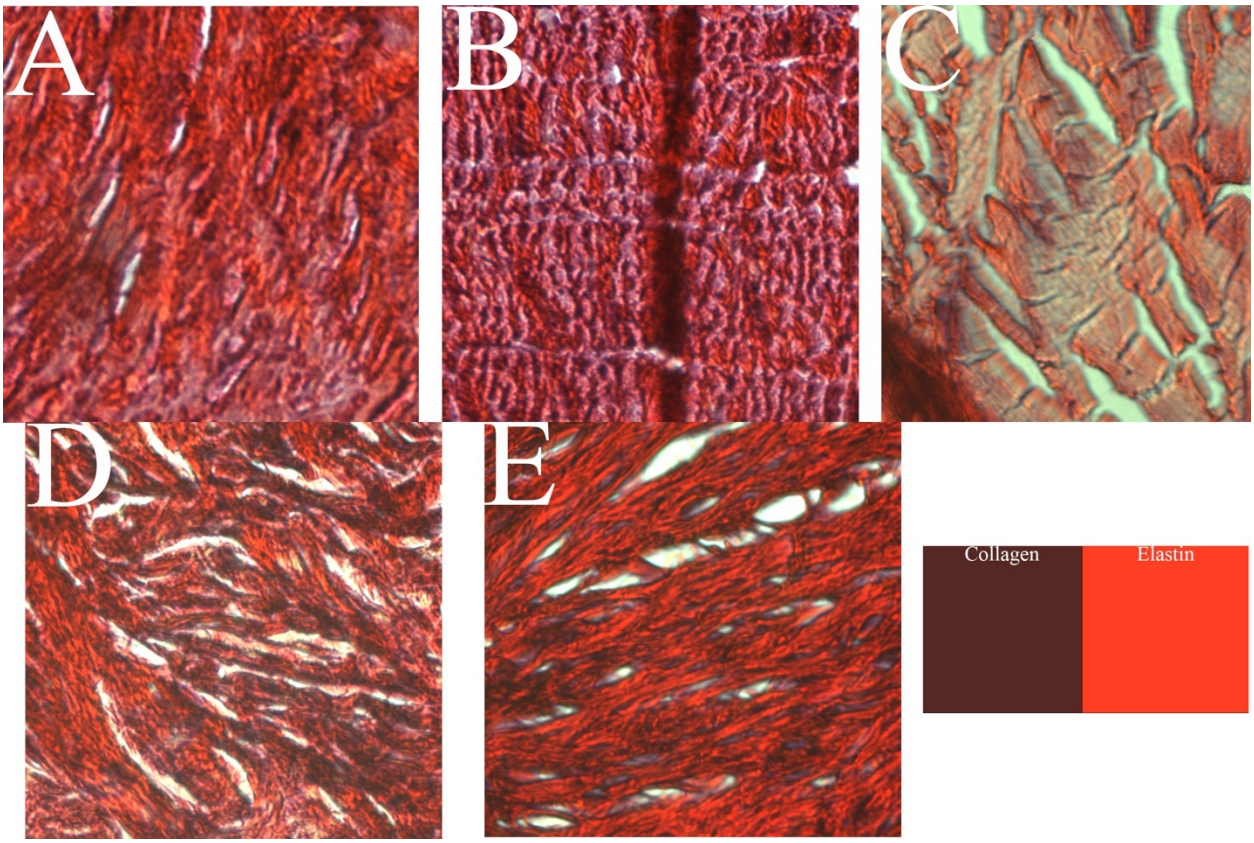

Figure 4. 5: Insets of histological slides from (A) *Bodianus rufus*, (B) *Lachnolaimus maximus*, (C) *Epibulus insidiator*, (D) *Sparisoma chrysopterum*, (E) *Scarus gucamaia.* Dark red signifies collagen whereas bright orange represents elastin. Colors for the collagen and elastin are given on the bottom right of the figure.

DISCUSSION

The mechanical properties of soft tissues are an important axis of biomechanical variability in vertebrate function. Here we show that in labrids, extraordinarily low modulus of elasticity in the ligaments is present across an iconic radiation of coral reef fishes. A central finding of this research is that suction feeding fishes have a stiffer, less tough and less stretchy IOPM ligament compared to species that bite. These results show that suction feeding fishes in two disparate clades of wrasses have evolved a stiffer IOPM ligament for rapid force transfer. The coronomaxillary ligament is shown to be stiffer in the hypsigenyines and more compliant in the scarines, and cheilines. The CM, therefore, has evolved more for damping of forces in the musculoskeletal system of labrids than for rapid force transfer. Resilience is high in all labrids, potentially indicating the energy storage capabilities of the CM and IOPM ligaments in labrids. We sought to understand the interplay between tissue level and mechanical level biomechanics and found more collagen in suction feeding species' IOPM ligaments compared to the parrotfishes. We explore the role of these ligaments in the timing and force transfer in suction feeding, the feeding mechanisms of parrotfishes, and the dynamic relationship these ligaments have with skull function, specifically in terms of computational modeling of the teleost skull.

Implications for suction feeding

The timing of muscle activation and skeletal movements affects the ligaments and the mechanical properties of the ligaments. The two ligaments we focused on in this study have different locations and timings for when they are stretched during feeding motions. In teleost fishes, there is an anterior to posterior wave of motion in skeletal timings (Lauder 1982) and the

opposite in the muscle activation patterns (Liem 1978; Turingan and Wainwright 1993; Alfaro and Westneat 1999; Camp and Brainerd 2014). The CM is the first ligament to move during a biting or suction event due to the oral jaws being the first skeletal element to move in a suction or biting event (Lauder 1982; Alfaro and Westneat 1999; Alfaro et al. 2001; Gartner et al. 2022; Whitlow et al. 2022), but it would be the last ligament to incur forces from the epaxial and hypaxial muscles. The ligament mechanical properties surprisingly are not affected by feeding behavior, and instead show a phylogenetic pattern of evolving high stiffness once in *Oxycheilinus unifasciatus*. This may point to damping as being a strong driver of compliance in this ligament or the ability to modulate their jaws. The CM is the most compliant ligament consistently compared to the IOPM (Fig. 4.2 & 4.4). Many fish species are able to modulate their skeletal movements during feeding (Liem 1978; Sanford 2001; Lemberg et al. 2019; Olsen et al. 2019; Whitlow et al. 2022). This modulation in the oral jaws may be a central factor in the patterns in compliance in the CM.

A second hypothesis to be considered is that force damping may be an important factor in the high compliance of the CM ligament. In many biomechanical systems there is damping within the ligaments and tendons of various connective tissue systems (Ker 1981; Long et al. 1997, 2002). Damping causes the dissipation of stress and is beneficial when a sudden high force enters a musculoskeletal system. In parrotfishes, a large amount of force may occur suddenly for the feeding system when an individual slams their beaks into the rock or coral when feeding. This force event may require damping to occur so that force reverberations in the skull are minimized. Similarly, the sling-jaw wrasse is likely to experience high inputs of force when they suction feed due to the extreme jaw protrusion used during prey capture. This high impact, high velocity suction feeding event may necessitate the damping of forces at the end of the feeding

system, at the junction between the coronoid process and the maxilla. In this way both the parrotfish and the sling-jaw wrasse use the damping functions of their CM ligaments during feeding in different ways.

The hypsigenyines possess a stiff CM ligament which may be because *Lachnolaimus maximus* and *Bodianus rufus* bite more often compared to the cheilines. The hypsigenyines are benthic foragers; they search the bottom for small fishes or hard-shelled invertebrates and exhibit a pecking behavior when foraging (Hoffman 1983). *B. rufus* takes one to two bites in a 30 sec time frame (Hoffman 1983) and *L. maximus* has 95% of its diet to be hard-shelled invertebrates with winnowing being the most frequent feeding behavior (Clifton and Motta 1998). *O. unifasciatus,* on the other hand, has small fishes composing up to 83% of its diet (Westneat 1994) and has similar muscle timings during feeding as suction feeding fishes (Alfaro and Westneat 1999). The sling-jaw wrasse, *Epibulus insidiator*, solely suction feeds and is able to protrude its jaws to an extreme distance (Westneat and Wainwright 1989; Westneat 1994). These differences in diet and feeding behavior may be an underlying ecomorphological explanation for why hypsigenyines and cheilines have different stiffness levels in the CM ligament.

The IOPM ligament is the next ligament in the series to stretch due to its position in the skull. The material properties of this ligament are strongly associated with feeding behavior and are stiffer in species that suction feed. Additionally, this ligament is less tough and has a lower breaking strain in suction feeding fishes compared to biting species. This indicates the IOPM ligament can absorb a smaller amount of energy before fracture and cannot stretch as much compared to parrotfishes. When an individual suction feeds they are able to move force through the opercular linkage system more efficiently than parrotfishes. The IOPM ligament is pivotal to the four-bar linkage systems in the fish skull (Westneat 1990; Olsen et al. 2017). Force is

transferred from the retraction of the interopercle to the lower jaw through the IOPM (Westneat 1990; Olsen et al. 2017), influencing the opercular four-bar linkage function. In stiffer IOPM ligaments, force is transferred faster and directly towards the oral jaws whereas in more compliant ligaments the connected bones can modulate their movements. We suggest that the higher stiffness in the IOPM is acting like a rope and is transmitting forces more efficiently, with less damping, than the CM ligament, indicating the function of the IOPM is to rapidly transfer force and motion for rapid prey capture.

Scarines and their morphological innovations

Previous studies have found differences in myology (Bellwood and Choat 1990; Streelman et al. 2002; Wainwright et al. 2004), motor control patterns (Alfaro and Westneat 1999) and in bite rates (Ong and Holland 2010; Holzer et al. 2013; Peoples, N. unpublished data) between species that are excavators vs. scrapers (i.e., species from the seagrass clade vs. reef clade). Due to this variation in bite rate and feeding behavior, we predicted that we might discover material property variation in ligaments that would reflect the differing demands of the less frequent bites in seagrass parrotfishes vs. the reef clade species. However, with our current sample we don't find a significant difference in mechanical properties of cranial ligaments in different groups of parrotfishes. Rather, we find that parrotfishes show highly compliant properties in both the CM and IOPM across all species studied and appear to act as springs in the feeding musculoskeletal system. It is notable that the cranial ligaments of all species examined are highly compliant, with low E, among the lowest stiffness values found for any ligamentous structure tested across the vertebrate tree (see Chapter 3 Fig 3.7). Compliant ligaments are beneficial for species as they allow for damping of forces and for more movement between the

bones (Biewener 2008). Perhaps our most important conclusion is that parrotfishes essentially have two highly efficient, springs in their heads that help to damp forces and absorb shock when feeding by biting chunks of coral off reefs or scraping algae, leading to a very forceful bite that may be modulated both actively via muscle activity patterns (Alfaro and Westneat 1999) and passively by ligament material properties.

An emerging theme from this research that warrants further investigation is the idea that with changes in morphology, there are likely to be concurrent changes in the soft tissues of feeding systems. Scarines occupy a distinct location in the labrid morphospace compared to the rest of Labridae (Larouche et al. 2022; Gartner et al. in review). These differences in morphometric shape may be driven by the evolution of beaks (Evans et al. in review) and by the evolution of the mobile intramandibular joint (Price et al. 2010). These changes in morphology both decrease kinesis, with the fusion of teeth, and increase kinesis, with an additional mobile joint. The association of morphometric variation in skull morphology with anatomical and biomechanical features of the soft tissue is an intriguing area for future work.

Comparative Histology of the IOPM ligament

We sought to understand the relationship between the tissue structure of a ligament and the function of that ligament. We found suction feeding species, *Bodianus rufus, Lachnolaimus maximus,* and *Epibulus insidiator*, to have more collagen in their ligaments compared to biting species, *Scarus guacamaia* and *Sparisoma chrysopterum*. In this study, we examined the tissue histologically for the presence of collagen and the proportion of collagen in each ligament. The ligaments exhibited differences in the amount of collagen present in the slides, indicating a continuum of collagen content in these fibrous tissues. These quantitative and qualitative

analyses of the tissue relate to the functional roles of the ligaments. Tissue tensile properties are derived from the collagen content (Eleswarapu et al. 2011) as well as other extracellular matrix components, like elastin (Smith et al. 2011). Therefore, it was hypothesized that the mechanical tensile properties of the ligaments would reflect tissue level characteristics. As expected, the tensile properties align with the trends in collagen content. Suction feeding fishes have more collagen and less elastin in their tissues compared to parrotfishes. This elucidates important structure-function relationships that can help to inform future hypotheses on the biomechanics and biochemistry of fish cranial ligaments.

Modeling of skull mechanics

The skull is a complex skeletal system that differs in kinesis across vertebrates. With variability in kinesis there are often differences in soft tissue, like muscles and ligaments. Few ligaments have been studied in the skull across vertebrates, mainly mammalian sutural ligaments (Sharp et al. 2023) and fish cranial ligaments (see Chapter 3). In our study the IOPM is important for fish feeding due to the pattern in its stiffness, whereas the function of sutural ligaments is still being debated (Rafferty and Herring 1999; Rayfield 2005; Popowics and Herring 2007). However, many models of the sutural ligaments have been created, and have led to more accurate computational models of the skull (Rafferty et al. 2003; Rayfield 2005; Moazen et al. 2009; Jones et al. 2017; Sharp et al. 2023).

Sutures in the cranium are composed of cartilaginous and fibrous soft tissue that combines to create a series of ligaments (Rafferty and Herring 1999; Moazen et al. 2009). Sutural ligaments have a low Young's Modulus (Popowics and Herring 2007), are viscoelastic (Tanaka et al. 2000; Popowics and Herring 2007), and show regional and age specific trends

(Popowics and Herring 2007). Much of the research on sutural ligaments involves computer models which use lower Young's Moduli than previously measured in vivo (Moazen et al. 2009; Jones et al. 2017; Sharp et al. 2023) and are more broadly sampled taxonomically (e.g., Jones et al., 2017; Moazen et al., 2009; Popowics and Herring, 2007; Rafferty et al., 2003; Rafferty and Herring, 1999; Rayfield, 2005; Sharp et al., 2023). Because sutural ligaments have a lower stiffness than the surrounding bone, these areas become a strain "sink" (Rafferty et al. 2003; Rayfield 2005) where it is hypothesized strain is high in order to protect the surrounding bone from damage. The inclusion of this soft tissue in musculoskeletal models creates conditions similar to *in vivo* measurements, indicating the inclusion of soft tissue mechanics is critical for understanding skeletal mechanics.

We suggest that a deeper understanding of the mechanical properties of cranial ligaments in fishes provides an opportunity to incorporate these structures and their function into computational models of the skull. The fish skull and its linkage systems have often been modeled (Westneat 1990, 1994, 2003; Olsen and Westneat 2016; Olsen et al. 2017) and the 3D motions of fish skulls measured *in vivo* (Camp and Brainerd 2014; Camp et al. 2015; Brainerd et al. 2016; Olsen et al. 2017; Laurence-Chasen et al. 2019; Gartner et al. 2022; Whitlow et al. 2022). Future modeling studies may benefit from including the cranial ligaments into their models due to our findings that the IOPM and CM ligaments play an important role during feeding. Inclusion of important soft tissues into these biomechanical models will further help to predict the sources of variation in fish feeding mechanics across a diversity of species.

CONCLUSION

Parrotfishes are shown here to possess highly compliant properties in both the coronomaxillary and interoperculomandibular ligaments, two important collagenous tissues that transfer force and motion within the fish feeding system. Parrotfishes appear to have evolved compliant ligaments for more kinesis between the bones and for forces to be damped during frequent contact with hard surfaces. This evolution of compliant ligaments allows parrotfish to feed in unique ways that help keep reefs healthy by enabling parrotfish to constantly scrape and excavate hard surfaces throughout the day. Extreme suction feeders, like the sling-jaw wrasse, consistently have the highest stiffness in their IOPM ligament, but exhibit low stiffness in their CM ligament due to the high force and high velocity suction feeding behavior. With a growing understanding of soft tissue material properties, we will likely have a more complete understanding of fish feeding mechanics which will provide additional parameters for computational biomechanical models and enable a more detailed study of the evolutionary patterns of skeletal and soft tissue components in fish skull mechanics on a broad scale.

CHAPTER 5: CONCLUSIONS

This thesis examines the geometric morphometrics and biomechanics of the four-bar linkage systems in the fish skull and the interactions between the cranial ligaments and the skeletal system. Three-dimensional geometric morphometrics analysis of μCT scanned skulls provides insight into the morphology of the skeletal system, and exploration of the mechanical properties of ligaments reveals the function of soft tissues in transmitting forces during feeding. Combining these two techniques in a biomechanical system, such as linkage mechanisms in the teleost skull, increases our understanding of the phylogenetic patterns and functional implications of change in four-bar linkage systems of the skull in labrid fishes, and reveals the diverse and novel roles of ligaments in the complex feeding mechanisms of teleost fishes. Notably, this thesis research has opened a previously unexplored area of research on the biomechanics of soft tissues in fish feeding mechanics that will change the way biomechanical modeling is performed in future research.

Previous studies using three-dimensional morphometrics in fishes have quantified the mosaic evolution of the skull (Evans et al. 2019; Larouche et al. 2022), revealed effects of the evolution of the skull associated with feeding specializations and morphologies (Evans et al. 2017, 2022), and highlighted the modular evolution of the skull (Evans et al. 2019; Larouche et al. 2022; Chapter 2). The research prior to this dissertation has shown functional patterns of modularity, rather than developmental modularity patterns, are strongly supported in explaining the skull diversity seen within wrasses. Additionally, this previous work (Larouche et al. 2022) has shown that the functional modules found for the wrasse skull evolve at different rates and under different modes, indicating the tempo and mode of evolution influences the evolutionary change in the labrid skull. Building on this prior work, the research presented here (Chapter 2) on

linkage modularity and integration shows that linkage systems often coevolve in an integrated way yet have become separate modules in several groups of labrid fishes, with implications for the evolution of morphological novelties and specialty behaviors in wrasse skulls and for the overall evolution of diversity in teleost fishes.

The testing and analysis of material properties in ligaments and tendons has been a central part of vertebrate biomechanics for decades. Most studies have been on locomotor structures like intervertebral disks (Long et al. 1997, 2002) and caudal tendons in fishes (Shadwick 1990; Shadwick et al. 2002), tendons in the hindlimbs of mammals (Ker 1981; Ker et al. 1986; Woo et al. 1986; Bennett et al. 1989; Danto and Woo 1993; Moon et al. 2006), and tendons in the feeding systems of cartilaginous fishes and hagfishes (Summers et al. 2002, 2003). These studies have found tendons and ligaments to be viscoelastic, to have relatively high stiffness values, and to have force damping capabilities. This previous research has shown that tendons and ligaments act as force transfer structures and shock absorbers. Relatively few studies have looked into the mechanical properties of the ligamentous system in the vertebrate skull, primarily exploring tensile tissues in mammalian skull mechanics (Moazen et al., 2009; Popowics and Herring, 2007; Rafferty and Herring, 1999; Tanaka et al., 2000). These studies have found ligaments in mammalian skulls to vary based on viscoelasticity and stiffness, however, these studies have mainly been limited to computational studies (Tanaka et al. 2000; Moazen et al. 2009) rather than experimental models (Popowics and Herring 2007). Similarly, in fishes there is a relatively unexplored area of research in the material properties and biomechanical roles of soft tissues that this dissertation has begun to investigate. The results of this dissertation (Chapter 3 and 4), break new ground in this area, with the extreme tensile

elasticity found in the ligaments of wrasses and parrotfishes representing a potentially transformative discovery impacting our understanding of skull function in fishes.

This dissertation has explored three-dimensional geometric morphometrics to assess patterns of evolution in linkage modularity and integration and use mechanical testing and histology to understand the role of ligaments in the function of the four-bar linkage systems in the teleost skull. Specifically, the research presented in this thesis yields new insights into the morphology and function of the four-bar linkage systems, skull modularity and ligament biomechanics. In the sections below, broader conclusions and future directions are developed to establish a framework for research on geometric morphometrics, analysis of the function of the four-bar linkage systems and expanding the present studies to broader phylogenetic contexts.

Insights into the three-dimensional geometry of the labrid skull

Wrasses are a diverse group of coral reef fishes that have been shown to differ in linear metrics (Wainwright et al. 2004), muscle activation patterns (Alfaro and Westneat 1999), and three-dimensional shape (Larouche et al. 2022). These fishes also have very diverse diets from wrasses that clean parasites off other fish (Grutter 1996) to parrotfishes that browse and excavate hard coral skeletons (Bellwood and Choat 1990; Nicholson and Clements 2020). With all these differences, there are some features that are shared among wrasses, mainly in the mechanics of their skull. All wrasses have at least three four-bar linkage systems (Westneat 1990), an engineering principle in which four rotational joints are connected by four links and for which predictions of movement can be quantified. The feeding systems in wrasses, like other teleosts, are made up of skeletal, muscular, and ligamentous elements that also function to hold together and move the skull. This thesis has demonstrated that the linkage systems in wrasse skulls are

modular compared to the remainder of the skull (i.e., neurocranium, nasals, pharyngeal jaws, and premaxilla) and that modularity is a potential factor in the evolution of morphological novelties in the labrid skull. The labrid pattern of modularity splits the skull into two subunits of traits: the linkage systems and the neurocranium. These two modules are evolving independently of one another, suggesting that evolutionary processes may influence these two units separately. This allows for the linkage systems in wrasses to evolve separately and potentially to increase the likelihood of new anatomical configurations in the labrid feeding system.

This thesis has further shown there to be differences between the modularity patterns across four wrasse tribes: scarines, cheilines, julidines, and hypsigenyines. In the scarines a pattern of increased modularization of the skull was found, with the skull being partitioned into a multitude of different subunits of traits. This pattern may have driven the multiple skeletal differences in the scarines, including a mobile intramandibular joint and a beak for their oral jaws. These differences are a central influence in the phylomorphospace for the group, in which scarines occupy a region separate from the other wrasses. Cheilines also have more modular skulls compared to the overall family-level labrid pattern of modularity. The cheilines have extreme differences in their skeletal morphology as well, ranging from the small amphipod predator *Wetmorella* to the giant hump-head wrasse to the unusual sling-jaw wrasse. The hypsigenyines and julidines have a similar modularity pattern to the overall family pattern of linkages sharing a single module, and yet these tribes also exhibit diversity in skull shape. An interesting area of research might involve analyzing the detailed kinematics of labrid cranial linkages during live feeding in wrasses and more broadly, to test the idea that patterns of structural diversity are reflected in feeding behavior.

Similarly, with 200 of the 630 species analyzed here, additional 3D morphometrics work will be informative. Future work on the geometric morphometrics of the wrasse skull should be focused on increasing the sample size for the remainder of the tribes and to investigate the population level modularity patterns. In order to understand the evolutionary patterns of modularity across the labrid tree, the patterns of modularity for each tribe must be investigated. This thesis looked at four of the tribes in the wrasse phylogeny, but there are still four tribes left to be analyzed. To do this, more μCT scans need to be collected from species in these tribes. From a broader sample of other tribes analyzed in this suggested dataset, we might examine patterns of modularity and function in intriguing groups such as the cleaner wrasses (Labrichthyinini) and razorfishes (Novaculini).

Next, population level patterns should be investigated. This would require collection of μCT scans of many individuals from the same species of wrasse. The dataset would further help to understand some of the developmental and functional modularity patterns within wrasses. Does specialty feeding behavior confer differences in the pattern of modularity? Does the sling-jaw wrasse have a different pattern of modularity than the cheilines? Do all julidines show a more integrated pattern of modularity in their skull? We hypothesize that understudied groups and specialized feeding guilds such as the sling-jaw, cleaner wrasses, and the herbivorous odacines with specialty feeding behaviors are likely to exhibit increased modularization of the skull, similar to scarines. This might greatly enhance the number of ways in which we understand how modularity influences the diversity of novel morphologies and behaviors in wrasses.

Insights into the material properties of cranial ligaments in labrids

This thesis has shown wrasse cranial ligaments to be highly variable, often possessing tensile properties that are associated with species-specific feeding behavior. Ligaments are an essential fibrous tissue that connects bone to bone in the musculoskeletal system. In the fish skull, ligaments are essential for transferring force from the epaxial and hypaxial musculature to the oral jaws for suction feeding or biting (Camp et al. 2015). Three of the main ligaments in the fish skull, the coronomaxillary (CM), interoperculomandibular (IOPM), and interoperculohyoid (IOPH), are pivotal for the fish skull to work. Without ligaments, bones would not be able to move cohesively, and forces would not be transferred through the skull efficiently.

The CM appears to show an interesting relationship with feeding behavior. The position of the ligament is in an important place in the skull, between the oral jaws, so this may be influencing the mechanical properties of the ligament. *Oxycheilinus unifasciatus* and *Epibulus insidiator* are mainly piscivorous and they have one of the most compliant ligaments compared to the majority of biting and mixed feeding species. *O. unifasciatus* is able to protrude their jaws for evasive prey capture (Westneat 1994), while *E. insidiator* is known for having one of the most protrusible jaws in teleosts (Westneat and Wainwright 1989; Westneat 1991). One of the surprising findings of this thesis research is that having protrusible jaws may confer a need for CM ligament compliance to damp forces at the tip of the feeding system (i.e., the oral jaws) in order to dissipate the forces resulting from the jaws contacting prey or the substrate during the feeding strike.

Two wrasses sampled from the hogfish clade of the Hypsigenyini, *Bodianus rufus* and *Lachnolaimus maximus*, have CM stiffness resembling examples measured in parrotfishes. Such similarity might result from similar functional demands on the oral jaws. Modulation of the oral

jaws has been measured in multiple species of fish (Sanford 2001; Camp et al. 2009; Van Wassenbergh and De Rechter 2011). The ability to actively or passively tune the movements of the oral jaws may allow biting species to better set up their oral jaws for the multiple bites during feeding bouts. Future studies should compare behavioral modulation, or variability of kinematics under different conditions, of the oral jaws between suction feeding and biting species to better understand the kinematics and the role of ligament tensile properties associated with these feeding behaviors.

The properties of the IOPM are closely associated with feeding behavior. In suction feeding fishes, the IOPM is stiffer compared to species that solely bite or scrape the substrate. Suction feeding involves bones stretching apart, pulling on the interconnecting soft tissues (Camp and Brainerd 2014), and thereby stretching the IOPM which is a part of the opercular four-bar linkage system (Westneat 1990; Olsen et al. 2017). The opercular linkage system helps transmit force from the epaxial musculature to the opercular apparatus through the IOPM, and also contributes to the depression of the lower jaw (Westneat 1990; Camp and Brainerd 2014; Olsen et al. 2017). Additionally, the linkage system emphasizes moving the jaw rapidly rather than forcefully when the jaw opens (Westneat 1994). This relates to the function of the IOPM which, when compared to the other ligaments, has the mechanical properties (i.e., high stiffness) required for transferring force rapidly through suspensorial and mandibular systems.

The IOPH is the final ligament in the series and has a fairly consistent set of compliant, low modulus properties across all species measured. The IOPH is in the posterior region of the skull and stretches during feeding and breathing, or when the ceratohyal depresses and the operculum abducts. Being positioned away from the feeding apparatus may be the reason this ligament is not as finely tuned to the feeding habits of labrids as the IOPM. The IOPH has a low

Young's Modulus with a high breaking strain and high resilience, indicating this ligament is acting much like a spring in its operculo-hyoid connection. The hyoid apparatus is an important structure for the success of suction feeding and processing of prey (Camp and Brainerd 2015; Weller et al. 2020; Gartner et al. 2022; Whitlow et al. 2022). Being able to modulate the complex rotations of the ceratohyal may be important for the successful intake and processing of prey. Therefore, the IOPH is most likely allowing for mechanical flexibility between the ceratohyal and interopercle to occur, possibly leading to changes in the speed and motion of the ceratohyal and hyoid apparatus.

Overall, a central insight from this research is that the stiffness versus compliance of cranial ligaments is essential to the musculoskeletal system and is influenced by feeding behavior and habits across wrasses. Compliant ligaments appear to be a way to damp high forces entering the feeding apparatus when eating hard prey or during a forceful suction feeding event. In contrast, stiff ligaments allow for forces to be transferred faster through the tissue, getting forces to the oral jaws rapidly. The function of the ligaments affects how labrid species are able to feed on a variety of prey items and represent an important trait of complex fish feeding mechanisms.

Comparison of the function of the parrotfish beak

The parrotfish beak is an evolutionary innovation of the labrid tribe Scarini which allows these fish to graze, scrape, and excavate coral. The beak is one of the hardest biomaterials that has been measured (Marcus et al. 2017) and is defined as a coalescence of teeth into a cutting edge of the upper and lower jaws (Bellwood and Choat 1990; Bellwood 1994). Parrotfishes have

evolved these beaks that are a specialized morphology to allow them access to a new resource not available to other wrasses.

We surprisingly find no differences in ligament material properties between the reef clade (*Scarus and Chlorurus*) and the seagrass clade (*Sparisoma and Calotomus*). The muscle activation patterns differ between these two clades (Alfaro and Westneat 1999), the overall shape of the skull differs in morphospace (see Chapter 2 Fig 2.4), and the bite rate differs between the two clades (Holzer et al., 2013; Ong and Holland, 2010; Peoples, N. unpublished data). Due to these differences we expected to find differences in their ligament properties as well, but our data do not support any significant differences between the groups with our current sample. Instead, the parrotfish have highly compliant ligaments for all three tested ligaments. Parrotfishes graze algae and bite hard coral skeletons in high frequency bouts during daylight hours. This may be the reason parrotfishes have highly compliant ligaments because they frequently stretch their ligaments throughout the day. Compliant ligaments function to reduce susceptibility to damage over frequent loading cycles (Thornton et al. 2007; Biewener 2008). Having compliant ligaments likely enables parrotfishes to constantly feed through the day regardless of the bite rate, muscle activation patterns, or presence of a mobile intramandibular joint.

Many species have evolved novel morphologies within their feeding systems to access resources they otherwise couldn't get. The beak of the parrotfishes has given these fish access to resources other wrasses cannot attain and the beak seems to act as a hammer when feeding, like the woodpecker beak. The woodpecker beak has a keratinized outer layer, spongy middle layer, and bony inner layer (Lee et al. 2014) which helps to increase stiffness in the beak. The spongy middle layer, as well as the enlarged hyoid and tongue, has been hypothesized to act as a shock absorbing system and/or damping systems (Jung et al. 2016), but this hypothesis was recently

revised (Van Wassenbergh et al. 2022). Instead, the beak has evolved to act like a stiff hammer where woodpeckers decrease their impact time to increase their performance of their beaks (Van Wassenbergh et al. 2022). However, the soft tissues, like the tongue and cranial ligaments, may still be dissipating stress when the woodpecker pecks as the revised hypothesis does not talk about the soft tissue mechanical properties. Woodpeckers use their beaks to access a new food resource they couldn't access without this specialized morphology. Parrotfish also exhibit this phenomenon where they have evolved specialized morphology to access a new resource.

The parrotfish beak may be acting similarly like a hammer as the woodpecker beak functions, but there is one main difference: if parrotfish increase their impact time, the beak's performance would increase by enabling larger chunks of prey to be acquired. This leads to the conclusion that no two hammers are the same. Therefore, the parrotfish can't be using their beaks as a stiff hammer and must be using their beaks as a shock absorbing system. In addition, the compliant ligaments this thesis has found in the parrotfish skull may be aiding this system. By having compliant ligaments, parrotfish can increase impact time and dissipate the shock added to the system. The compliant ligaments allow parrotfish to increase the performance of their feeding system and absorb the shock added to the system every time an individual feeds. In this way, the parrotfish beak is acting like a hammer with a spring attached.

The future of fish skull modeling

The few models of fish skulls that have been created have focused on the four-bar linkage systems (Westneat 1990, 2003; Olsen and Westneat 2016; Olsen et al. 2017) or are models that come from time intensive methods, like X-ray Reconstruction of Moving Morphology (XROMM) (Gidmark et al. 2013; Camp and Brainerd 2014; Camp et al. 2015; Laurence-Chasen

et al. 2019; Gartner et al. 2022; Kaczmarek et al. 2022; Whitlow et al. 2022). So far, there have been no models using material properties of the musculoskeletal system integrated into a 3D model. Finite element analysis (FEA) is a static modeling method that estimates the stress or strain across a skull (Rayfield et al. 2001). This method uses the mechanical properties of the bone and muscle to understand how the skull receives stress from an input force (e.g., bite force). With the new information on ligament material properties in this thesis, we may be able to also model the ligaments as FEA models to understand how ligaments permit stress in certain areas of the skull. Future studies should integrate the information from this thesis with skeletal material properties of fish to understand the static changes in the skull during suction feeding or biting.

Additionally, new work on a dynamic FEA model has been ongoing in the medical field using Artisynth (Lloyd et al. 2012). This type of model can be built from many components like muscles and ligaments, unilateral and bilateral constraints, and other skeletal or muscular elements. Artisynth is a physics simulator that was originally created to model the mechanics of speech production. It has expanded to modeling the head and neck region in physiology, dentistry, medicine and linguistics (Lloyd et al. 2012). However, with the understanding of the material properties of ligaments and muscle activation patterns in fishes (Alfaro and Westneat 1999; Friel and Wainwright 1999; Alfaro et al. 2001; Grubich 2001), we could theoretically use Artisynth to model fish skulls during suction feeding or biting behaviors. Therefore, we can model the lengthening and compression of ligaments and from this one can understand how the ligaments affect the movement of the skeletal components in the skull. Future studies should focus on using Artisynth to model multibody, dynamic fish skulls more accurately. In this way we can further understand skull mechanics without going through arduous and time-consuming methods.

Future Studies: Strain Rate, XROMM, and Phylogenetic Breadth

Due to the integrative nature of the studies, there remain more questions than answers. Future work should focus on 1) quantifying the effect strain rate has on the mechanical properties; 2) understanding the *in vitro* vs. *in vivo* mechanical properties of the ligaments and 3) broadening the phylogenetic study to understand if the relationship in fishes is similar across varying taxa.

Understanding Strain Rate Effects

I want to investigate the effect of strain rate on Young's Modulus (E) in fishes. In the mammal literature, strain rate has a significant effect on E where the higher the strain rate, the higher the E measured. In this thesis, strain rate was based off previous literature and the frequency of biting by parrotfishes. I want to understand how changing this rate affects E because parrotfish and the sling-jaw wrasse feed at vastly different rates. I want to see how strain affects the cranial ligament to better understand how the ligaments function *in vivo.* Previous literature has shown a relationship between strain rate and E, but it becomes more complicated for other mechanical properties measured (Danto and Woo 1993). Understanding how strain rate affects the mechanical properties can help when choosing a strain rate for a broad phylogenetic study. Should strain rate remain the same across species? Or should it vary for each species based on the frequency of jaw movement. These are some of the questions I hope will be answered with this research.

Using XROMM data for in vivo measurements

XROMM or X-ray Reconstruction of Moving Morphology is a widely used technique in which you can measure 3D movements of skeletal elements from live animals. This technique has recently been used more in fishes to understand the movements of a complex system. With previously collected XROMM data, we can start to ask questions beyond the skeletal movements and more about the musculoskeletal system. Movement of the bones correspond to movements in the soft tissue of the animal. By understanding the placement of ligaments, we can begin to model the stretch-relaxation cycles of these ligaments. Additionally, modeling the ligaments *in vivo* can help to understand how these ligaments are functioning in real time.

Additionally, new XROMM data should be collected on varying fish species. During my tenure at the University of Chicago, I collected some preliminary XROMM data on a parrotfish, *Scarus taeniopterus*. Due to logistical challenges, I was unable to collect a full dataset on this species. I want to continue this study and collect more XROMM data from parrotfishes. This will help elucidate how biting species are using their ligaments. There is still debate on when the ligaments are being held in tension (i.e., when the mouth is opening or closing) and when the ligaments are slack. By using XROMM data on parrotfish, we can begin to understand the solution to these questions for such a quintessential biting species.

Broadening the phylogenetic study

Throughout this thesis, I focused on the ligaments and linkages in teleost fishes, specifically in wrasses. Future work should include adding more teleost fishes and other species with kinetic skulls, in order to understand how soft tissues function in kinetic environments. One of the main goals of this thesis is to provide the foundation for more studies on ligament material

properties. Questions on the mechanical and histological properties of ligaments should be asked to understand the large-scale evolutionary patterns of soft tissue. Other species throughout the tree of life have kinetic skulls that are connected by soft tissues, such as birds. Birds have a shared trait of cranial kinesis with fishes, and they have ligaments that help transmit force through the skull. Investigating birds would allow for the discovery of potentially similar patterns with specialized behavior to those found in wrasses. This can increase our knowledge about ligament properties across different vertebrate clades. This project can also help us to understand the ecology of the birds further by quantifying the interactions between the musculoskeletal system of birds.

Alongside ligaments in kinetic structures, I am also interested in ligaments that help stabilize joints, like the anterior cruciate ligament (ACL) in humans, or ligaments that have ossified over evolutionary time, like the postorbital ligament in birds vs. the skeletal postorbital bar in lizards. Ligaments are essential soft tissue to the musculoskeletal system, yet they are often understudied. Understanding the mechanical properties of ligaments in vertebrates can help to understand how joints are stabilized, how shock is dissipated, and how force moves through a musculoskeletal system. Understanding ligaments is inter-disciplinary in nature and can further our knowledge of soft tissue biomechanics.

APPENDIX A – SUPPLEMENTARY TABLES AND FIGURES FOR CHAPTER 2

Appendix A Figure 1 – 3D model of the landmark (blue dots) and semi-landmark (red dot) positions. Illustrated on a *Halichoeres bivittatus* specimen.
Taken with permission from Larouche et al. 2022.

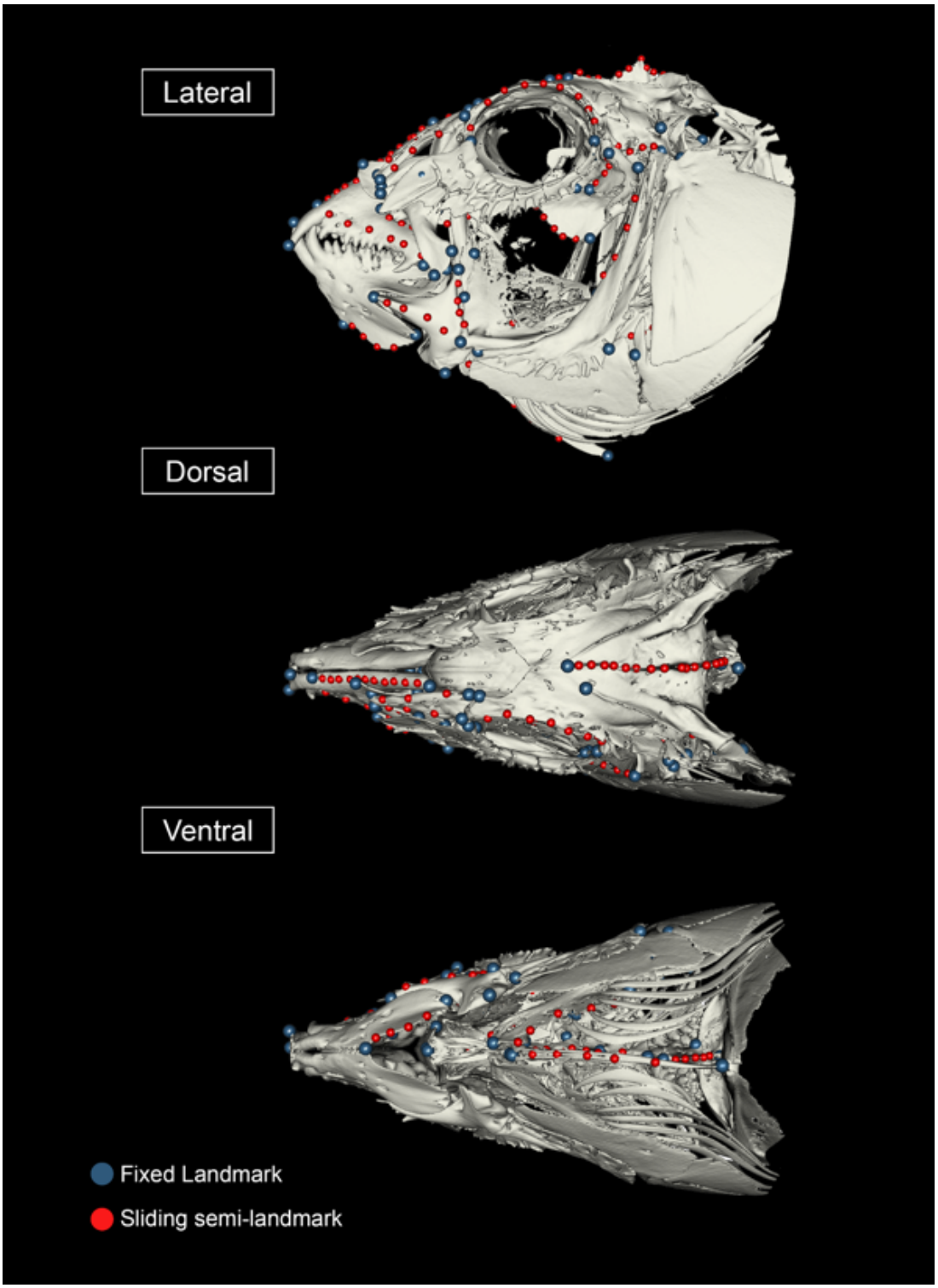

Appendix A Table 1 – Materials examined for the three-dimensional geometric morphometric analysis of 206 skull shape in wrasses.
BMNH= British Museum of Natural History, ANSP= Academy of Natural Sciences of Drexel University, FMNH= Field Museum of Natural History, uncat= uncatalogued, AMNH= American museum of Natural History, AM= Australian Museum, UWFC= Burke Museum of Natural History, USNM=Smithsonian Museum of Natural history, BPBM= Bernice Pauahi Bishop Museum. Adapted from Evans et al. 2022.

Species	Museum Code	Catalog number
Acantholabrus palloni	BMNH	5492
Achoerodus gouldii	ANSP	13450
Anampses chrysocephalus	FMNH	63668
Anampses cuvier	FMNH	63669
Anampses femininus	Uncat	
Anampses geographicus	FMNH	110638
Anampses melanurus	Uncat	
Anampses meleagrides	FMNH	124439
Anampses neoguinaicus	FMNH	120173
Anampses twistii	FMNH	119451
Austrolabrus maculatus	FMNH	138043
Bodianus axillaris	FMNH	124032
Bodianus bilunulatus	Uncat	
Bodianus diana	FMNH	124487
Bodianus dictynna	FMNH	124034
Bodianus loxozonus	FMNH	112723
Bodianus mesothorax	FMNH	126755
Bodianus pulchellus	FMNH	73534
Bolbometopon muricatum	FMNH	119522
Calotomus carolinus	FMNH	123890
Calotomus japonicus	FMNH	572478
Calotomus spinidens	FMNH	110792
Centrolabrus exoletus	BMNH	1975-8-18
Cetoscarus bicolor	FMNH	110797
Cheilinus abudjubbe	FMNH	
Cheilinus bimaculatus	FMNH	
Cheilinus chlorourus	FMNH	120176
Cheilinus fasciatus	FMNH	124051
Cheilinus lunulatus	FMNH	
Cheilinus oxycephalus	FMNH	120182
Cheilinus trilobatus	FMNH	126786
Cheilinus undulatus	FMNH	110658
Cheilio inermis	FMNH	126789
Chlorurus bleekeri	FMNH	118756
Chlorurus bowersi	FMNH	138383

Chlorurus capistratoides	FMNH	123894
Chlorurus gibbus	FMNH	110803
Chlorurus japanensis	FMNH	118758
Chlorurus microrhinos	FMNH	119524
Chlorurus oedema	FMNH	110932
Chlorurus perspicillatus	FMNH	73775
Chlorurus spilurus	FMNH	
Choerodon anchorago	FMNH	119442
Choerodon oligacanthus	FMNH	51758
Choerodon schoenleinii	FMNH	110673
Choerodon zosterophorus	FMNH	110674
Cirrhilabrus cyanopleura	FMNH	126811
Cirrhilabrus exquisitus	FMNH	126814
Cirrhilabrus punctatus	FMNH	134111
Cirrhilabrus scottorum	FMNH	127220
Cirrhilabrus temminckii	FMNH	126819
Clepticus parrae	FMNH	62916
Coris aygula	FMNH	112777
Coris batuensis	FMNH	110680
Coris dorsomacula	FMNH	112778
Coris gaimard	FMNH	110684
Coris julis	FMNH	46108
Coris pictoides	FMNH	126830
Coris venusta	FMNH	128476
Cryptotomus roseus	FMNH	65595
Ctenolabrus rupestris	BMNH	1986-8-7
Cymolutes torquatus	FMNH	110686
Decodon puellaris	FMNH	66713
Diproctacanthus xanthurus	FMNH	118887
Doratonotus megalepis	FMNH	61535
Epibulus insidiator	FMNH	86378
Eupetrichthys angustipes	FMNH	138034
Gomphosus caeruleus	FMNH	80054
Gomphosus varius	FMNH	127214
Haletta semifasciata	AMNH	I.20180013
Halichoeres argus	FMNH	124452
Halichoeres binotopsis	FMNH	75982
Halichoeres bivittatus	FMNH	45567
Halichoeres chloropterus	FMNH	126858
Halichoeres chrysus	FMNH	110699
Halichoeres dispilus	FMNH	72294
Halichoeres garnoti	FMNH	65314
Halichoeres hartzfeldii	FMNH	110701

Halichoeres hortulanus	FMNH	126864
Halichoeres leucurus	FMNH	120159
Halichoeres maculipinna	FMNH	65217
Halichoeres margaritaceus	FMNH	112803
Halichoeres marginatus	FMNH	124460
Halichoeres melanochir	FMNH	126991
Halichoeres melanurus	FMNH	124110
Halichoeres melasmapomus	FMNH	119486
Halichoeres nebulosus	FMNH	40651
Halichoeres podostigma	FMNH	110709
Halichoeres poeyi	FMNH	67745
Halichoeres prosopeion	FMNH	120160
Halichoeres richmondi	FMNH	124120
Halichoeres scapularis	FMNH	118725
Halichoeres trimaculatus	FMNH	112810
Hemigymnus fasciatus	FMNH	127216
Hemigymnus melapterus	FMNH	80132
Heteroscarus acroptilus	AM	15751-005
Hipposcarus harid	ANSP	103766
Hipposcarus longiceps	FMNH	119526
Hologymnosus doliatus	FMNH	121072
Iniistius bimaculatus	FMNH	127213
Iniistius dea	FMNH	57355
Iniistius pavo	UWFC	7203
Iniistius pentadactylus	FMNH	47707
Iniistius umbrilatus	FMNH	128485
Labrichthys unilineatus	FMNH	120192
Labroides pectoralis	FMNH	119497
Labropsis australis	FMNH	127211
Labrus merula	FMNH	109161
Labrus mixtus	BMNH	FS492
Labrus viridis	FMNH	109162
Lachnolaimus maximus	ANSP	49141
Leptoscarus vaigiensis	FMNH	110821
Macropharyngodon geoffroy	FMNH	63593
Macropharyngodon meleagris	FMNH	124602
Macropharyngodon negrosensis	Uncat	
Malapterus reticulatus	FMNH	107424
Neodax balteatus	AM	I.20179-015
Nicholsina usta	USNM	202348.5062
Notolabrus gymnogenis	FMNH	135921
Novaculichthys taeniourus	FMNH	118735
Novaculoides macrolepidotus	FMNH	110729

Odax cyanoallix	AMNH	17019008
Odax pullus	AMNH	123364001
Olisthops cyanomelas	AMNH	I.17019008
Ophthalmolepis lineolata	FMNH	137991
Oxycheilinus arenatus	BPBM	24119
Oxycheilinus celebicus	FMNH	127140
Oxycheilinus digramma	FMNH	124596
Oxycheilinus nigromarginatus	FMNH	
Oxycheilinus orientalis	FMNH	127162
Oxycheilinus unifasciatus	FMNH	
Oxyjulis californica	FMNH	77933
Paracheilinus filamentosus	FMNH	127167
Pictilabrus laticlavius	FMNH	137988
Pseudocheilinops ataenia	FMNH	124174
Pseudocheilinus evanidus	FMNH	130899
Pseudocheilinus hexataenia	FMNH	112884
Pseudocheilinus octotaenia	FMNH	118982
Pseudocoris yamashiroi	FMNH	119504
Pseudodax moluccanus	FMNH	119120
Pseudojuloides cerasinus	FMNH	127186
Pseudolabrus guentheri	FMNH	135927
Pseudolabrus luculentus	FMNH	137990
Pteragogus cryptus	FMNH	127188
Scarus chameleon	FMNH	110833
Scarus coelestinus	ANSP	75173
Scarus coeruleus	FMNH	46860
Scarus dimidiatus	FMNH	127258
Scarus dubius	FMNH	49154
Scarus festivus	FMNH	118765
Scarus flavipectoralis	FMNH	123906
Scarus forsteni	FMNH	127261
Scarus frenatus	ANSP	151966
Scarus globiceps	ANSP	9279
Scarus guacamaia	JFBM	29376
Scarus hypselopterus	FMNH	110849
Scarus maculipinna	FMNH	117286
Scarus niger	FMNH	127266
Scarus oviceps	FMNH	118773
Scarus prasiognathos	ANSP	151958
Scarus psittacus	FMNH	110857
Scarus quoyi	FMNH	127343
Scarus rubroviolaceus	ANSP	51097
Scarus russelii	ANSP	103714

Scarus schlegeli	ANSP	122616
Scarus spinus	FMNH	119521
Scarus taeniopterus	ANSP	9290
Scarus tricolor	FMNH	118780
Scarus viridifucatus	ANSP	109275
Semicossyphus pulcher	FMNH	62769
Siphonognathus argyrophanes	AMNH	120180014
Siphonognathus radiatus	AMNH	I.200228008
Sparisoma aurofrenatum	FMNH	108733
Sparisoma axillare	FMNH	74653
Sparisoma choati	UF	179646
Sparisoma chrysopterum	FMNH	67987
Sparisoma cretense	ANSP	9281
Sparisoma radians	FMNH	5391
Sparisoma rubripinne	ANSP	9294
Sparisoma viride	ANSP	75014
Stethojulis balteata	FMNH	80145
Stethojulis bandanensis	FMNH	110746
Stethojulis interrupta	FMNH	124466
Suezichthys gracilis	FMNH	127196
Symphodus mediterraneus	FMNH	109164
Symphodus ocellatus	FMNH	63840
Symphodus rostratus	FMNH	109168
Symphodus tinca	FMNH	46103
Tautoga onitis	FMNH	5857
Tautogolabrus adspersus	JFBM	14932
Terelabrus dewapyle	FMNH	133681
Thalassoma amblycephalum	FMNH	130928
Thalassoma ballieui	FMNH	129436
Thalassoma bifasciatum	FMNH	108729
Thalassoma cupido	FMNH	89117
Thalassoma duperrey	FMNH	128475
Thalassoma hardwicke	FMNH	127202
Thalassoma lunare	FMNH	120214
Thalassoma lutescens	FMNH	121076
Thalassoma quinquevittatum	FMNH	127208
Wetmorella nigropinnata	FMNH	130978
Xenojulis margaritaceus	FMNH	110771
Xiphocheilus typus	FMNH	110772
Xyrichtys martinicensis	JFBM	19343
Xyrichtys novacula	FMNH	46615

Appendix A Table 2 - Descriptions of homologous anatomical landmarks and curves for sliding semi-landmarks adapted from Larouche et al. 2022.
The three points added to this study are bolded (192-194).

Homologous anatomical landmarks	
Landmark #	**Definition**
1	Most distal point of first tooth on premaxilla
2	Base of first tooth
3	Most distal point of ascending process of premaxilla
4	Proximal vertex between ascending and descending processes of premaxilla
5	Most distal point of descending process of premaxilla
6	Most distal point of first tooth on dentary
7	Posterior-most point on dentary flange
8	Ventral-most point of mental symphysis on dentary
9	Antero-distal-most point of articular/angular
10	Distal-most point of coronoid process
11	Ventral, posterior-most point of dentary
12	Center of jaw joint on quadrate
13	Posterior-most point on retroarticular
14	Most anterior point of vomer
15	Left, distal-most point on anterior of vomer (used to approximate width of vomer)
16	Proximal lachrymal-lateral ethmoid margin
17	Proximal lateral ethmoid-parasphenoid margin
18	Dorsal-most point of lachrymal
19	Proximal-most point of lateral ethmoid frontal margin
20	Origin of supraoccipital
21	Posterior frontal sub-orbital margin
22	Pterosphenoid-parasphenoid margin
23	Mid-point parasphenoid-basioccipital margin
24	Prootic foramen
25	Frontal parietal margin
26	Posterior-most point of supraoccipital
27	Ventral epiotic-post temporal margin
28	Distal-most dorsal point of basioccipital
29	Pterotic-post temporal margin
30	Distal-most ventral point of basioccipital
31	Anterior most point of lower pharyngeal jaw plate
32	Descending process of lower pharyngeal jaw plate
33	Lateral-central most point of pharyngeal tooth plate
34	Ventral base of descending process of pharyngeal tooth plate
35	Lateral wing of pharyngeal tooth plate
36	Posterior center-most point of pharyngeal tooth plate
87	Distal, dorsal anterior margin of maxilla
88	Distal, dorsal posterior margin of maxilla
89	Distal, ventral anterior margin of maxilla

90	Distal, ventral posterior margin of maxilla
91	Proximal, dorsal anterior margin of maxilla
92	Proximal, dorsal posterior margin of maxilla
93	Anterior-most point of the proximal descending process of maxilla
94	anterior-most point of contact on the distal face of the hyomandibula between hyomandibula and sphenotic
95	posterior-most point of contact on the distal face of the hyomandibula between the hyomandibula and the pterotic
96	Distal-most point of lateral projection of hyomandibula
97	Anterior-ventral most point of hyomandibula
98	Ventral-most point of hyomandibula
99	Anterior, proximal-most point of nasal
100	Anterior, distal-most point of nasal
101	Posterior, proximal-most point of nasal
102	Posterior, distal-most point of nasal
150	Dorsal, anterior-most point of urohyal
151	Ventral anterior-most point of urohyal
152	Dorsal, posterior-most point of urohyal
153	Ventral, posterior-most point of urohyal
154	Anterior-most point of ceratohyal
155	Interior-ridge of ceratohyal
156	Dorsal ceratohyal-epihyal margin
157	Posterior-most point of epihyal
158	Ventral ceratohyal-epihyal margin
179	left outside angle of preoperculum
180	left anterior tip of preoperculum
181	left interopercle-opercle joint
182	left joint between preoperculum and neurocranium
183	left joint between hyomandibula and operculum
184	left anterior tip of palatine
185	left dorsal point on curve of palatine
186	left ventral tip of palatine at pterygoid joint
187	left dorsal tip of palatine at pterygoid joint
188	anterior tip of hypohyal
189	posterior tip of hypohyal
190	joint between hypohyal and ceratohyal
191	left dorsal tip of interhyal
192	**left ventral tip of pectoral girdle**
193	**left joint between cleithrum and supracleithrum**
194	**left joint between supracleithrum and posttemporal**
195	left side of joint between upper pharyngeal jaws
196	left dorsal point of upper pharyngeal jaws
197	left ventral point of upper pharyngeal jaws
198	left lateral point on upper pharyngeal jaws
199	left upper pharyngeal jaw joint
200	left uppermost tip of upper pharyngeal jaw

Homologous curves for the positioning of sliding semi-landmarks

Landmark #	Definition
37-47	Curve 1: Ascending process of premaxilla, between landmarks 2 and 3
48-51	Curve 2: Ventral margin of dentary, between landmarks 8 and 11
52-62	Curve 3: Ventral margin of parasphenoid, between landmarks 14 and 23
63-77	Curve 4: Supraoccipital crest, between landmarks 20 and 26
78-86	Curve 5: Orbital margin, between landmarks 18 and 21
103-106	Curve 6: Angular ascending process, between landmarks 10 and 12
107-110	Curve 7: Angular lateral process, between landmarks 9 and 12
111-115	Curve 8: Lateral arm of lower pharyngeal tooth plate, between landmarks 34 and 35
116-120	Curve9: Descending process of lower pharyngeal tooth plate, between landmarks 34 and 32
121-126	Curve 10: Descending arm of premaxilla, between landmarks 4 and 5
127-131	Curve 11: Lateral arm of premaxilla, between landmarks 2 and 5
132-135	Curve 12: Anterior face of hyomandibula, between landmarks 94 and 97
136-139	Curve 13: Dorsal surface of hyomandibula, between landmarks 94 and 95
140-143	Curve 14: Posterior face of hyomandibula, between landmarks 96 and 98
144-146	Curve 15: Nasal interior surface, between landmarks 99 and 101
147-149	Curve 16: Nasal outer edge, between landmarks 100 and 102
159-163	Curve 17: Urohyal dorsal edge, between landmarks 150 and 152
164-168	Curve 18: Urohyal ventral edge, between landmarks 151 and 153
169-173	Curve 19: Ceratohyal dorsal ridge, between landmarks 154 and 156
174-178	Curve 20: Ceratohyal ventral ridge, between landmarks 154 and 158

Appendix Table 3 – Covariance ratio (CR) effect size values for Labridae

Hypothesis	CR effect size
No_Modules	0
AllSpec.CR.phy[[1]]	-12.37992
AllSpec.CR.phy[[2]]	-16.329085
AllSpec.CR.phy[[3]]	-17.075366
AllSpec.CR.phy[[4]]	-9.9120865
AllSpec.CR.phy[[5]]	-9.0603876
AllSpec.CR.phy[[6]]	-6.1918992
AllSpec.CR.phy[[7]]	-6.6640179
AllSpec.CR.phy[[8]]	-7.1986239
AllSpec.CR.phy[[9]]	-7.329061
AllSpec.CR.phy[[10]]	-11.009643
AllSpec.CR.phy[[11]]	-10.853098
AllSpec.CR.phy[[12]]	-11.575224
AllSpec.CR.phy[[13]]	-11.814297

Appendix A Table 4 – Deviance information criterion (DIC) scores for Labridae from the distance matrix approach

nullhyp	mod1	mod2	mod3	mod4	mod5
0	2319.12689	200.173624	330.226414	602.649376	734.442172
0	539.709583	128.970009	138.422857	209.469841	225.426291
mod6	mod7	mod8	mod9	mod10	mod11
514.225701	710.239417	916.701412	1114.45514	288.774675	484.788382
222.687347	293.807795	303.187175	380.811218	193.706785	264.827232
mod12	mod13	type			
691.250404	889.004129	GPA_notsepManS			
274.206613	351.830657	GPA_sepManS			

Appendix A Table 5 – Covariance ratio (CR) effect size values for hypsigenyines

Hypothesis	CR effect size
No_Modules	0
AllSpec.CR.phy.hypsigenyines[[1]]	-7.279996
AllSpec.CR.phy.hypsigenyines[[2]]	-11.863176
AllSpec.CR.phy.hypsigenyines[[3]]	-8.5617445
AllSpec.CR.phy.hypsigenyines[[4]]	-9.957714
AllSpec.CR.phy.hypsigenyines[[5]]	-8.6428508
AllSpec.CR.phy.hypsigenyines[[6]]	-8.867686
AllSpec.CR.phy.hypsigenyines[[7]]	-10.014061
AllSpec.CR.phy.hypsigenyines[[8]]	-10.800087
AllSpec.CR.phy.hypsigenyines[[9]]	-11.770895
AllSpec.CR.phy.hypsigenyines[[10]]	-14.77759
AllSpec.CR.phy.hypsigenyines[[11]]	-15.872447
AllSpec.CR.phy.hypsigenyines[[12]]	-15.142948
AllSpec.CR.phy.hypsigenyines[[13]]	-15.810583

Appendix A Table 6 – Deviance information criterion (DIC) scores for hypsigenyines from the distance matrix approach

nullhyp	mod1	mod2	mod3	mod4	mod5
0	208.854651	-34.528144	-37.652346	-16.746062	-10.199658
0	-42.188402	-44.708539	-55.148257	-75.120273	-76.026436
mod6	mod7	mod8	mod9	mod10	mod11
-24.415863	-24.018623	-6.6337833	3.43406142	-30.969211	-30.571971
-47.42493	-58.242332	-77.836665	-79.120512	-44.922827	-55.740228
mod12	mod13	type			
-13.187131	-3.1192864	GPA_notsepManS			
-75.334561	-76.618409	GPA_sepManS			

Appendix A Table 7 – Covariance ratio (CR) effect size values for julidines

Hypothesis	CR effect size
No_Modules	0
AllSpec.CR.phy.julidines_total[[1]]	-8.0608979
AllSpec.CR.phy.julidines_total[[2]]	-20.000761
AllSpec.CR.phy.julidines_total[[3]]	-18.54865
AllSpec.CR.phy.julidines_total[[4]]	-12.264103
AllSpec.CR.phy.julidines_total[[5]]	-10.197422
AllSpec.CR.phy.julidines_total[[6]]	-7.2649969
AllSpec.CR.phy.julidines_total[[7]]	-8.0128111
AllSpec.CR.phy.julidines_total[[8]]	-6.9696481
AllSpec.CR.phy.julidines_total[[9]]	-8.8585326
AllSpec.CR.phy.julidines_total[[10]]	-12.723507
AllSpec.CR.phy.julidines_total[[11]]	-13.363246
AllSpec.CR.phy.julidines_total[[12]]	-12.718983
AllSpec.CR.phy.julidines_total[[13]]	-14.228812

Appendix A Table 8 – Deviance information criterion (DIC) scores for julidines from the distance matrix approach

nullhyp	mod1	mod2	mod3	mod4	mod5
0	469.295453	2.45716529	72.0784424	49.2593013	123.292467
0	48.4405775	-0.2873989	-7.0958363	-19.694909	-18.069026
mod6	mod7	mod8	mod9	mod10	mod11
46.5070867	131.008325	93.3092155	182.222343	25.0602975	109.561536
16.7876774	28.388694	-2.6198339	17.4155002	15.1297863	26.7308029
mod12	mod13	type			
71.8624279	160.775555	GPA_notsepManS			
-4.2777249	15.7576091	GPA_sepManS			

Appendix A Table 9 –Covariance ratio (CR) effect size values for cheilines

Hypothesis	CR effect size
No_Modules	0
AllSpec.CR.phy.cheilines[[1]]	-4.8732662
AllSpec.CR.phy.cheilines[[2]]	-21.92082
AllSpec.CR.phy.cheilines[[3]]	-22.647654
AllSpec.CR.phy.cheilines[[4]]	-4.6307092
AllSpec.CR.phy.cheilines[[5]]	-5.5818614
AllSpec.CR.phy.cheilines[[6]]	-4.5394685
AllSpec.CR.phy.cheilines[[7]]	-5.2072976
AllSpec.CR.phy.cheilines[[8]]	-4.8306483
AllSpec.CR.phy.cheilines[[9]]	-5.6673857
AllSpec.CR.phy.cheilines[[10]]	-7.2068512
AllSpec.CR.phy.cheilines[[11]]	-10.011084
AllSpec.CR.phy.cheilines[[12]]	-7.3065138
AllSpec.CR.phy.cheilines[[13]]	-9.4999432

Appendix A Table 10 – Deviance information criterion (DIC) scores for cheilines from the distance matrix approach

nullhyp	mod1	mod2	mod3	mod4	mod5
0	3.28539792	-53.661451	-63.215824	-75.981871	-75.425856
0	-127.03711	-53.494818	-65.207026	-110.18092	-111.28268
mod6	mod7	mod8	mod9	mod10	mod11
-58.629177	-72.33949	-80.949597	-84.549524	-56.961554	-70.671868
-63.315802	-80.285713	-120.00191	-126.36137	-59.579491	-76.549402
mod12	mod13	type			
-79.281975	-82.881901	GPA_notsepMan S			
-116.2656	-122.62506	GPA_sepManS			

Appendix A Table 11 – Covariance ratio (CR) effect size values for scarines

Hypothesis	CR effect size
No_Modules	0
AllSpec.CR.phy.scarines[[1]]	-6.3019055
AllSpec.CR.phy.scarines[[2]]	-13.766668
AllSpec.CR.phy.scarines[[3]]	-13.455071
AllSpec.CR.phy.scarines[[4]]	-7.9921599
AllSpec.CR.phy.scarines[[5]]	-6.9940092
AllSpec.CR.phy.scarines[[6]]	-5.9780134
AllSpec.CR.phy.scarines[[7]]	-6.5316646
AllSpec.CR.phy.scarines[[8]]	-6.7948549
AllSpec.CR.phy.scarines[[9]]	-7.6333135
AllSpec.CR.phy.scarines[[10]]	-10.226172
AllSpec.CR.phy.scarines[[11]]	-11.044106
AllSpec.CR.phy.scarines[[12]]	-10.18895
AllSpec.CR.phy.scarines[[13]]	-10.878221

Appendix A Table 12 – Deviance information criterion (DIC) scores for scarines from the distance matrix approach

nullhyp	mod1	mod2	mod3	mod4	mod5
0	-65.757089	-44.723894	-56.572778	-90.737055	-91.552856
0	-183.58255	-69.895916	-82.486147	-151.55676	-153.55225
mod6	mod7	mod8	mod9	mod10	mod11
-38.042471	-45.086456	-84.055633	-80.066534	-50.06033	-57.104314
-77.581949	-91.093539	-159.24279	-162.15964	-76.455396	-89.966986
mod12	mod13	type			
-96.073491	-92.084392	GPA_notsepManS			
-158.11624	-161.03309	GPA_sepManS			

Appendix A Table 13 – Planarity values for the anterior jaw linkage, opercular linkage, and hyoid linkage systems

Species	Anterior Jaw linkage	Opercular Linkage	Hyoid Linkage
Acantholabrus_palloni	0.8164	0.8565	0.5973
Achoerodus_gouldii	0.9995	0.9375	0.8656
Anampses_chrysocephalus	0.9813	0.9495	0.7985
Anampses_cuvier	0.9755	0.9571	0.817
Anampses_femininus	0.9987	0.962	0.8815
Anampses_geographicus	0.9886	0.9491	0.8471
Anampses_melanurus	0.9942	0.9402	0.8838
Anampses_meleagrides	0.9699	0.9086	0.815
Anampses_neoguinaicus	0.9692	0.9242	0.8264
Anampses_twistii	0.9887	0.946	0.8207
Austrolabrus_maculatus	0.9592	0.9505	0.8376
Bodianus_axillaris	0.8771	0.9288	0.6446
Bodianus_bilunulatus	0.8098	0.9359	0.7281
Bodianus_diana	0.7269	0.9106	0.5754
Bodianus_dictynna	0.6688	0.9041	0.6466
Bodianus_loxozonus	0.992	0.9516	0.8062
Bodianus_mesothorax	0.7148	0.9083	0.6318
Bodianus_pulchellus	0.7274	0.8744	0.641
Bolbometopon_muricatum	0.9998	0.9559	0.5662
Calotomus_carolinus	0.9908	0.9477	0.5973
Calotomus_japonicus	0.9996	0.9248	0.5489
Calotomus_spinidens	0.9177	0.9339	0.6415
Centrolabrus_exoletus	0.9996	0.9326	0.9104
Cetoscarus_bicolor	0.9695	0.9333	0.6014
Cheilinus_abudjubbe	0.9363	0.9207	0.6266
Cheilinus_bimaculatus	0.8401	0.8748	0.585
Cheilinus_chlorourus	0.9379	0.8888	0.6515
Cheilinus_fasciatus	0.8793	0.9165	0.7853
Cheilinus_lunulatus	0.9581	0.9213	0.6121
Cheilinus_oxycephalus	0.6614	0.9101	0.8134
Cheilinus_trilobatus	0.9041	0.8892	0.7783
Cheilinus_undulatus	0.9705	0.9212	0.6472
Cheilio_inermis	0.9956	0.9088	0.8562
Chlorurus_bleekeri	0.9289	0.8925	0.6313
Chlorurus_bowersi	0.8385	0.9014	0.6108

Chlorurus_capistratoides	0.9393	0.898	0.6856
Chlorurus_gibbus	0.9123	0.9018	0.5894
Chlorurus_japanensis	0.8837	0.9269	0.622
Chlorurus_microrhinos	0.8523	0.9975	0.5454
Chlorurus_oedema	0.9554	0.9122	0.557
Chlorurus_perspicillatus	0.918	0.8893	0.679
Chlorurus_spilurus	0.904	0.8947	0.5483
Choerodon_anchorago	0.9046	0.927	0.6434
Choerodon_oligacanthus	0.8814	0.9152	0.6146
Choerodon_schoenleinii	0.8438	0.9578	0.5662
Choerodon_zosterophorus	0.927	0.8834	0.54
Cirrhilabrus_cyanopleura	0.7584	0.9037	0.5971
Cirrhilabrus_exquisitus	0.7117	0.9629	0.645
Cirrhilabrus_punctatus	0.7065	0.898	0.563
Cirrhilabrus_scottorum	0.9622	0.9272	0.7725
Cirrhilabrus_temminckii	0.9756	0.9791	0.7643
Clepticus_parrae	0.8022	0.9334	0.7213
Coris_aygula	0.9443	0.9419	0.8169
Coris_batuensis	0.9501	0.9539	0.8644
Coris_dorsomacula	0.9642	0.9384	0.8588
Coris_gaimard	0.9649	0.925	0.7584
Coris_julis	0.9618	0.933	0.7072
Coris_pictoides	0.9407	0.932	0.7968
Coris_venusta	0.7101	0.9463	0.6759
Cryptotomus_roseus	0.9629	0.8854	0.6965
Ctenolabrus_rupestris	0.6219	0.8804	0.656
Cymolutes_torquatus	0.9416	0.9341	0.6844
Decodon_puellaris	0.8318	0.9047	0.5919
Diproctacanthus_xanthurus	0.8447	0.914	0.9353
Doratonotus_megalepis	0.6499	0.8953	0.7161
Epibulus_insidiator	0.9997	0.413	0.5676
Eupetrichthys_angustipes	0.8632	0.9261	0.7643
Gomphosus_caeruleus	0.9181	0.9394	0.7744
Gomphosus_varius	0.9704	0.9185	0.8788
Haletta_semifasciata	0.8153	0.9068	0.838
Halichoeres_argus	0.8157	0.9372	0.8004
Halichoeres_binotopsis	0.9203	0.9426	0.7325
Halichoeres_bivittatus	0.886	0.9581	0.6616
Halichoeres_chloropterus	0.9826	0.921	0.9029

Halichoeres_chrysus	0.9207	0.9349	0.8146
Halichoeres_dispilus	0.9668	0.9234	0.7704
Halichoeres_garnoti	0.9874	0.9404	0.8461
Halichoeres_hartzfeldii	0.8952	0.9566	0.677
Halichoeres_hortulanus	0.9577	0.9471	0.7588
Halichoeres_leucurus	0.9762	0.9077	0.8619
Halichoeres_maculipinna	0.7216	0.928	0.7287
Halichoeres_margaritaceus	0.9187	0.9219	0.8779
Halichoeres_marginatus	0.9756	0.9395	0.8293
Halichoeres_melanochir	0.9933	0.9234	0.8927
Halichoeres_melanurus	0.9879	0.9087	0.8971
Halichoeres_melasmapomus	0.8459	0.9465	0.8181
Halichoeres_nebulosus	0.7984	0.9276	0.703
Halichoeres_podostigma	0.8875	0.9291	0.7946
Halichoeres_poeyi	0.9543	0.9237	0.7529
Halichoeres_prosopeion	0.8282	0.9443	0.8142
Halichoeres_richmondi	0.9819	0.9223	0.8872
Halichoeres_scapularis	0.9516	0.9298	0.7737
Halichoeres_trimaculatus	0.8859	0.926	0.6962
Hemigymnus_fasciatus	0.9291	0.8944	0.7927
Hemigymnus_melapterus	0.9765	0.9181	0.8432
Heteroscarus_acroptilus	0.9709	0.8804	0.8946
Hipposcarus_harid	0.9751	0.9244	0.6098
Hipposcarus_longiceps	0.9653	0.9047	0.6053
Hologymnosus_doliatus	0.9886	0.9519	0.8146
Iniistius_bimaculatus	0.9673	0.9364	0.7585
Iniistius_dea	0.9591	0.9327	0.6597
Iniistius_pavo	0.9332	0.9597	0.599
Iniistius_pentadactylus	0.9862	0.9511	0.6753
Iniistius_umbrilatus	0.9908	0.9283	0.5522
Labrichthys_unilineatus	0.7429	0.9325	0.7646
Labroides_pectoralis	0.7174	0.923	0.9157
Labropsis_australis	0.7245	0.909	0.9606
Labrus_merula	0.705	0.8322	0.6431
Labrus_mixtus	0.9491	0.8238	0.8339
Labrus_viridis	0.6688	0.8497	0.7079
Lachnolaimus_maximus	0.991	0.9589	0.7843
Leptoscarus_vaigiensis	0.9487	0.9478	0.5151
Macropharyngodon_geoffroy	0.9245	0.9758	0.7194

Macropharyngodon_meleagris	0.9993	0.952	0.8265
Macropharyngodon_negrosensis	0.9434	0.9682	0.7322
Malapterus_reticulatus	0.9876	0.8994	0.8565
Neoodax_balteatus	0.9689	0.8653	0.7937
Nicholsina_usta	0.975	0.9249	0.581
Notolabrus_gymnogenis	0.8582	0.9331	0.7806
Novaculichthys_taeniourus	0.7682	0.9127	0.7599
Novaculoides_macrolepidotus	0.9025	0.9408	0.6824
Odax_cyanoallix	0.9762	0.9334	0.871
Odax_pullus	0.8753	0.9179	0.8109
Olisthops_cyanomelas	0.9726	0.8897	0.8116
Ophthalmolepis_lineolata	0.9809	0.9387	0.8349
Oxycheilinus_arenatus	0.9268	0.8865	0.7647
Oxycheilinus_celebicus	0.972	0.8492	0.7944
Oxycheilinus_digramma	0.8615	0.8629	0.6952
Oxycheilinus_nigromarginatus	0.7667	0.8484	0.6727
Oxycheilinus_orientalis	0.7963	0.8588	0.6145
Oxycheilinus_unifasciatus	0.8498	0.8956	0.5998
Oxyjulis_californica	0.9852	0.9435	0.7925
Paracheilinus_filamentosus	0.8026	0.8992	0.5511
Pictilabrus_laticlavius	0.9838	0.9268	0.8338
Pseudocheilinops_ataenia	0.9961	0.8892	0.8238
Pseudocheilinus_evanidus	0.9202	0.9218	0.7281
Pseudocheilinus_hexataenia	0.9875	0.8799	0.8699
Pseudocheilinus_octotaenia	0.8399	0.8554	0.587
Pseudocoris_yamashiroi	0.951	0.9238	0.7336
Pseudodax_moluccanus	0.8952	0.9389	0.7295
Pseudojuloides_cerasinus	0.8639	0.9183	0.8424
Pseudolabrus_guentheri	1	0.9359	0.8596
Pseudolabrus_luculentus	0.9157	0.8947	0.6138
Pteragogus_cryptus	0.9528	0.9333	0.7902
Scarus_chameleon	0.9796	0.9117	0.5617
Scarus_coelestinus	0.9983	0.9436	0.6907
Scarus_coeruleus	0.917	0.9157	0.639
Scarus_dimidiatus	0.8912	0.8824	0.6856
Scarus_dubius	0.9838	0.8971	0.6678
Scarus_festivus	0.9431	0.9372	0.6946
Scarus_flavipectoralis	0.9797	0.9077	0.6281
Scarus_forsteni	0.9239	0.8892	0.6332

Scarus_frenatus	0.9643	0.8659	0.5738
Scarus_globiceps	0.9971	0.8908	0.5516
Scarus_guacamaia	0.9149	0.942	0.6439
Scarus_hypselopterus	0.9858	0.9132	0.5689
Scarus_maculipinna	0.986	0.8688	0.6234
Scarus_niger	0.9766	0.8739	0.6022
Scarus_oviceps	0.9881	0.8724	0.5792
Scarus_prasiognathos	0.9866	0.8479	0.5951
Scarus_psittacus	0.9896	0.8545	0.631
Scarus_quoyi	0.9755	0.8607	0.6505
Scarus_rubroviolaceus	0.9781	0.9338	0.7508
Scarus_russelii	0.8335	0.8804	0.6674
Scarus_schlegeli	0.9589	0.8889	0.612
Scarus_spinus	0.9877	0.8745	0.5448
Scarus_taeniopterus	0.9757	0.9039	0.6275
Scarus_tricolor	0.9764	0.8534	0.6794
Scarus_viridifucatus	0.9734	0.856	0.6307
Semicossyphus_pulcher	0.8213	0.8965	0.6724
Siphonognathus_argyrophanes	0.8004	0.8417	0.8542
Siphonognathus_radiatus	0.8878	0.8944	0.8771
Sparisoma_aurofrenatum	0.9619	0.9582	0.6576
Sparisoma_axillare	0.9567	0.9516	0.6043
Sparisoma_choati	0.9664	0.961	0.6453
Sparisoma_chrysopterum	0.9921	0.944	0.6058
Sparisoma_cretense	0.987	0.9157	0.5381
Sparisoma_radians	0.9641	0.9602	0.5708
Sparisoma_rubripinne	0.9347	0.9511	0.5762
Sparisoma_viride	0.9386	0.9277	0.5786
Stethojulis_balteata	0.8417	0.9009	0.7963
Stethojulis_bandanensis	0.8347	0.8843	0.7523
Stethojulis_interrupta	0.7738	0.8404	0.7303
Suezichthys_gracilis	0.8448	0.9221	0.7145
Symphodus_mediterraneus	0.9989	0.9375	0.9105
Symphodus_ocellatus	0.9701	0.9021	0.9058
Symphodus_rostratus	0.9933	0.8607	0.892
Symphodus_tinca	0.7223	0.8473	0.7475
Tautoga_onitis	0.8376	0.902	0.7561
Tautogolabrus_adspersus	0.7905	0.8332	0.7619
Terelabrus_dewapyle	0.6735	0.8104	0.6415

Thalassoma_amblycephalum	0.7258	0.9022	0.785
Thalassoma_ballieui	0.8223	0.8805	0.9517
Thalassoma_bifasciatum	0.7938	0.8895	0.7336
Thalassoma_cupido	0.9525	0.9074	0.8073
Thalassoma_duperrey	0.9908	0.9362	0.8769
Thalassoma_hardwicke	0.8428	0.9145	0.7854
Thalassoma_lunare	0.8361	0.9148	0.7861
Thalassoma_lutescens	0.8706	0.9384	0.7844
Thalassoma_quinquevittatum	0.8754	0.9411	0.8592
Wetmorella_albofasciata	0.7829	0.8655	0.8636
Wetmorella_nigropinnata	0.8721	0.9089	0.9039
Xenojulis_margaritaceus	0.9379	0.9502	0.7243
Xiphocheilus_typus	0.9893	0.8622	0.5767
Xyrichtys_martinicensis	0.9141	0.9557	0.5574
Xyrichtys_novacula	0.9576	0.9205	0.733

APPENDIX B – SUPPLEMENTARY TABLES AND FIGURES FOR CHAPTER 3

Appendix B Table 1 – P-adjusted values from Tukey Test from the ANOVA of Species v. E for the CM

Species comparison	**p-adjusted value**
Calotomus_carolinus-Bodianus_rufus	0
Chlorurus_spilurus-Bodianus_rufus	0
Epibulus_insidiator-Bodianus_rufus	0
Lachnolaimus_maximus-Bodianus_rufus	0.00496439
Oxycheilinus_unifasciatus-Bodianus_rufus	0
Scarus_frenatus-Bodianus_rufus	0
Scarus_globiceps-Bodianus_rufus	0
Scarus_guacamaia-Bodianus_rufus	0
Scarus_psittacus-Bodianus_rufus	0
Scarus_taeniopterus-Bodianus_rufus	0
Sparisoma_chrysopterum-Bodianus_rufus	0
Sparisoma_viride-Bodianus_rufus	7.25E-08
Chlorurus_spilurus-Calotomus_carolinus	0
Epibulus_insidiator-Calotomus_carolinus	0
Lachnolaimus_maximus-Calotomus_carolinus	0
Oxycheilinus_unifasciatus-Calotomus_carolinus	0
Scarus_frenatus-Calotomus_carolinus	0
Scarus_globiceps-Calotomus_carolinus	0
Scarus_guacamaia-Calotomus_carolinus	0
Scarus_psittacus-Calotomus_carolinus	0
Scarus_taeniopterus-Calotomus_carolinus	2.32E-08
Sparisoma_chrysopterum-Calotomus_carolinus	0.56746642
Sparisoma_viride-Calotomus_carolinus	0
Epibulus_insidiator-Chlorurus_spilurus	0
Lachnolaimus_maximus-Chlorurus_spilurus	0
Oxycheilinus_unifasciatus-Chlorurus_spilurus	0
Scarus_frenatus-Chlorurus_spilurus	0.9859429
Scarus_globiceps-Chlorurus_spilurus	0
Scarus_guacamaia-Chlorurus_spilurus	0
Scarus_psittacus-Chlorurus_spilurus	0.02661491
Scarus_taeniopterus-Chlorurus_spilurus	0
Sparisoma_chrysopterum-Chlorurus_spilurus	0
Sparisoma_viride-Chlorurus_spilurus	0
Lachnolaimus_maximus-Epibulus_insidiator	0

Oxycheilinus_unifasciatus-Epibulus_insidiator	0
Scarus_frenatus-Epibulus_insidiator	0
Scarus_globiceps-Epibulus_insidiator	0.59014685
Scarus_guacamaia-Epibulus_insidiator	0
Scarus_psittacus-Epibulus_insidiator	0
Scarus_taeniopterus-Epibulus_insidiator	0
Sparisoma_chrysopterum-Epibulus_insidiator	0
Sparisoma_viride-Epibulus_insidiator	0
Oxycheilinus_unifasciatus-Lachnolaimus_maximus	0
Scarus_frenatus-Lachnolaimus_maximus	0
Scarus_globiceps-Lachnolaimus_maximus	0
Scarus_guacamaia-Lachnolaimus_maximus	0
Scarus_psittacus-Lachnolaimus_maximus	0
Scarus_taeniopterus-Lachnolaimus_maximus	0
Sparisoma_chrysopterum-Lachnolaimus_maximus	0
Sparisoma_viride-Lachnolaimus_maximus	0
Scarus_frenatus-Oxycheilinus_unifasciatus	0
Scarus_globiceps-Oxycheilinus_unifasciatus	0
Scarus_guacamaia-Oxycheilinus_unifasciatus	0
Scarus_psittacus-Oxycheilinus_unifasciatus	0
Scarus_taeniopterus-Oxycheilinus_unifasciatus	0
Sparisoma_chrysopterum-Oxycheilinus_unifasciatus	0
Sparisoma_viride-Oxycheilinus_unifasciatus	0
Scarus_globiceps-Scarus_frenatus	0
Scarus_guacamaia-Scarus_frenatus	0
Scarus_psittacus-Scarus_frenatus	0.0003555
Scarus_taeniopterus-Scarus_frenatus	0
Sparisoma_chrysopterum-Scarus_frenatus	0
Sparisoma_viride-Scarus_frenatus	0
Scarus_guacamaia-Scarus_globiceps	0
Scarus_psittacus-Scarus_globiceps	0
Scarus_taeniopterus-Scarus_globiceps	0
Sparisoma_chrysopterum-Scarus_globiceps	0
Sparisoma_viride-Scarus_globiceps	0
Scarus_psittacus-Scarus_guacamaia	0
Scarus_taeniopterus-Scarus_guacamaia	0
Sparisoma_chrysopterum-Scarus_guacamaia	0

Sparisoma_viride-Scarus_guacamaia	0
Scarus_taeniopterus-Scarus_psittacus	0
Sparisoma_chrysopterum-Scarus_psittacus	2.79E-06
Sparisoma_viride-Scarus_psittacus	0
Sparisoma_chrysopterum-Scarus_taeniopterus	0
Sparisoma_viride-Scarus_taeniopterus	0.99653209
Sparisoma_viride-Sparisoma_chrysopterum	0

Appendix B Table 2 – P-adjusted values from Tukey Test from the ANOVA of Species v. E for the IOPM

Species comparison	**p-adjusted value**
Calotomus_carolinus-Bodianus_rufus	1.33E-11
Chlorurus_spilurus-Bodianus_rufus	1.33E-11
Epibulus_insidiator-Bodianus_rufus	1.33E-11
Lachnolaimus_maximus-Bodianus_rufus	1.34E-11
Oxycheilinus_unifasciatus-Bodianus_rufus	1.34E-11
Scarus_frenatus-Bodianus_rufus	1.33E-11
Scarus_globiceps-Bodianus_rufus	1.33E-11
Scarus_guacamaia-Bodianus_rufus	1.33E-11
Scarus_psittacus-Bodianus_rufus	1.33E-11
Scarus_taeniopterus-Bodianus_rufus	1.33E-11
Sparisoma_chrysopterum-Bodianus_rufus	1.33E-11
Sparisoma_viride-Bodianus_rufus	1.33E-11
Chlorurus_spilurus-Calotomus_carolinus	0.99956724
Epibulus_insidiator-Calotomus_carolinus	1.33E-11
Lachnolaimus_maximus-Calotomus_carolinus	1.33E-11
Oxycheilinus_unifasciatus-Calotomus_carolinus	1.33E-11
Scarus_frenatus-Calotomus_carolinus	1.96E-06
Scarus_globiceps-Calotomus_carolinus	0.99999957
Scarus_guacamaia-Calotomus_carolinus	0.36399316
Scarus_psittacus-Calotomus_carolinus	2.75E-09
Scarus_taeniopterus-Calotomus_carolinus	0.98317994
Sparisoma_chrysopterum-Calotomus_carolinus	1.34E-11
Sparisoma_viride-Calotomus_carolinus	1.01E-10
Epibulus_insidiator-Chlorurus_spilurus	1.33E-11
Lachnolaimus_maximus-Chlorurus_spilurus	1.33E-11
Oxycheilinus_unifasciatus-Chlorurus_spilurus	1.33E-11
Scarus_frenatus-Chlorurus_spilurus	3.69E-08
Scarus_globiceps-Chlorurus_spilurus	0.99451038
Scarus_guacamaia-Chlorurus_spilurus	0.04304757
Scarus_psittacus-Chlorurus_spilurus	3.76E-11
Scarus_taeniopterus-Chlorurus_spilurus	0.99999695
Sparisoma_chrysopterum-Chlorurus_spilurus	1.34E-11
Sparisoma_viride-Chlorurus_spilurus	1.40E-11
Lachnolaimus_maximus-Epibulus_insidiator	1.33E-11
Oxycheilinus_unifasciatus-Epibulus_insidiator	1.33E-11

Scarus_frenatus-Epibulus_insidiator	1.33E-11
Scarus_globiceps-Epibulus_insidiator	1.33E-11
Scarus_guacamaia-Epibulus_insidiator	1.33E-11
Scarus_psittacus-Epibulus_insidiator	1.33E-11
Scarus_taeniopterus-Epibulus_insidiator	1.33E-11
Sparisoma_chrysopterum-Epibulus_insidiator	1.33E-11
Sparisoma_viride-Epibulus_insidiator	1.33E-11
Oxycheilinus_unifasciatus-Lachnolaimus_maximus	0.99998546
Scarus_frenatus-Lachnolaimus_maximus	1.33E-11
Scarus_globiceps-Lachnolaimus_maximus	1.33E-11
Scarus_guacamaia-Lachnolaimus_maximus	1.33E-11
Scarus_psittacus-Lachnolaimus_maximus	1.33E-11
Scarus_taeniopterus-Lachnolaimus_maximus	1.33E-11
Sparisoma_chrysopterum-Lachnolaimus_maximus	1.33E-11
Sparisoma_viride-Lachnolaimus_maximus	1.33E-11
Scarus_frenatus-Oxycheilinus_unifasciatus	1.33E-11
Scarus_globiceps-Oxycheilinus_unifasciatus	1.33E-11
Scarus_guacamaia-Oxycheilinus_unifasciatus	1.33E-11
Scarus_psittacus-Oxycheilinus_unifasciatus	1.33E-11
Scarus_taeniopterus-Oxycheilinus_unifasciatus	1.33E-11
Sparisoma_chrysopterum-Oxycheilinus_unifasciatus	1.33E-11
Sparisoma_viride-Oxycheilinus_unifasciatus	1.33E-11
Scarus_globiceps-Scarus_frenatus	0.00202914
Scarus_guacamaia-Scarus_frenatus	0.02532335
Scarus_psittacus-Scarus_frenatus	0.99998479
Scarus_taeniopterus-Scarus_frenatus	1.79E-07
Sparisoma_chrysopterum-Scarus_frenatus	0.85477138
Sparisoma_viride-Scarus_frenatus	0.99741987
Scarus_guacamaia-Scarus_globiceps	0.96645048
Scarus_psittacus-Scarus_globiceps	5.68E-05
Scarus_taeniopterus-Scarus_globiceps	0.95177472
Sparisoma_chrysopterum-Scarus_globiceps	2.25E-08
Sparisoma_viride-Scarus_globiceps	6.88E-06
Scarus_psittacus-Scarus_guacamaia	0.00056681
Scarus_taeniopterus-Scarus_guacamaia	0.03995557
Sparisoma_chrysopterum-Scarus_guacamaia	2.90E-08
Sparisoma_viride-Scarus_guacamaia	5.26E-05

Scarus_taeniopterus-Scarus_psittacus	5.67E-10
Sparisoma_chrysopterum-Scarus_psittacus	0.99593412
Sparisoma_viride-Scarus_psittacus	0.99999985
Sparisoma_chrysopterum-Scarus_taeniopterus	1.34E-11
Sparisoma_viride-Scarus_taeniopterus	4.04E-11
Sparisoma_viride-Sparisoma_chrysopterum	0.99998498

Appendix B Table 3 – P-adjusted values from Tukey Test from the ANOVA of Species v. E for the IOPH

	p adj
Calotomus_carolinus-Bodianus_rufus	3.07E-09
Chlorurus_spilurus-Bodianus_rufus	3.07E-09
Epibulus_insidiator-Bodianus_rufus	0.09379585
Lachnolaimus_maximus-Bodianus_rufus	3.07E-09
Oxycheilinus_unifasciatus-Bodianus_rufus	3.07E-09
Scarus_frenatus-Bodianus_rufus	0.53638573
Scarus_globiceps-Bodianus_rufus	3.07E-09
Scarus_guacamaia-Bodianus_rufus	1.17E-08
Scarus_psittacus-Bodianus_rufus	3.07E-09
Scarus_taeniopterus-Bodianus_rufus	0.99994861
Sparisoma_chrysopterum-Bodianus_rufus	3.07E-09
Sparisoma_viride-Bodianus_rufus	0.57398014
Chlorurus_spilurus-Calotomus_carolinus	3.07E-09
Epibulus_insidiator-Calotomus_carolinus	3.07E-09
Lachnolaimus_maximus-Calotomus_carolinus	0.99999
Oxycheilinus_unifasciatus-Calotomus_carolinus	3.07E-09
Scarus_frenatus-Calotomus_carolinus	1.62E-08
Scarus_globiceps-Calotomus_carolinus	0.00072182
Scarus_guacamaia-Calotomus_carolinus	0.27560875
Scarus_psittacus-Calotomus_carolinus	0.99340236
Scarus_taeniopterus-Calotomus_carolinus	3.07E-09
Sparisoma_chrysopterum-Calotomus_carolinus	0.9830824
Sparisoma_viride-Calotomus_carolinus	1.12E-08
Epibulus_insidiator-Chlorurus_spilurus	3.07E-09
Lachnolaimus_maximus-Chlorurus_spilurus	3.07E-09
Oxycheilinus_unifasciatus-Chlorurus_spilurus	3.07E-09
Scarus_frenatus-Chlorurus_spilurus	3.07E-09
Scarus_globiceps-Chlorurus_spilurus	3.07E-09
Scarus_guacamaia-Chlorurus_spilurus	3.07E-09
Scarus_psittacus-Chlorurus_spilurus	3.07E-09
Scarus_taeniopterus-Chlorurus_spilurus	3.07E-09
Sparisoma_chrysopterum-Chlorurus_spilurus	3.07E-09
Sparisoma_viride-Chlorurus_spilurus	3.07E-09
Lachnolaimus_maximus-Epibulus_insidiator	3.07E-09
Oxycheilinus_unifasciatus-Epibulus_insidiator	3.07E-09
Scarus_frenatus-Epibulus_insidiator	0.99999897

Scarus_globiceps-Epibulus_insidiator	3.07E-09
Scarus_guacamaia-Epibulus_insidiator	8.46E-09
Scarus_psittacus-Epibulus_insidiator	3.07E-09
Scarus_taeniopterus-Epibulus_insidiator	4.63E-09
Sparisoma_chrysopterum-Epibulus_insidiator	3.07E-09
Sparisoma_viride-Epibulus_insidiator	0.99999536
Oxycheilinus_unifasciatus-Lachnolaimus_maximus	3.07E-09
Scarus_frenatus-Lachnolaimus_maximus	6.50E-09
Scarus_globiceps-Lachnolaimus_maximus	0.00995778
Scarus_guacamaia-Lachnolaimus_maximus	0.09851948
Scarus_psittacus-Lachnolaimus_maximus	0.99999564
Scarus_taeniopterus-Lachnolaimus_maximus	3.07E-09
Sparisoma_chrysopterum-Lachnolaimus_maximus	0.99999306
Sparisoma_viride-Lachnolaimus_maximus	5.20E-09
Scarus_frenatus-Oxycheilinus_unifasciatus	3.07E-09
Scarus_globiceps-Oxycheilinus_unifasciatus	3.07E-09
Scarus_guacamaia-Oxycheilinus_unifasciatus	3.07E-09
Scarus_psittacus-Oxycheilinus_unifasciatus	3.07E-09
Scarus_taeniopterus-Oxycheilinus_unifasciatus	3.07E-09
Sparisoma_chrysopterum-Oxycheilinus_unifasciatus	3.07E-09
Sparisoma_viride-Oxycheilinus_unifasciatus	3.07E-09
Scarus_globiceps-Scarus_frenatus	3.07E-09
Scarus_guacamaia-Scarus_frenatus	0.00021921
Scarus_psittacus-Scarus_frenatus	4.56E-09
Scarus_taeniopterus-Scarus_frenatus	0.00349179
Sparisoma_chrysopterum-Scarus_frenatus	3.12E-09
Sparisoma_viride-Scarus_frenatus	1
Scarus_guacamaia-Scarus_globiceps	3.38E-08
Scarus_psittacus-Scarus_globiceps	0.09301869
Scarus_taeniopterus-Scarus_globiceps	3.07E-09
Sparisoma_chrysopterum-Scarus_globiceps	0.03542537
Sparisoma_viride-Scarus_globiceps	3.07E-09
Scarus_psittacus-Scarus_guacamaia	0.0376588
Scarus_taeniopterus-Scarus_guacamaia	3.07E-09
Sparisoma_chrysopterum-Scarus_guacamaia	0.00601005
Sparisoma_viride-Scarus_guacamaia	0.00015385
Scarus_taeniopterus-Scarus_psittacus	3.07E-09

Sparisoma_chrysopterum-Scarus_psittacus	1
Sparisoma_viride-Scarus_psittacus	4.01E-09
Sparisoma_chrysopterum-Scarus_taeniopterus	3.07E-09
Sparisoma_viride-Scarus_taeniopterus	0.00463302
Sparisoma_viride-Sparisoma_chrysopterum	3.10E-09

Appendix B Table 4 – Literature review of Young's Modulus

Ligament Type	E	Resource
Rabbit ACL	930	Danto and woo 1993
Human 48-86 ACL	65.3	Noyes and Grood 1976
Human 16-26 ACL	111	Noyes and Grood 1976
Rhesus monkey ACL	186	Noyes and Grood 1976
Human peridontal ligament	3.8	Atkinson and Ralph 1977
Human PCL	248	Race and Amis 1994
Horse nuchal ligament	0.84	Gellman and Bertram 2002
Rabbit MCL	970	Woo et al. 1990
Human ligamentum flavum	4.358	Mihara et al. 2021
Human patellar ligament	459.3	Stäubli et al. 1999
Canine cranial cruciate ligament	478.6	Butler et al. 1983
Parrotfish CM	4.33	Gartner and Westneat
Parrotfish IOPM	10.62	Gartner and Westneat
Parrotfish OPH	1.87	Gartner and Westneat
Suction feeding CM	1.67	Gartner and Westneat
Suction feeding IOPM	75.01	Gartner and Westneat
Suction feeding OPH	1.31	Gartner and Westneat
Mixed CM	5.35	Gartner and Westneat
Mixed IOPM	47.23	Gartner and Westneat
Mixed OPH	1.48	Gartner and Westneat
Horse suspensory ligament 1	148.02	Souza, MV et al.
Horse suspensory ligament 2	81.11	Souza, MV et al.
Young pig sutural ligament	43	Popowics and Herring 2007
Older pig sutural ligament	70	Popowics and Herring 2008

APPENDIX C – SUPPLEMENTARY TABLES AND FIGURES FOR CHAPTER 4

Appendix C Figure 1 – Boxplots of Young's Modulus (E) vs. Species for the CM. A represents the E in the toe region; B is the E in the middle third of the loading curve; C is the upper third of the loading curve. In red are the biting species, parrotfishes, in green are the mixed feeding species, and in blue are the suction feeding species.

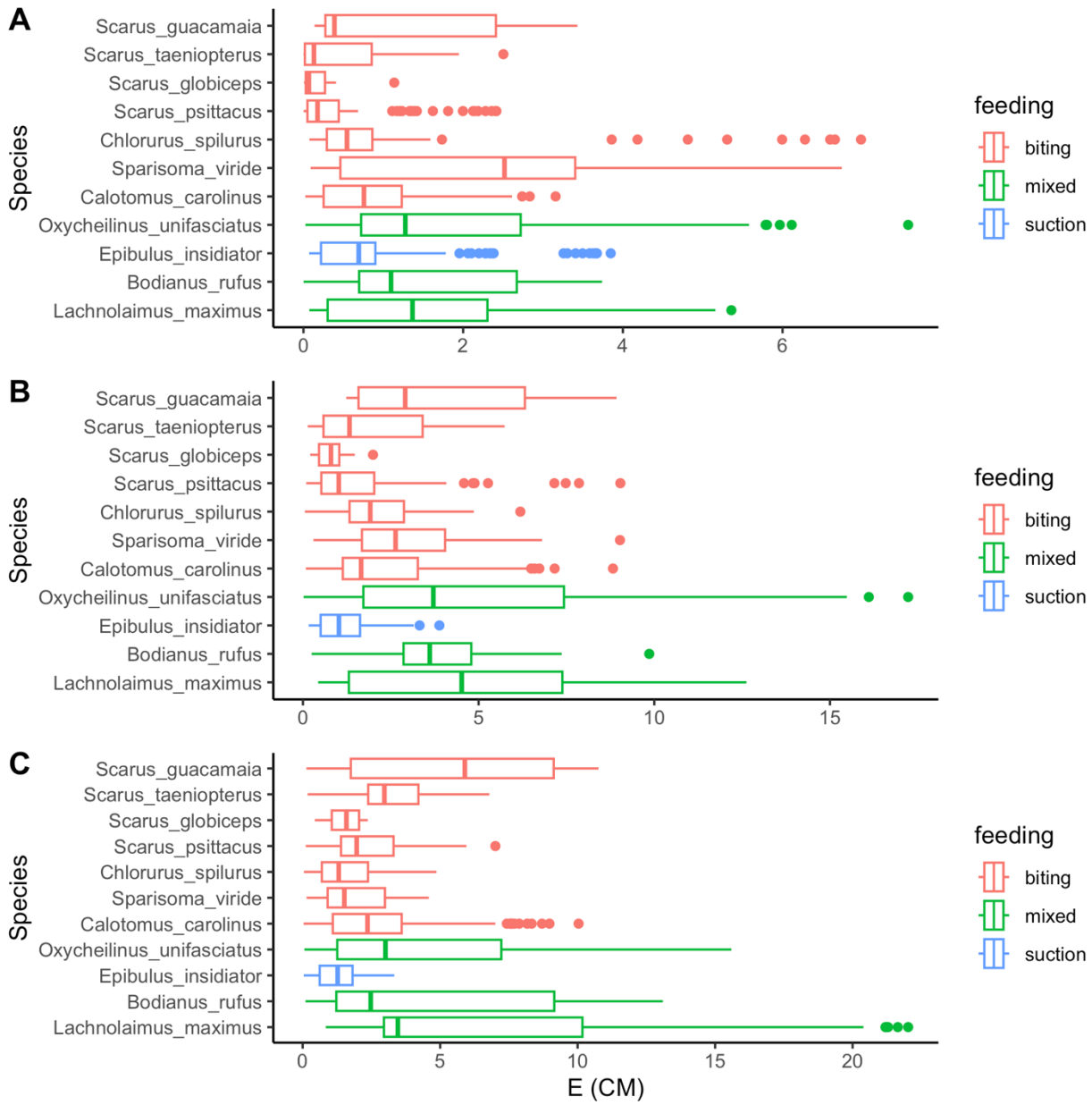

Appendix C Figure 2 – Boxplots of E vs. Species for the IOPM. A represents the E in the toe region; B is the E in the middle third of the loading curve; C is the upper third of the loading curve. In red are the biting species, parrotfishes, in green are the mixed feeding species, and in blue are the suction feeding species.

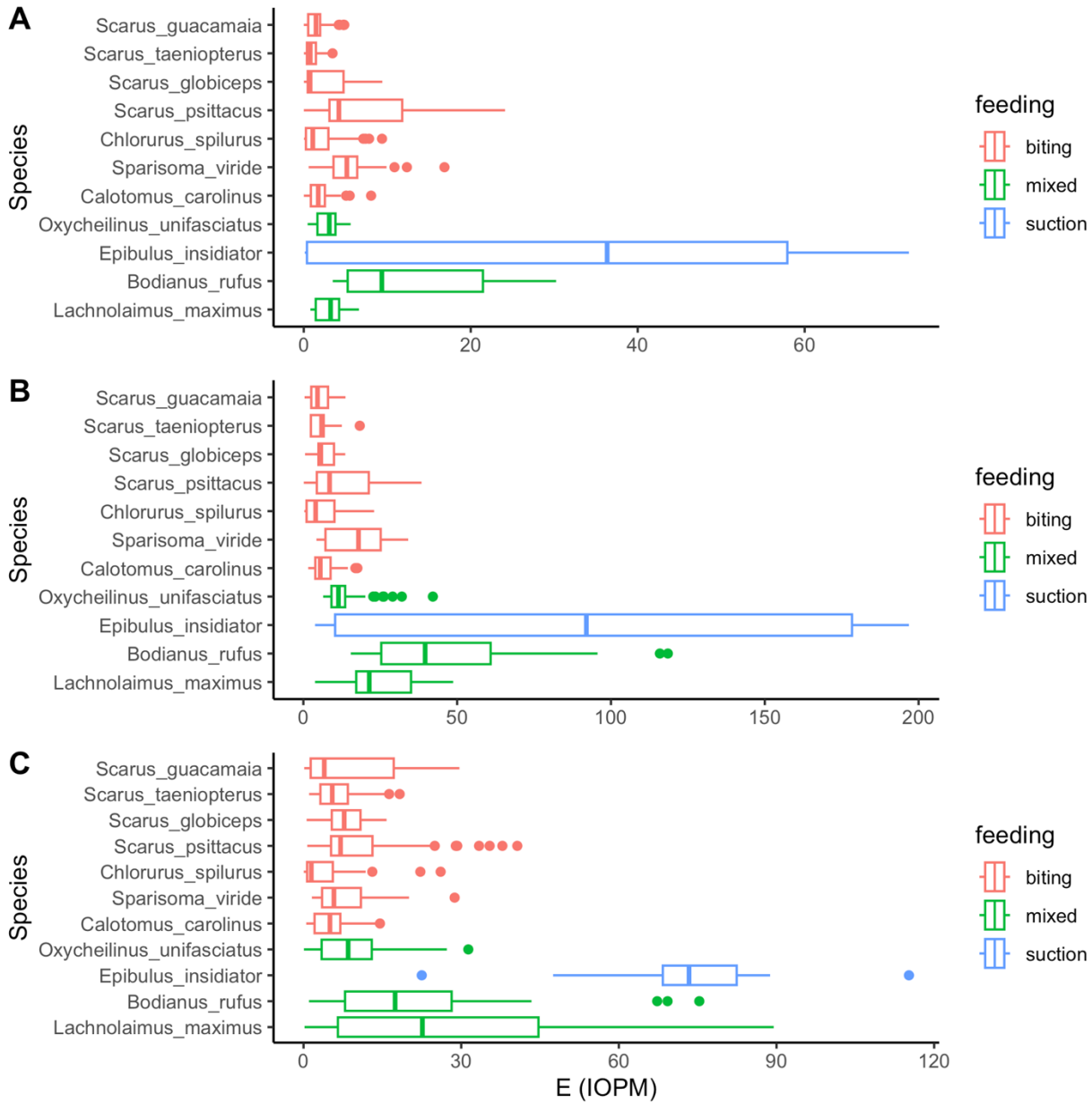

REFERENCES

Abe T, Hashiguchi A, Yamazaki K, Ebinuma H, Saito H, Kumada H, Izumi N, Masaki N, Sakamoto M. 2013. Quantification of collagen and elastic fibers using whole-slide images of liver biopsy specimens. Pathol Int 63:305–10.

Adams DC, Collyer ML. 2019. Comparing the strength of modular signal, and evaluating alternative modular hypotheses, using covariance ratio effect sizes with morphometric data. Evolution (N Y) 73:2352–67.

Adams DC, Collyer ML, Kaliontzopoulou A, Baken EK. 2022. Geomorph: Software for geometric morphometric analyses. R package version 4.0.4. .

Afeworki Y, Zekeria ZA, Videler JJ, Bruggemann JH. 2013. Food intake by the parrotfish *Scarus ferrugineus* varies seasonally and is determined by temperature, size and territoriality. Mar Ecol Prog Ser 489:213–24.

Aiello BR, Westneat MW, Hale ME. 2017. Mechanosensation is evolutionarily tuned to locomotor mechanics. Proc Natl Acad Sci 114:4459–64.

Albertson RC, Streelman JT, Kocher TD, Yelick PC. 2005. Integration and evolution of the cichlid mandible: The molecular basis of alternate feeding strategies. Proc Natl Acad Sci U S A 102:16287–92.

Alexander RMN. 1989. Elastic mechanisms in the locomotion of vertebrates. Netherlands J Zool.

Alfaro M, Westneat MW. 1999. Motor patterns of herbivorous feeding: Electromyographic analysis of biting in the parrotfishes *Cetoscarus bicolor* and *Scarus iseri*. Brain Behav Evol 54:205–22.

Alfaro ME, Janovetz J, Westneat MW. 2001. Motor control across trophic strategies: Muscle activity of biting and suction feeding fishes. Am Zool 41:1266–79.

Anker GC. 1974. Morphology and kinetics of the head of the stickleback, *Gasterosteus aculeatus* . Trans Zool Soc London 32:311–416.

Bardua C, Fabre AC, Bon M, Das K, Stanley EL, Blackburn DC, Goswami A. 2020. Evolutionary integration of the frog cranium. Evolution (N Y) 74:1200–1215.

Bardua C, Wilkinson M, Gower DJ, Sherratt E, Goswami A. 2019. Morphological evolution and modularity of the caecilian skull. BMC Evol Biol 19:1–23.

Barel CDN. 1982. Towards a constructional morphology of cichlid fishes (Teleostei, Perciformes). Netherlands J Zool.

Baumgart A, Anderson P. 2018. Finding the weakest link: Mechanical sensitivity in a fish cranial linkage system. R Soc Open Sci 5.

Bellwood DR. 1994. A phylogenetic study of the parrotfish family Scaridae (Pisces: Labroidea), with a revision of genera. Rec Aust Museum, Suppl 20:1–86.

Bellwood DR, Choat JH. 1990. A functional analysis of grazing in parrotfishes (family Scaridae): the ecological implications. Environ Biol Fishes 28:189–214.

Bennett MB, Ker RF, Alexander RMN. 1989. Elastic strain energy storage in the feet of running monkeys. J Zool 217:469–75.

Betancur RR, Wiley EO, Arratia G, Acero A, Bailly N, Miya M, Lecointre G, Ortí G. 2017. Phylogenetic classification of bony fishes. BMC Evol Biol 17:1–40.

Biewener AA. 2008. Tendons and Ligaments: Structure, Mechanical Behavior and Biological Function. In: Collagen: Structure and Mechanics p. 269–84.

Birch HL, Thorpe CT, Rumian AP. 2013. Specialisation of extracellular matrix for function in tendons and ligaments. Muscles Ligaments Tendons J 3:12–22.

Bon M, Bardua C, Goswami A, Fabre AC. 2020. Cranial integration in the fire salamander, *Salamandra salamandra* (Caudata: Salamandridae). Biol J Linn Soc 130:178–94.

Bonaldo RM, Krajewski JP, Sazima C, Sazima I. 2006. Foraging activity and resource use by three parrotfish species at Fernando de Noronha Archipelago, tropical West Atlantic. Mar Biol 149:423–33.

Brainerd EL, Moritz S, Ritter DA. 2016. XROMM analysis of rib kinematics during lung ventilation in the green iguana, *Iguana iguana*. J Exp Biol 219:404–11.

Buschmann J, Meier Bürgisser G. 2017. Structure and function of tendon and ligament tissues. Biomech Tendons Ligaments 3–29.

Camp AL, Brainerd EL. 2014. Role of axial muscles in powering mouth expansion during suction feeding in largemouth bass *(Micropterus salmoides)*. J Exp Biol 217:1333–45.

Camp AL, Brainerd EL. 2015. Reevaluating musculoskeletal linkages in suction-feeding fishes with X-Ray reconstruction of moving morphology (XROMM). Integr Comp Biol 55:36–47.

Camp AL, Konow N, Sanford CPJ. 2009. Functional morphology and biomechanics of the tongue-bite apparatus in salmonid and osteoglossomorph fishes. J Anat 214:717–28.

Camp AL, Roberts TJ, Brainerd EL. 2015. Swimming muscles power suction feeding in largemouth bass. Proc Natl Acad Sci U S A 112:8690–95.

Cardini A, O'Higgins P, Rohlf FJ. 2019. Seeing distinct groups where there are none: Spurious patterns from between-group PCA. Evol Biol 46:303–16.

Cheverud JM. 1982. Phenotypic, genetic, and environmental morphological integration in the cranium. Evolution (N Y) 36:499.

Cheverud JM. 1995. Morphological integration in the saddle-back tamarin *(Saguinus fuscicollis)* cranium. Am Nat 145:63–89.

Churchill M, Miguel J, Beatty BL, Goswami A, Geisler JH. 2019. Asymmetry drives modularity of the skull in the common dolphin *(Delphinus delphis)*. Biol J Linn Soc 126:225–39.

Claverie T, Patek SN. 2013. Modularity and rates of evolutionary change in a power-amplified prey capture system. Evolution (N Y) 67:3191–3207.

Clifton KB, Motta PJ. 1998. Feeding morphology , diet , and ecomorphological relationships among five Caribbean labrids (Teleostei , Labridae). Copeia 1998:953–66.

Clune J, Mouret JB, Lipson H. 2013. The evolutionary origins of modularity. Proc R Soc B Biol Sci 23.

Cross R. 2008. Differences between bouncing balls, springs, and rods. Am J Phys 76:908–15.

Daley MA, Usherwood JR, Felix G, Biewener AA. 2006. Running over rough terrain: Guinea fowl maintain dynamic stability despite a large unexpected change in substrate height. J Exp Biol 209:171–87.

Danto MI, Woo SL. 1993. The mechanical properties of skeletally mature rabbit anterior cruciate ligament and patellar tendon over a range of strain rates. J Orthop Res 11:58–67.

Datovo A, Vari RP. 2013. The jaw adductor muscle complex in teleostean fishes: Evolution, homologies and revised nomenclature (Osteichthyes: Actinopterygii). PLoS One 8.

Denton JSS, Adams DC. 2015. A new phylogenetic test for comparing multiple high-dimensional evolutionary rates suggests interplay of evolutionary rates and modularity in lanternfishes (Myctophiformes; Myctophidae). Evolution (N Y) 69:2425–40.

Durie CJ, Turingan RG. 2004. The effects of opercular linkage disruption on prey-capture kinematics in the teleost fish *Sarotherodon melanotheron*. J Exp Zool Part A Comp Exp Biol 301:642–53.

Eleswarapu S V., Responte DJ, Athanasiou KA. 2011. Tensile properties, collagen content, and crosslinks in connective tissues of the immature knee joint. PLoS One 6:1–7.

Evans KM, Larouche O, Gartner SM, Faucher RE, Dee SG, Westneat MW. 2023. Beaks promote rapid morphological diversification along distinct evolutionary trajectories in

labrid fishes (Eupercaria: Labridae). Rev.

Evans KM, Larouche O, West JJL, Gartner SM, Westneat MW. 2022. Burrowing constrains patterns of skull shape evolution in wrasses. Evol Dev.

Evans KM, Vidal-García M, Tagliacollo VA, Taylor SJ, Fenolio DB. 2019. Bony patchwork: Mosaic patterns of evolution in the skull of electric fishes (Apteronotidae: Gymnotiformes). Integr Comp Biol 59:420–31.

Evans KM, Waltz B, Tagliacollo V, Chakrabarty P, Albert JS. 2017. Why the short face? Developmental disintegration of the neurocranium drives convergent evolution in neotropical electric fishes. Ecol Evol 7:1783–1801.

Ferry-Graham LA. 1998. Effects of prey size and mobility on prey-capture kinematics in leopard sharks Triakis semifasciata. J Exp Biol 201:2433–44.

Fill TS, Carey JP, Toogood RW, Major PW. 2011. Experimentally determined mechanical properties of, and models for, the periodontal ligament: Critical review of current literature. J Dent Biomech 2:1–10.

Friel, Wainwright. 1999. Evolution of complexity in motor patterns and jaw musculature of tetraodontiform fishes. J Exp Biol 202:867–80.

Gartner SM, Whitlow KR, Laurence-Chasen JD, Kaczmarek EB, Granatosky MC, Ross CF, Westneat MW. 2022. Suction feeding of West African lungfish *(Protopterus annectens)*: An XROMM analysis of jaw mechanics, cranial kinesis, and hyoid mobility. Biol Open 11.

Gellman KS, Bertram JEA. 2002a. The equine nuchal ligament 1: Structural and material properties. Vet Comp Orthop Traumatol.

Gellman KS, Bertram JEA. 2002b. The equine nuchal ligament 2: Passive dynamic energy exchange in locomotion. Vet Comp Orthop Traumatol 15:7–14.

Gidmark NJ, Konow N, LoPresti E, Brainerd EL. 2013. Bite force is limited by the force-length relationship of skeletal muscle in black carp, *Mylopharyngodon piceus*. Biol Lett 9.

Gobalet KW. 2017. Cranial specializations of parrotfishes, genus Scarus (Scarinae, Labridae) for scraping reef surfaces. In: Hoey AS, Bonaldo RM, editors. The Biology of Parrotfishes. 1st ed CRC Press. p. 1–25.

Gosline WA. 1971. Functional morphologgy and classification of teleostean fishes Honolulu: University of Hawaii Press.

Goswami A, Polly PD. 2010. Methods for studying morphological integration and modularity. Paleontol Soc Pap 16:213–43.

Goswami A, Watanabe A, Felice RN, Bardua C, Fabre AC, Polly PD. 2019. High-density morphometric analysis of shape and integration: The good, the bad, and the not-really-a-problem. Integr Comp Biol 59:669–83.

Gregory WK. 1933. Fish Skulls: A Study of the Evolution of Natural Mechanisms. Trans Am Philos Soc 23:i.

Grubich JR. 2001. Prey capture in actinopterygian fishes: A review of suction feeding motor patterns with new evidence from an elopomorph fish, *megalops atlanticus*. Am Zool 41:1258–65.

Grubich JR, Huskey S, Crofts S, Orti G, Porto J. 2012. Mega-Bites: Extreme jaw forces of living and extinct piranhas (Serrasalmidae). Sci Rep 2:1–9.

Grubich JR, Rice AN, Westneat MW. 2008. Functional morphology of bite mechanics in the great barracuda *(Sphyraena barracuda)*. Zoology 111:16–29.

Grubich JR, Westneat MW, Bos AR. 2014. Fish Gristle: mechanical performance of IOPM ligaments among functionally diverse jaws. Integr Comp Biol 54.

Grutter A. 1996. Parasite removal rates by the cleaner wrasse *Labroides dimidiatus*. Mar Ecol Prog Ser 130:61–70.

Hansen TF, Houle D. 2008. Measuring and comparing evolvability and constraint in multivariate characters. J Evol Biol 21:1201–19.

Hoffman SG. 1983. Sex-related foraging behavior in sequentially hermaphroditic hogfishes (Bodianus Spp .). Ecol Soc Am 64:798–808.

Holzer KK, Seekell DA, McGlathery KJ. 2013. Bucktooth parrotfish *Sparisoma radians* grazing on Thalassia in Bermuda varies seasonally and with background nitrogen content. J Exp Mar Bio Ecol 443:27–32.

Hughes LC, Nash CM, White WT, Westneat MW. 2022. Concordance and discordance in the phylogenomics of the wrasses and parrotfishes (Teleostei: Labridae). Syst Biol.

Jiang Y, Guan Y, Lan Y, Chen S, Li T, Zou S, Hu Z, Ye Q. 2021. Mechanosensitive piezo1 in periodontal ligament cells promotes alveolar bone remodeling during orthodontic tooth movement. Front Physiol 12.

Johnson CD. 1995. Design of passive damping systems. J Mech Des Trans ASME 117:171–76.

Jones MEH, Gröning F, Dutel H, Sharp A, Fagan MJ, Evans SE. 2017. The biomechanical role of the chondrocranium and sutures in a lizard cranium. J R Soc Interface 14.

Jones RS, Nawana NS, Pearcy MJ, Learmonth D, Bickerstaff DR, Costi JJ, Paterson RS. 1995.

Mechanical properties of the human anterior cruciate ligament. Clin Biomech 10:339–44.

Jung JY, Naleway SE, Yaraghi NA, Herrera S, Sherman VR, Bushong EA, Ellisman MH, Kisailus D, McKittrick J. 2016. Structural analysis of the tongue and hyoid apparatus in a woodpecker. Acta Biomater 37:1–13.

Kaczmarek EB, Gartner SM, Westneat MW, Brainerd EL. 2022. Air breathing and suction feeding kinematics in West African lungfish. Integr Comp Biol 62:865–77.

Ker RF. 1981. Dynamic tensile properties of the plantaris tendon of sheep (Ovis aries). J Exp Biol 93:283–302.

Ker RF, Dimery NJ, Alexander RMN. 1986. The role of tendon elasticity in hopping in a wallaby Macropus rufogriseus. J Zool 208:417–28.

Klingenberg CP. 2008. Morphological integration and developmental modularity. Annu Rev Ecol Evol Syst 39:115–32.

Larouche O, Gartner SM, Westneat MW, Evans KM. 2022. Mosaic evolution of the skull in labrid fishes involves differences in both tempo and mode of morphological change. Syst Biol.

Larouche O, Zelditch ML, Cloutier R. 2018. Modularity promotes morphological divergence in ray-finned fishes. Sci Rep 8:1–6.

Lauder G V. 1979. Feeding mechanics in primitive teleosts and in the halecomorph fish *Amia calva*. J Zool London 187:543–78.

Lauder BYG V. 1983. Prey capture hydrodynamics in fishes: Experimental tests of two models. J Exp Biol 104:1–13.

Lauder G V. 1982. Patterns of evolution in the feeding mechanism of actinopterygian fishes. Am Zool 22:275–85.

Laurence-Chasen JD, Ramsay JB, Brainerd EL. 2019. Shearing overbite and asymmetrical jaw motions facilitate food breakdown in a freshwater stingray, *Potamotrygon motoro*. J Exp Biol.

Lee N, Horstemeyer MF, Rhee H, Nabors B, Liao J, Williams LN. 2014. Hierarchical multiscale structure - Property relationships of the red-bellied woodpecker (Melanerpes carolinus) beak. J R Soc Interface 11.

Lemberg JB, Shubin NH, Westneat MW. 2019. Feeding kinematics and morphology of the alligator gar (*Atractosteus spatula* , Lacépède, 1803). J Morphol 1548–70.

Lewis SM. 2010. The role of herbivorous fishes in the organization of a caribbean reef

community. Ecol Soc Am 56:183–200.

Liem KF. 1970. Comparative functional anatomy of the nandidae (Pisces: Teleostei). Fieldiana Zool 56:1–166.

Liem KF. 1978. Modulatory multiplicity in the functional repertoire of the feeding mechanism in cichlid fishes. I. Piscivores. J Morphol 158:323–60.

Lloyd JE, Stavness I, Fels S. 2012. ArtiSynth: A fast interactive biomechanical modeling toolkit combining multibody and finite element simulation. Stud Mechanobiol Tissue Eng Biomater 11:355–94.

Long JH, Adcock B, Root RG. 2002. Force transmission via axial tendons in undulating fish: A dynamic analysis. Comp Biochem Physiol - A Mol Integr Physiol 133:911–29.

Long JH, Pabst DA, Shepherd WR, McLellan WA. 1997. Locomotor design of dolphin vertebral columns: Bending mechanics and morphology of *Delphinus delphis*. J Exp Biol 200:65–81.

Mandel U, Dalgaard P, Vidik A. 1986. A biomechanical study of the periodontal ligament. J Biomech 19:637–45.

Marchetti GM. 2006. Independencies induced from a graphical markov model after marginalization and conditioning: The R package ggm. J Stat Softw 15.

Marcus MA, Amini S, Stifler CA, Sun CY, Tamura N, Bechtel HA, Parkinson DY, Barnard HS, Zhang XXX, Chua JQI, Miserez A, Gilbert PUPA. 2017. Parrotfish Teeth: Stiff Biominerals Whose Microstructure Makes Them Tough and Abrasion-Resistant to Bite Stony Corals. ACS Nano 11:11856–65.

Matthews LS, Ellis D. 1968. Viscoelastic properties of cat tendon: Effects of time after death and preservation by freezing. J Biomech 1:65–71.

Mihara A, Nishida N, Jiang F, Ohgi J, Imajo Y, Suzuki H, Funaba M, Yamagata H, Chen X, Sakai T. 2021. Tensile test of human lumbar ligamentum flavum: Age-related changes of stiffness. Appl Sci 11.

Moazen M, Curtis N, O'Higgins P, Jones MEH, Evans SE, Fagan MJ. 2009. Assessment of the role of sutures in a lizard skull: A computer modelling study. Proc R Soc B Biol Sci 276:39–46.

Monteiro LR, Bonato V, Dos Reis SF. 2005. Evolutionary integration and morphological diversification in complex morphological structures: Mandible shape divergence in spiny rats (Rodentia, Echimyidae). Evol Dev 7:429–39.

Montuelle SJ, Herrel A, Libourel PA, Daillie S, Bels VL. 2012. Prey capture in lizards: Differences in jaw-neck-forelimb coordination. Biol J Linn Soc 105:607–22.

Moon DK, Woo SLY, Takakura Y, Gabriel MT, Abramowitch SD. 2006. The effects of refreezing on the viscoelastic and tensile properties of ligaments. J Biomech 39:1153–57.

Muller M. 1989. A quantitative theory of expected volume changes of the mouth during feeding in teleost fishes. J Zool London 217:639–62.

Nakagawa H, Mikawa Y, Watanabe R. 1994. Elastin in the human posterior longitudinal ligament and spinal dura: A histologic and biochemical study. Spine (Phila Pa 1976) 19:2164–69.

Nemeth DH. 1997. Modulation of attack behavior and its effect on feeding performance in a trophic generalist fish, Hexagrammos decagrammus. J Exp Biol 200:2155–64.

Nicholls M, Aspelund T, Ingvarsson T, Briem K. 2018. Nationwide study highlights a second peak in ACL tears for women in their early forties. Knee Surgery, Sport Traumatol Arthrosc 26:648–54.

Nicholson GM, Clements KD. 2020. Resolving resource partitioning in parrotfishes (Scarini) using microhistology of feeding substrata. Coral Reefs 39:1313–27.

Olsen AM, Camp AL, Brainerd EL. 2017. The opercular mouth-opening mechanism of largemouth bass functions as a 3D four-bar linkage with three degrees of freedom. J Exp Biol 220:4612–23.

Olsen AM, Hernández LP, Camp AL, Brainerd EL. 2019. Channel catfish use higher coordination to capture prey than to swallow. Proc R Soc B Biol Sci 286.

Olsen AM, Westneat MW. 2016. Linkage mechanisms in the vertebrate skull: Structure and function of three-dimensional, parallel transmission systems. J Morphol 277:1570–83.

Olson EC, Miller RL. 1999. Morphological integration University of Chicago Press.

Ong L, Holland KN. 2010. Bioerosion of coral reefs by two Hawaiian parrotfishes: Species, size differences and fishery implications. Mar Biol 157:1313–23.

Ornelas-García CP, Bautista A, Herder F, Doadrio I. 2017. Functional modularity in lake-dwelling characin fishes of Mexico. PeerJ 2017:1–22.

Paradis E, Claude J, Strimmer K. 2004. APE: Analyses of phylogenetics and evolution in R language. Bioinformatics.

Parsons KJ, Cooper WJ, Albertson RC. 2011. Modularity of the oral jaws is linked to repeated changes in the craniofacial shape of African cichlids. Int J Evol Biol 2011:1–10.

Parsons KJ, Márquez E, Craig Albertson R. 2012. Constraint and opportunity: The genetic basis

and evolution of modularity in the cichlid mandible. Am Nat 179:64–78.

Pigliucci M. 2008. Is evolvability evolvable? Nat Perspect 9:75–82.

Popowics TE, Herring SW. 2007. Load transmission in the nasofrontal suture of the pig, *Sus scrofa* . J Biomech 40:837–44.

Price SA, Wainwright PC, Bellwood DR, Kazancioglu E, Collar DC, Near TJ. 2010. Functional innovations and morphological diversification in parrotfish. Evolution (N Y) 64:3057–68.

Rafferty KL, Herring SW. 1999. Craniofacial sutures: Morphology, growth, and in vivo masticatory strains. J Morphol 242:167–79.

Rafferty KL, Herring SW, Marshall CD. 2003. Biomechanics of the rostrum and the role of facial sutures. J Morphol 257:33–44.

Rayfield EJ. 2005. Using finite-element analysis to investigate suture morphology: A case study using large carnivorous dinosaurs. Anat Rec - Part A Discov Mol Cell Evol Biol 283:349–65.

Rayfield EJ, Norman DB, Horner CC, Horner JR, Smith PM, Thomason JJ, Upchurch P. 2001. Cranial design and function in a large theropod dinosaur. Nature 409:1033–37.

Revell LJ. 2012. phytools: An R package for phylogenetic comparative biology (and other things). Methods Ecol Evol.

Ristaniemi A, Stenroth L, Mikkonen S, Korhonen RK. 2018. Comparison of elastic, viscoelastic and failure tensile material properties of knee ligaments and patellar tendon. J Biomech 79:31–38.

Roberts TJ, Azizi E. 2011. Flexible mechanisms: The diverse roles of biological springs in vertebrate movement. J Exp Biol 214:353–61.

Rohlf FJ, Slice D. 1990. Extensions of the procrustes method for the optimal superimposition of landmarks. Syst Zool 39:40–59.

Ross CF, Dharia R, Herring SW, Hylander WL, Liu ZJ, Rafferty KL, Ravosa MJ, Williams SH. 2007. Modulation of mandibular loading and bite force in mammals during mastication. J Exp Biol 210:1046–63.

RStudio. 2012. RStudio: Integrated development environment for R. J Wildl Manage.

Sanford CPJ. 2001. Kinematic analysis of a novel feeding mechanism in the brook trout *Salvelinus fontinalis* (Teleostei: Salmonidae): Behavioral modulation of a functional novelty. J Exp Biol 204:3905–16.

Sass GG, Motta PJ. 2002. The effects of satiation on strike mode and prey capture kinematics in the largemouth bass, Micropterus salmoides. Environ Biol Fishes 65:441–54.

Schatzmann L, Brunner P, Stäubli HU. 1998. Effect of cyclic preconditioning on the tensile properties of human quadriceps tendons and patellar ligaments. Knee Surgery, Sport Traumatol Arthrosc.

Shadwick RE. 1990. Elastic energy storage in tendons: Mechanical differences related to function and age. J Appl Physiol 68:1033–40.

Shadwick RE, Rapoport HS, Fenger JM. 2002. Structure and function of tuna tail tendons. Comp Biochem Physiol - A Mol Integr Physiol 133:1109–25.

Shantz AA, Ladd MC, Burkepile DE. 2020. Overfishing and the ecological impacts of extirpating large parrotfish from Caribbean coral reefs. Ecol Monogr 90:1–17.

Sharp AC, Dutel H, Watson PJ, Gröning F, Crumpton N, Fagan MJ, Evans SE. 2023. Assessment of the mechanical role of cranial sutures in the mammalian skull: Computational biomechanical modelling of the rat skull. J Morphol.

Sidlauskas B. 2008. Continuous and arrested morphological diversification in sister clades of characiform fishes: A phylomorphospace approach. Evolution (N Y) 62:3135–56.

Smith KD, Vaughan-Thomas A, Spiller DG, Innes JF, Clegg PD, Comerford EJ. 2011. The organisation of elastin and fibrillins 1 and 2 in the cruciate ligament complex. J Anat 218:600–607.

Smith LL, Fessler JL, Alfaro ME, Streelman JT, Westneat MW. 2008. Phylogenetic relationships and the evolution of regulatory gene sequences in the parrotfishes. Mol Phylogenet Evol 49:136–52.

Smith TB. 2008. Temperature effects on herbivory for an Indo-Pacific parrotfish in Panamá: Implications for coral-algal competition. Coral Reefs 27:397–405.

Souza M V., Van Weeren PR, Van Schie HTM, Van de Lest CHA. 2010. Regional differences in biochemical, biomechanical and histomorphological characteristics of the equine suspensory ligament. Equine Vet J 42:611–20.

Stäubli HU, Schatzmann L, Brunner P, Rincón L, Nolte LP. 1999. Mechanical tensile properties of the quadriceps tendon and patellar ligament in young adults. Am J Sports Med 27:27–34.

Streelman JT, Alfaro M, Westneat MW, Bellwood DR, Karl SA. 2002. Evolutionary history of the parrotfishes: Biogeography, ecomorphology, and comparative diversity. Evolution (N Y) 56:961–71.

Summers AP, Koob-Emunds MM, Kajiura SM, Koob TJ. 2003. A novel fibrocartilaginous

tendon from an elasmobranch fish *(Rhinoptera bonasus)*. Cell Tissue Res 312:221–27.

Summers AP, Koob TJ, Romer AS. 2002. The evolution of tendon — morphology and material properties. Comp Biochem Physiol Part A 133:1159–70.

Tanaka E, Miyawaki Y, Del Pozo R, Tanne K. 2000. Changes in the biomechanical properties of the rat interparietal suture incident to continuous tensile force application. Arch Oral Biol 45:1059–64.

Thornton GM, Schwab TD, Oxland TR. 2007. Fatigue is more damaging than creep in ligament revealed by modulus reduction and residual strength. Ann Biomed Eng 35:1713–21.

Tokita M, Kiyoshi T, Armstrong KN. 2007. Evolution of craniofacial novelty in parrots through developmental modularity and heterochrony. Evol Dev 9:590–601.

Turingan RG, Wainwright PC. 1993. Morphological and functional bases of durophagy in the queen triggerfish, *Balistes vetula* (Pisces, tetraodontiformes). J Morphol 215:101–18.

Van Wassenbergh S, De Rechter D. 2011. Piscivorous cyprinid fish modulates suction feeding kinematics to capture elusive prey. Zoology 114:46–52.

Van Wassenbergh S, Herrel A, Adriaens D, Aerts P. 2007. Interspecific variation in sternohyoideus muscle morphology in clariid catfishes: Functional implications for suction feeding. J Morphol 268:232–42.

Van Wassenbergh S, Ortlieb EJ, Mielke M, Böhmer C, Shadwick RE, Abourachid A. 2022. Woodpeckers minimize cranial absorption of shocks. Curr Biol 32:3189-3194.e4.

Vogel S. 2013. Comparative biomechanics: Life's physical world. Second. ed Princeton: Princeton University Press.

Wagner GP. 1996. Homologues, natural kinds and the evolution of modularity. Am Zool 36:36–43.

Wagner GP, Altenberg L. 1996. Complex adaptations and the evolution of evolvability. Evolution (N Y) 50:967–76.

Wagner GP, Pavlicev M, Cheverud JM. 2007. The road to modularity. Nat Rev Genet 8:921–31.

Wainwright PC. 1987. Biomechanical limits to ecological performance: mollusc-crushing by the Caribbean hogfish, Lachnolaimus maximus (Labridae). J Zool 213:283–97.

Wainwright PC, Bellwood DR, Westneat MW, Grubich JR, Hoey AS. 2004. A functional morphospace for the skull of labrid fishes: Patterns of diversity in a complex biomechanical system. Biol J Linn Soc 82:1–25.

Weller HI, Olsen AM, Camp AL, Manafzadeh AR, Hernandez LP, Brainerd EL. 2020. An XROMM Study of Food Transport and Swallowing in Channel Catfish. Integr Org Biol 2.

Westneat MW. 1990. Feeding mechanics of teleost fishes (Labridae; Perciformes): A test of four-bar linkage models. J Morphol 205:269–95.

Westneat MW. 1991. Linkage biomechanics and evolution of the unique feeding mechanism of *Epibulus insidiator* (Labridae: Teleostei). J Exp Biol 159:165–84.

Westneat MW. 1993. Phylogenetic relationships of the tribe cheilinini (Labridae: Perciformes). Bull Mar Sci 52:351–94.

Westneat MW. 1994. Transmission of force and velocity in the feeding mechanisms of labrid fishes (Teleostei, Perciformes). Zoomorphology 114:103–18.

Westneat MW. 2003. A biomechanical model for analysis of muscle force, power output and lower jaw motion in fishes. J Theor Biol 223:269–81.

Westneat MW. 2006. Skull biomechanics and suction feeding in fishes. Fish Physiol 23:29–75.

Westneat MW, Alfaro ME. 2005. Phylogenetic relationships and evolutionary history of the reef fish family Labridae. Mol Phylogenet Evol 36:370–90.

Westneat MW, Alfaro ME, Wainwright PC, Bellwood DR, Grubich JR, Fessler JL, Clements KD, Smith LL. 2005. Local phylogenetic divergence and global evolutionary convergence of skull function in reef fishes of the family labridae. Proc R Soc B Biol Sci 272:993–1000.

Westneat MW, Wainwright PC. 1989. Feeding mechanism of *Epibulus insidiator* (Labridae; Teleostei): Evolution of a novel functional system. J Morphol 202:129–50.

Whitlow KR. 2022. Biomechanics, evolution and modulation of suction feeding mechanisms in fishesUniv Chicago.

Whitlow KR, Ross CF, Gidmark NJ, Laurence-Chasen JD, Westneat MW. 2022. Suction feeding biomechanics of *Polypterus bichir*: Investigating linkage mechanisms and the contributions of cranial kinesis to oral cavity volume change. J Exp Biol 225.

William Fielding J, Burstein AH, Frankel VH. 1976. The Nuchal Ligament. Spine (Phila Pa 1976) 1:3–14.

Winterbottom R. 1974. A Descriptive Synonymy of the Striated Muscles of the Teleostei. Proc Acad Nat Sci Philadelphia 125:225–317.

Woo SLY, Orlando CA, Camp JF, Akeson WH. 1986. Effects of postmortem storage by freezing on ligament tensile behavior. J Biomech 19:399–404.

Zelditch ML, Goswami A. 2021. What does modularity mean? Evol Dev 23:377–403.

Zelditch ML, Swiderski DL, Sheets HD. 2012. Geometric morphometrics for biologists: a primer Academic Press.